5

III

THE APPLICATION OF ERTS IMAGERY TO MONITORING ARCTIC SEA ICE

ERT Document 0408-F

FEBRUARY 1974

TYPE III REPORT

June 1972 thru December 1973

JAMES C. BARNES
CLINTON J. BOWLEY

prepared for
NATIONAL AERONAUTICS AND SPACE ADMINISTRATION
GODDARD SPACE FLIGHT CENTER
GREENBELT, MARYLAND 20771

1126A
05/07/74

ENVIRONMENTAL RESEARCH & TECHNOLOGY, INC.
429 MARRETT ROAD, LEXINGTON, MASSACHUSETTS 02173

PREFACE

Because of the effect of sea ice on the heat balance of the Arctic and because of the expanding economic interest in arctic oil and other minerals, extensive monitoring and further study of sea ice is required. However, the inaccessibility of the polar regions has necessitated the use of slow and costly methods for data acquisition. Now, through the use of ERTS imagery, the potential exists for monitoring arctic sea ice on a more complete and economical basis than has heretofore been possible.

The application of ERTS data for mapping ice is evaluated for several arctic areas, including the Bering Sea, the eastern Beaufort Sea, parts of the Canadian Archipelago, and the Greenland Sea. Interpretive techniques are discussed, and the scales and types of ice features that can be detected are described. Ice conditions mapped from ERTS imagery are compared with the conditions depicted on aerial ice observation charts; for the Bering Sea, a sample of ERTS imagery is compared with visual ice reports and aerial photography from the NASA-CV-990 aircraft.

The results of the investigation demonstrate that ERTS imagery has substantial practical application for monitoring arctic sea ice. Ice features as small as 80-100 m in width can be detected, and the combined use of the visible and near-IR imagery is a powerful tool for identifying ice types. In the eastern Beaufort Sea, the combination of ERTS orbital overlap and a high incidence of cloud free conditions during the spring assures a high frequency of repetitive satellite coverage. With this repetitive coverage, the deformation and movement of ice features could be mapped throughout the early April to late June period. Ice features that can be identified in ERTS imagery include: the distinction between grey, grey-white, and older forms of ice, as well as the distinction between ice floes and surrounding brash ice; the growth and deterioration of leads; the formation of new grey ice within leads; the deterioration of the ice surface as evidenced by the formation of puddled areas and flooded ice; linear dry areas within flooded ice fields caused by the drainage of meltwater; and icebergs embedded in fast ice or close pack ice detectable by their shadows. Ice conditions in the Bering Sea during early March depicted in ERTS images are in close agreement with aerial photographs taken from the NASA CV-990 aircraft and with the ice conditions reported by the observer onboard the aircraft.

TABLE OF CONTENTS

LIST OF ILLUSTRATIONS

LIST OF ILLUSTRATIONS

Contd.

LIST OF ILLUSTRATIONS

Contd.

LIST OF TABLES

1. INTRODUCTION

1.1 Purpose and Objectives

The purpose of this investigation was to evaluate the application of ERTS data for detecting and mapping arctic sea ice. The specific objectives were to determine the spectral bands most suitable for detecting ice, to measure the scale and types of ice features that can be detected, and to develop interpretive techniques for differentiating ice from clouds and for mapping ice concentrations. Aerial survey ice charts and aircraft photography have been used as correlative data to determine the reliability with which ice boundaries and concentrations can be mapped from ERTS in comparison with other sources of ice observations. The ERTS data have been analyzed for various arctic regions including the Bering Sea, the eastern Beaufort Sea, Baffin Bay, and the Greenland Sea.

Because of the inaccessibility of the polar regions, sea ice monitoring is, by its very nature, a problem that can benefit from space technology. The results of this study will lead eventually to the operational use of future satellite data and, thus, to a more cost-effective means for obtaining ice observations.

1.2 Requirement for Monitoring Arctic Sea Ice

Several scientists have pointed out that because of the critical effect of sea ice on the heat balance of the Arctic, the amount of ice may be an important and possibly a key factor in the climate of the Northern Hemisphere (Fletcher, 1966; Maykut and Untersteiner, 1969; and Committee on Polar Research, 1970). In another report, Fletcher (1968) states that the seasonal patterns of surface heat exchange over oceanic regions, which are directly related to ice distribution, are the most important factors to monitor in both the Arctic and Antarctic. The report of the Committee on Polar Research (1970) stresses that what is needed most in the Arctic is an observational program to provide input data for numerical models of the atmosphere and ocean.

Because of the enormous implications of ice, detailed scientific studies have been initiated. One such effort is Project AIDJEX, the Arctic Ice Dynamics Joint Experiment, the purpose of which is to gain a

quantitative understanding of the interaction between the fields of motion of the atmosphere, the pack ice, and the liquid ocean (Maykut, et al, 1972). Similarly, the POLEX program planned for the late 1970's will be a vast international effort to study the earth's polar regions (Borisenkov and Treshnikov, 1971). Extensive synoptic-scale ice data must be obtained as input to the numerical ice models under development in these and other programs.

The requirement for extensive monitoring and study of sea ice is further emphasized by recent interest in the economic exploitation of arctic regions. Exploration for oil and other minerals will, in itself, require increased shipping in arctic waters, demanding increasingly accurate ice-condition forecasting. The modern demands of the Canadian ice advisory service are summarized by Markham (1973). Furthermore, reliable ice statistics must be accumulated to plan properly for offshore oil drilling in arctic coastal areas; when drilling operations are actually undertaken, careful ice monitoring will be necessary to minimize the potential hazards.

1.3 Application of Satellite Data to Sea Ice Monitoring

The potential of the satellite for collecting ice data was recognized soon after the first pictures were returned by the early TIROS weather satellites more than a decade ago (Wark and Popham, 1962; Baliles and Neiss, 1963). This potential was emphasized at a conference on oceanography from space, where a panel recommended that systems for the detection of sea ice be among the very first to be incorporated into future satellites (Morse, 1964). In fact, it was in the mid-1960s that Fletcher (1966) stated that the "observational barrier" in the arctic was crumbling primarily under the impact of satellite observation systems.

Since the time of Fletcher's remarks concerning the impact of satellite observations on the arctic, further studies have been conducted to develop techniques to apply satellite data to marine resources problems. Studies such as those reported by McClain and Baliles (1971), Barnes, Chang, and Willand (1970, 1972), and Barnes, et al (1973) have demonstrated that useful ice information could be derived from the visible and thermal IR measurements made by existing meteorological satellites. Now, through the improved NOAA-2 operational system even greater use of spacecraft-acquired data for sea ice analysis is being made (McClain, 1973; Wiesnet, 1973). Despite

the usefulness of meteorological satellite data, however, much of the required ice information can only be acquired through the high-resolution sensors of the ERTS spacecraft. In particular, the information required as input to numerical ice models and to derive statistics of ice distributions useful for applications such as planning offshore oil drilling cannot be acquired from the lower resolution observations. The preliminary results of the investigation to evaluate the application of ERTS imagery to sea ice mapping were presented in papers by Barnes and Bowley (1973a, 1973b).

2. DATA SAMPLE

2.1 Locations of Test Sites

Three arctic regions were originally selected as test sites. These three regions, which are indicated on the map in Figure 2-1, are (1) Baffin Bay, (2) the Beaufort Sea, and (3) the Greenland Sea. A map of the region extending from the Eastern Beaufort Sea to Baffin Bay is shown in Figure 2-2.

Baffin Bay is an area of the arctic which has a relatively large amount of ship traffic, and for which ground-truth data are more plentiful than in most arctic regions. Furthermore, a number of studies of remote sensing applications for ice survey have concentrated on this area. Baffin Bay is ice-filled from about December through June, with the month of minimum ice coverage being September. Even during the minimum ice season, however, small ice floes and icebergs are common.

The Beaufort Sea is an important region economically because of the petroleum development of the North Slope of Alaska and the exploration for petroleum and other minerals in the islands and coastal waters of northern Canada. Furthermore, the Beaufort Sea is the location of the AIDJEX test site. Although the ice boundary retreats northward from the coastline of Alaska and Canada during the summer months, ice is found in the Beaufort Sea during all seasons.

The Greenland Sea is also a region of considerable scientific interest because it is the major area of outflow from the Arctic Ocean (Wittmann, 1966). Ice concentrations vary from season to season in the Greenland Sea, but some ice is found during all months. A map of Greenland is given in Figure 2-3.

A fourth test site selected later in the study is in the Bering Sea. This area was chosen because of the availability of correlative ice observations collected as part of the Bering Sea Expedition (BESEX), a joint effort between the United States and USSR that was conducted during the period from mid-February through early March 1973. The primary area of interest, shown in Figure 2-4, extended southward from St. Lawrence Island to beyond the edge of the pack ice. During the period of the expedition, the pack ice edge was well to the south, so that St. Lawrence, St. Matthew, and Nunivak Islands were all within the pack.

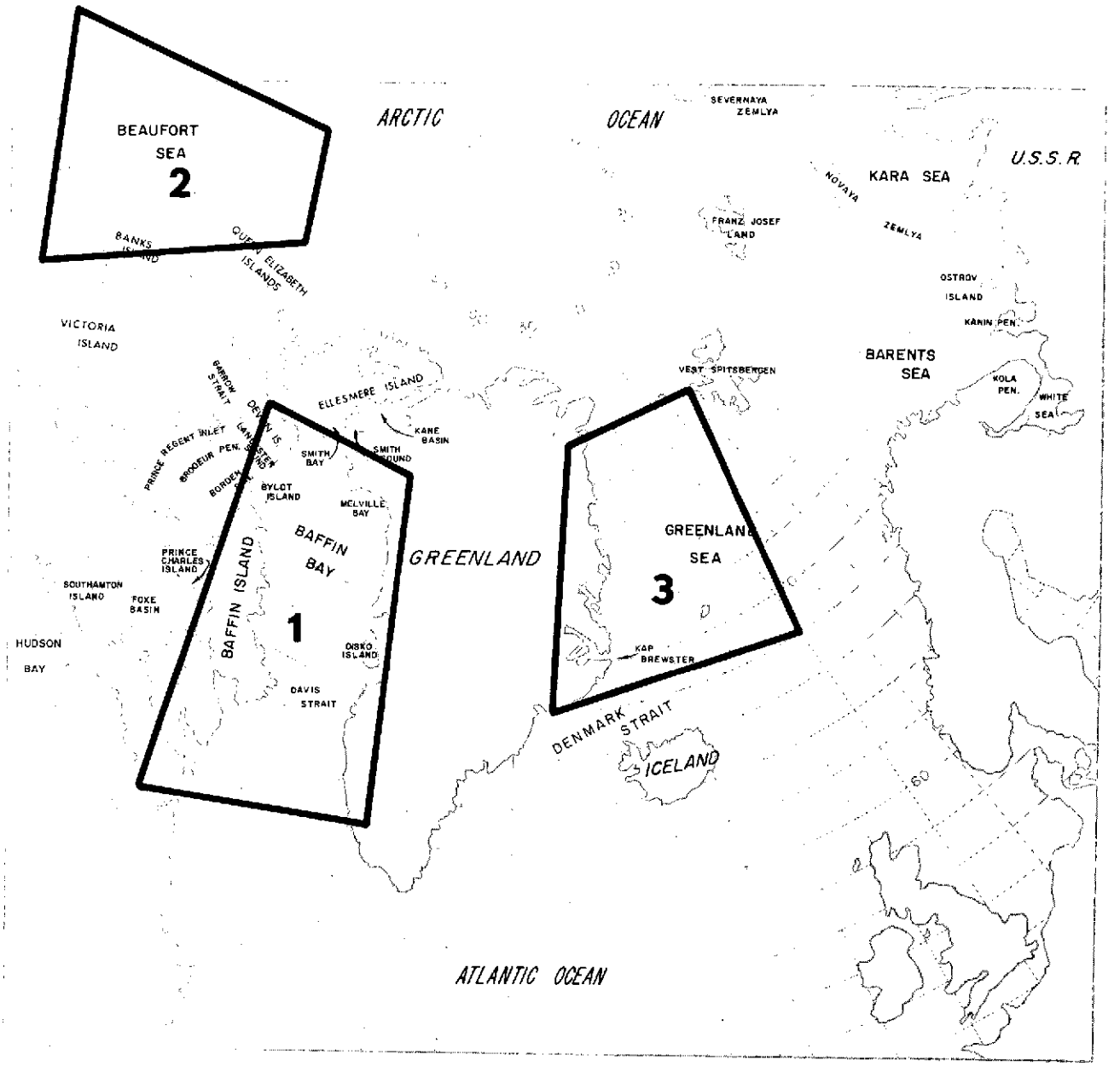

Figure 2-1 Map of Arctic with primary test sites indicated.

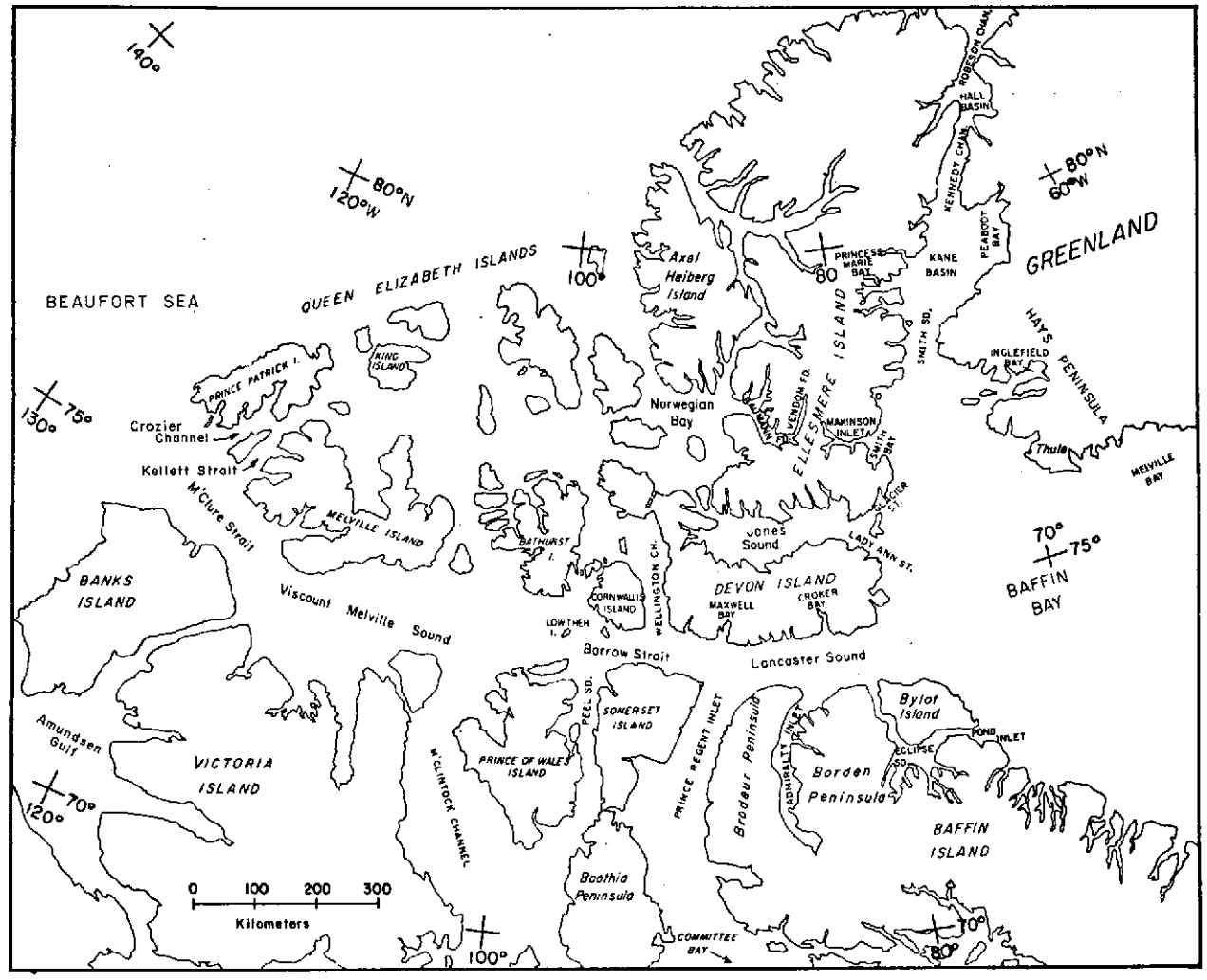

Figure 2-2 Map of Arctic showing area from eastern Beaufort Sea to Baffin Bay.

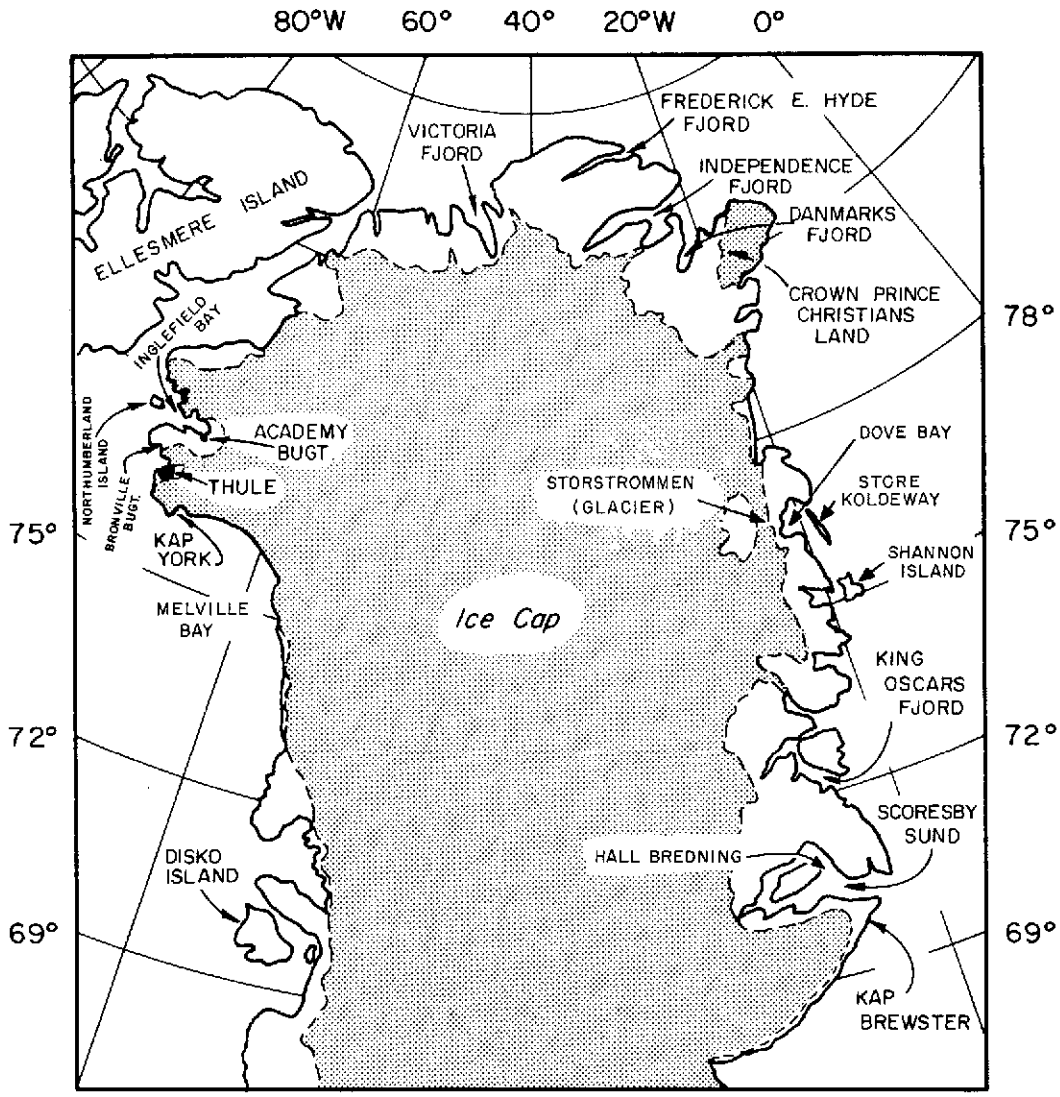

Figure 2-3 Map of Greenland; approximate boundaries of ice cap are indicated.

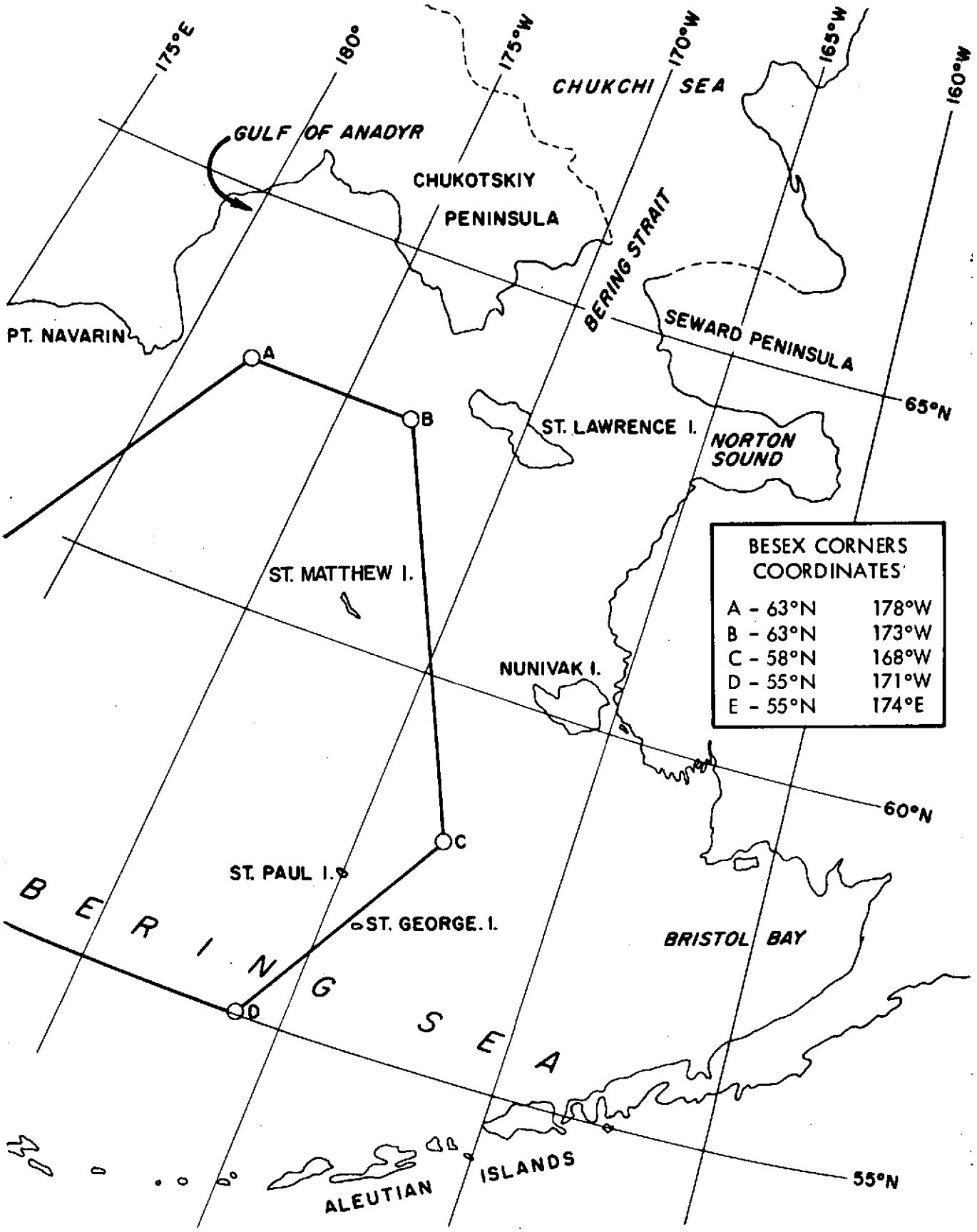

Figure 2-4 Map of Bering Sea Showing the BESEX (Bering Sea Expedition) Test Area

2.2 ERTS Data

ERTS-1 was placed into a near-polar, sun-synchronous orbit at a height of 900 km on 23 July 1972. Except for a brief period in early August of 1972, the MSS (Multi-Spectral Scanner) sensor system has operated continuously, returning approximately 188 data scenes each day, 44 of which are over the United States. The MSS views a swath 180 km wide, with coverage of the exact same area occurring every 18 days. Because of orbital overlap at the higher latitudes, however, coverage of arctic areas can occur as often as three or four consecutive days during each 18-day repeat cycle. The results of studies reported at the various symposia have indicated that features greater than about 70 m in width can be identified in ERTS imagery and can be mapped accurately to a scale of at least 1:250,000. The MSS senses in four spectral bands: MSS-4 (0.5-0.6 μm), MSS-5 (0.6-0.7 μm), MSS-6 (0.7-0.8 μm), and MSS-7 (0.8-1.1 μm).

The second sensor system on board ERTS-1 is the RBV (Return Beam Vidicon). Although this sensor was in operation for only a short period during late July and early August 1972, some RBV imagery of the arctic was collected. The area viewed by the RBV is identical to that of the MSS, and the ground resolutions are similar. The three spectral bands of this sensor are: RBV-1 (0.475-0.575 μm), RBV-2 (0.580-0.680 μm), and RBV-3 (0.690-0.830 μm).

The extensive MSS and very limited RBV data samples used in the investigation were comprised entirely of imagery; no digitized data were used. The imagery was acquired from the NASA Data Processing Facility (NDPF) in both the 70 mm negative transparency and 9.5-inch positive paper print formats through the standing order procedure. The data for the Bering Sea were acquired through a retrospective data request. In addition to black and white imagery, a limited sample of color composite prints was also examined.

ERTS-1 coverage of the arctic extended to about 80°N. Because of the winter dark period, however, illumination was not sufficient to permit usable data to be collected north of about 70°N during the period from late October to early April. The data sample used in this investigation, therefore, was during the periods from late July to late October 1972 and from early April to early July 1973. A few images were also acquired from

late March, and the BESEX data were from late February and early March. Under the scope of the study effort, it was not possible to analyze data collected later in the summer of 1973.

Because of the readout configuration for ERTS-1 and cloud obscuration, the majority of the usable data were for the eastern Beaufort Sea test site. On several dates, two ERTS orbital passes produced usable imagery over this test site; also, as a result of the overlapping of orbits at high latitudes, cloud-free coverage of the same area was frequently available on two consecutive days, and occasionally on three consecutive days. Tables 2-1 and 2-2 provide an indication of the size of the ERTS data sample for the specified test sites. In addition to the orbital passes indicated, ERTS data were collected on a total of four passes over the Bering Sea during the BESEX period. On two dates, 27 and 28 February, the ERTS passes crossed the easternmost part of the Bering Sea in the Nunivak Island area (ERTS Identifier No. 1219-21382 through -21391), and 1220-21440 through -21445). On 6 and 7 March, the passes crossed St. Lawrence Island and the prime BESEX area of interest (ERTS Identifier Nos. 1226-22165 through -22185, and 1227-22223 through -22241). The data for each of these four passes were acquired from the NDPF.

2.3 Correlative Data

The paucity of correlative ice data from the arctic underscores the need for satellite observations. Aerial survey ice charts prepared by the Ice Forecast Office of the U. S. Navy Fleet Weather Central and by the Canadian Ice Forecasting Central were acquired from the respective agencies; however, only a very few charts were available for the areas and dates covered by ERTS.

During the BESEX period, some 14 flights were made by the NASA CV-990 aircraft, operating out of Elmendorf Air Force Base in Anchorage. The targets for the flights were either precipitating cloud profile, ocean roughness, or ice mosaic. One flight, on 3 March, flew north to the Beaufort Sea to overfly the 1972 AIDJEX site. On all flights numerous on-board experiments were conducted including nearly continuous vertical viewing aerial photography. Although only one flight was made on a day with ERTS data, two other flights were within a day of an ERTS pass. Both the aircraft

TABLE 2-1

NUMBER OF ERTS ORBITAL PASSES PROVIDING CLOUD-FREE COVERAGE OF VARIOUS ARCTIC AREAS DURING THE PERIOD FROM LATE JULY TO LATE OCTOBER 1972

Area	No. of Passes
Mid-Beaufort Sea south to Alaska Coast	20
Prince Patrick Island, Melville Island, Banks Island, and Amundsen Gulf	24
Axel Heiberg, Ellef Ringnes, and Amund Ringnes Islands (Queen Elizabeth Islands)	2
Hudson Bay	3
Labrador Coast, Baffin Island, and Ellesmere Island	4
Devon Island, Cornwallis Island, Somerset Island, and Prince of Wales Island	5
Baffin Bay (along West Coast of Greenland)	2
Greenland Sea (along East Coast of Greenland)	7

TABLE 2-2

ERTS-1 ORBITAL PASSES PROVIDING CLOUD-FREE COVERAGE
OF VARIOUS ARCTIC AREAS DURING THE SPRING 1973

Date	Image Identifier	Geographic Area
24 March	1244-17032 thru 1244-17043	Baffin Bay & Thule, Greenland
25 March	1245-13412 thru 1245-13430	Greenland Sea & E.Coast of Greenland
28 March	1248-15451 thru 1248-15471	Baffin Bay & Baffin Island
1 April	1252-21150 thru 1252-21175	Beaufort Sea
8 April	1259-20130 thru 1259-20151	Prince Patrick Is, Eglinton Is, & Banks Is.
10 April	1261-20241 thru 1261-20264	Prince Patrick Is.&Beaufort Sea
11 April	1262-20295 thru 1262-20320	Prince Patrick Is.&Beaufort Sea
21 April	1272-21255 thru 1272-21285	Beaufort Sea
28 April	1279-20242 thru 1279-20251	Prince Patrick Is.&Beaufort Sea
2 May	1283-20463 thru 1283-20484	Banks Is. & Beaufort Sea
3 May	1284-20521 thru 1284-20535	Beaufort Sea
7 May	1288-21144 thru 1288-21165	Beaufort Sea
17 May	1298-20293 thru 1298-20302	Prince Patrick Is.&Beaufort Sea
20 May	1301-20462 thru 1301-20432	Prince Patrick Is.&Beaufort Sea
6 June	1318-20405 thru 1318-20432	Prince Patrick Is.&Beaufort Sea
10 June	1322-19223 and 1322-19230	Eastern Amundsen Gulf
12 June	1324-19334 thru 1324-19343	Prince of Wales Strait & Amundsen Gulf
13 June	1325-19394	Amundsen Gulf
16 June	1328-19554 thru 1328-19570	M'Clure Strait, Banks Is., & Amundsen Gulf
18 June	1330-21475 thru 1330-21505	Beaufort Sea
18 June	1330-20064 thru 1330-20085	Prince Patrick Is., Eglinton Is., Melville Is., M'Clure Strait, Banks Is., & Beaufort Sea
20 June	1332-20174 thru 1332-20183	Prince Patrick Is., Eglinton Is., M'Clure Strait, Banks Is.

photography and the comments by the on-board ice observer (listed in the BESEX Navigational Flight Data) provided excellent correlative information.

Standard meteorological charts for the arctic were acquired from the National Climatic Center.

3. DETECTION OF SEA ICE IN ERTS IMAGERY

3.1 Processing of Imagery

In general, the quality of the ERTS data products received from the NDPF was very good. Some of the 9.5-inch prints did appear to be either too light or too dark, however, with considerable variation in the overall density from pass to pass over the same test site. The 70 mm negatives received early in the study period were of a density that made their use difficult with standard photographic processing equipment; this difficulty was corrected in the later negatives. In some of the positive prints received from the NDPF later in the study period, the darkest features are surrounded by an area with an anomalously bright tone. This "halo" effect occurs, for example, when an open lead exists in a scene that is otherwise almost completely ice-covered. The effect does not appear to be present in the 70 mm negative, so is presumably a result of the "dodged print" processing announced in the ERTS Investigators Bulletin of 10 April 1973.

Several ERTS orbital passes contained more than one scene of interest for ice mapping. In these instances mosaics were prepared from the 9.5-inch prints received from the NDPF. Using the mosaics, it was possible to map ice features that extend through two or more ERTS scenes. In addition to working with the 9.5-inch prints, enlarged prints of selected scenes were processed from the 70 mm negatives at ERT's photographic laboratory. Although various scales of enlargements were made depending on the size of the area of interest, most of the reprocessed prints were made at a scale of 1:500,000 as compared to the original 1:1 million scale. For most of the analysis procedures the enlarged prints were found to be the more useful to work with because the ice features could be analyzed more easily at this scale.

In the reprocessing procedure, experiments were also conducted with the exposure time and contrast. Through the experimentation, it was found that when longer exposure times are used such that the snow-covered land areas become completely saturated, many sea ice features not visible in the original print can be detected. The differences between the original and reprocessed prints are particularly noticeable for ERTS scenes covering the eastern coast of Greenland in late summer, where extensive glaciated

land areas are in sharp contrast to the partially ice-free fiords. An illustration of the advantages of image reprocessing for ice detection is given in Figure 3-1 (a and b), in which original and reprocessed portions of an ERTS-1 scene covering Hall Bredning (Bay) at the northern end of Scoresby Sund on the east coast of Greenland are shown.

In the original print (Figure 3-1a), which was presumably processed through a standard photographic procedure applied to all images and directed toward enhancement of land features, detail in the land area is readily seen, whereas the fiord appears to be essentially ice-free. In the reprocessed print (Figure 3-1b), the land is completely saturated; however, areas that appeared to be ice-free in the original print are seen to be actually covered with a considerable amount of ice. In another enlargement, what appears to be bands of ice southeast of Kap Brewster (at the head of Scoresby Sund) in the original print, is seen to be actually the denser portions of a cirrus cloud band. Thus, for certain purposes, such as ice monitoring, the standard products processed at the NDPF may not be optimum.

3.2 Procedures for Detecting and Mapping Ice

3.2.1 Most Useful Spectral Band for Detecting Ice

The initial examination of the MSS data sample and very limited RBV sample indicated that sea ice can be identified in all of the spectral bands because of its high reflectance in contrast to that of the ice-free ocean surface. Overall, the spectral bands in the visible range (MSS-4 and MSS-5) appear to be the most useful for mapping the ice edge and for detecting areas of new or thin ice. Certain types of ice, such as newly forming ice or brash ice, can be detected more readily in these spectral bands than in the longer wavelength bands. In some instances, however, ice-covered areas are saturated in the MSS-4 band, resulting in a loss of ice detail and the obscuration of features on the ice surface. In these instances, the MSS-5 band (0.6 to 0.7 μm) was used in place of the MSS-4 data.

Although overall ice extent can be mapped best using the visible spectral bands, the use of the visible (MSS-4 or MSS-5) data together with the near-IR (MSS-7) data has been found to be a powerful tool for identifying ice types and certain ice surface characteristics. Most analyses were

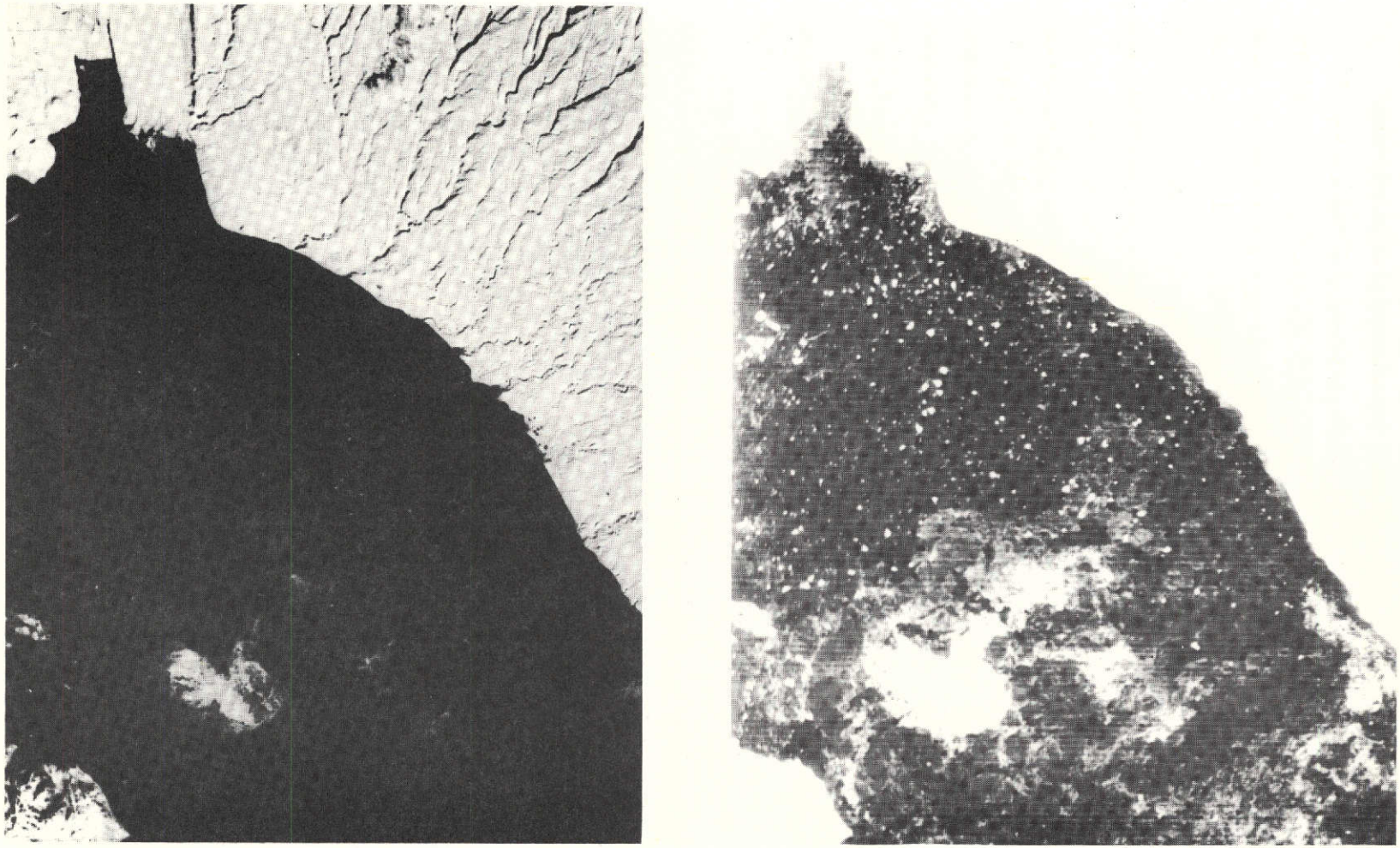

(a) (b)

Figure 3-1 ERTS-1 MSS-4 imagery (ID No. 1076-13032), 7 October 1972, showing part of Hall Bredning (Bay), east coast of Greenland: (2) Image processed to maintain detail in land area; (b) Reprocessed image in which ice features not visible in (a) can be detected.

conducted, therefore, using the MSS-7 imagery in combination with either the MSS-4 or MSS-5 imagery. The application of multispectral analysis to ice mapping is discussed in detail in Section 4.

3.2.2 Procedures for Distinguishing Between Ice and Clouds

Although ice and clouds may have a similar reflectance, ice can be distinguished through a number of interpretive keys. Moreover, ice can often be detected through a thin cloud layer, as illustrated in Figure 3-2. In this regard, cloud penetration is considerably greater in the MSS-7 data than in the shorter wavelengths; in fact, in several instances cloud shadows can be seen on the underlying ice surface in the MSS-7 image, even though the clouds themselves are difficult to detect. In some images, cracks in the ice and cloud shadows were found to have similar reflectances in the MSS-7 band, whereas the cracks appear significantly darker than the cloud shadows in the MSS-4 band. In general, the interpretive keys used to distinguish ice from clouds are as follows:

- The brightness of ice fields and large ice floes is often more uniform than that of clouds. Furthermore, ice floes and features such as leads and fractures within an ice field can at times be detected through thin cirriform cloud cover.

- Cloud shadows can often be detected on the underlying ice surface.

- Edges of most ice features, particularly ice floes, are more distinct than edges of clouds.

- Ice cover fits coastlines and islands, permitting land features to be recognized.

- The spatial frequencies of ice features are not characteristic of cloud patterns. These features include ice floes surrounded by broken ice, narrow ice bands, and spiral patterns induced by ocean currents.

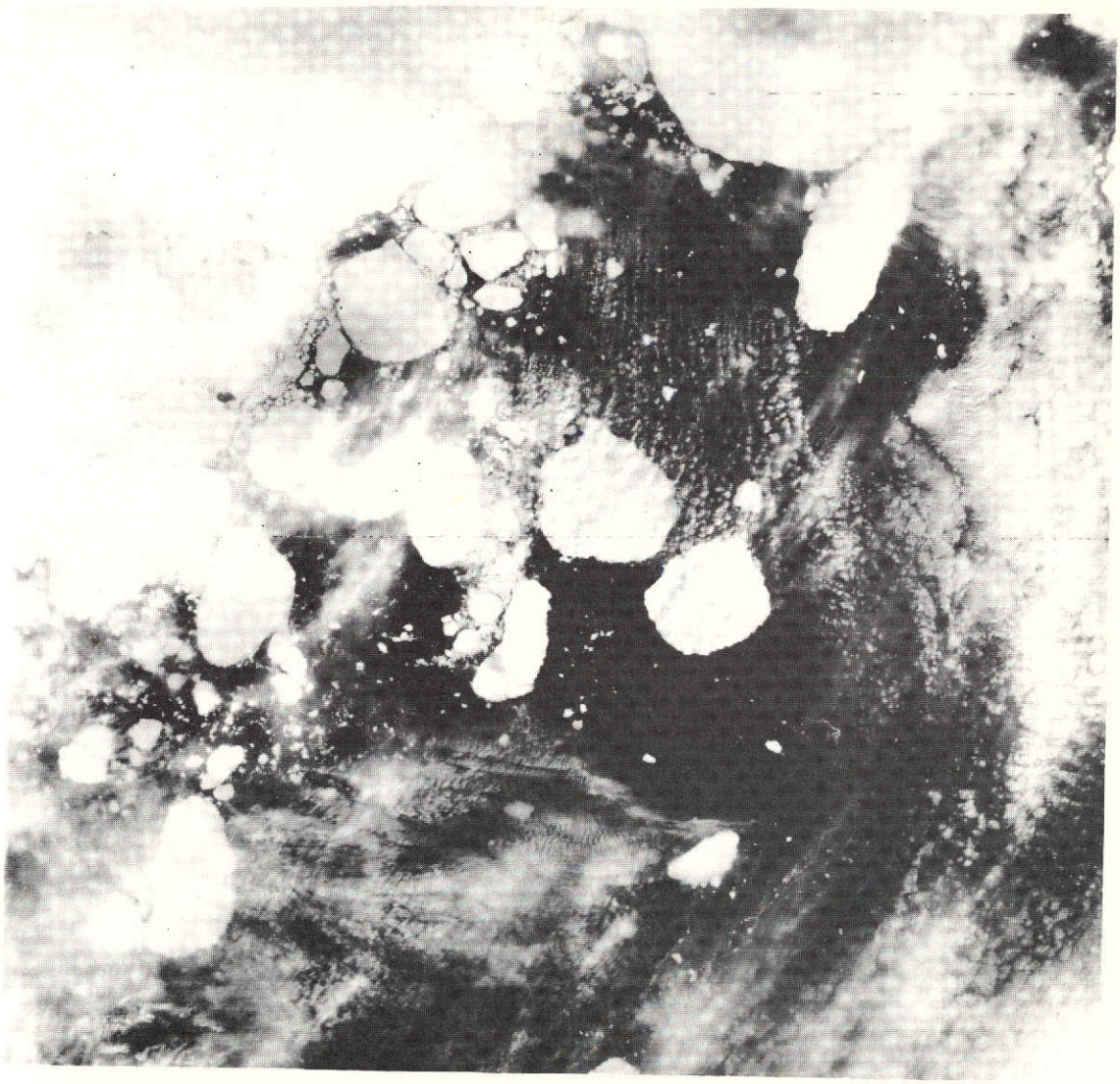

Figure 3-2 ERTS-1 MSS-5 image (ID No. 1065-20360), 26 September 1972, showing ice and clouds, eastern Beaufort Sea.

- When repetitive coverage is available, some ice features remain stable over the 24-hour interval between observations. Even at the longer periods between ERTS repeat cycles, some large floes can still be identified.

3.2.3 Mapping Procedures

Various ice features including the location of the pack ice edge, boundaries between differing ice concentrations and ice types, and certain ice surface characteristics, were mapped from the mosaics and the enlarged prints using transparent acetate overlays. The identification of the various features is based on their differing reflectances and spatial patterns. To attain the greatest mapping accuracy possible, the geographic gridding of the ERTS scenes was corrected if necessary. In most of the frames some correction was applied, the correction factor being generated by checking the locations of land features against standard maps. When no land reference is visible, such as in the data over the Beaufort Sea, the accuracy of the gridding cannot be checked. The maps found to be most useful for use in the analysis of the ERTS data are the Operational Navigation Charts (ONC Series). These maps are of a 1:1 million scale, essentially the same scale as that of the 9.5-inch prints.

Identification of ice types and the scales of the ice features has been made according to the terminology used in the WMO Sea Ice Nomenclature (see Appendix). Ice movements were mapped by transposing the positions of recognizeable features onto the same overlay. It was found that large ice floes could often be identified even after intervals of nearly a month through recognition of shape and surface features.

3.3 Scale of Detectable Ice Features

Ice features of a scale essentially as small as the limiting resolution of the ERTS sensors (about 70 m) can be detected. The detectable features include small ice floes against a water background and surface features or cracks within an ice field. In both cases, the contrast is large; in the former case the ice has a much higher reflectance than the background, whereas in the latter the cracks or surface features have a significantly lower reflectance than the surrounding ice. In fact, although difficult

to measure because of the lack of a reference feature of known size, it does appear that linear features of high contrast, such as cracks through ice fields, may be detectable even though their widths are below the nominal 70 m ERTS resolution.

The ERTS images shown in Figures 3-3 and 3-4 (a and b) provide examples of the scales of detectable ice features. Two scenes from an early ERTS-1 orbital pass (27 July 1972) covering a part of northern Hudson Bay are shown in Figure 3-3; portions of ERTS scenes viewing the same ice floes in the Eastern Beaufort Sea in early and late August 1972 are shown in Figure 3-4 (a and b).

In the MSS-5 imagery shown in Figure 3-3, a well-defined ice edge is evident southwest of Coats Island, with several bights and tongues apparently caused by a westerly surface wind flow. The ice along the immediate ice edge appears to consist mostly of brash or rotten ice, whereas the ice east of the edge consists of close or open pack ice. The majority of ice floes visible in these passes are vast, big, or medium sizes, although one giant ice floe is located near the center of the image[1]. An ice belt is visible off the south coast of Southhampton Island and some fast ice is apparent along the north coast of Coats Island. The comparative analysis between this imagery and concurrent aerial ice observations is discussed in Section 5.1.

In the imagery shown in Figure 3-4, the sea ice consists of individual floes that are more distinct than the ice in the previous figure. Surface features on the larger floes can also be detected. The image in Figure 3-4a is a portion of the complete MSS-7 scene viewing an area near 74°N,130°W on 2 August; the image in Figure 3-4b is a portion of the MSS-7 scene viewing the same area 20 days later. The area covered in both images is approximately 100 km across.

Three giant ice floes can be identified in the two images through reference to their shapes and surface characteristics. Because these floes have rather irregular edges and exhibit very little deterioration over the 20-day interval, they are deduced to be multi-year ice; first-year ice floes would be expected to have more rounded edges and to deteriorate during late

---

(1) In the WMO Sea Ice Nomenclature ice floes are subdivided according to their horizontal extent. The terminology used to define floes and other selected ice features is given in the Appendix.

summer. In a study by Campbell, et al (1973) using ERTS and Nimbus microwave data, the Eastern Beaufort Sea was found to have a greater frequency of multi-year floes, whereas the Western Beaufort Sea has a greater frequency of first-year floes.

The largest of the three identifiable floes has dimensions of about 60 by 50 km; the smallest detectable floes in these images are of the order of 80 to 100 m across. On 2 August, these floes are surrounded by ice concentrations consisting primarily of open pack (4/10 to 6/10) and close pack (7/10 to 8/10), with many various sized smaller floes. Twenty days later, the overall ice concentrations appear to have increased somewhat and now consist mostly of close pack and very close pack (9/10 to less than 10/10). This apparent increase in ice concentration is probably the result of the overall breakup of the numerous smaller "giant floes" (10 to 20 km across), which are greatly reduced in number in the 22 August data. Similarly, a comparison of the surface features of the individual floes indicates that noticeable changes do occur over the 20-day period. In particular, although the larger dark features can be readily identified on both dates, many of the smaller dark spots observed on 2 August are not visible on 22 August. It is possible, therefore, that the smaller dark spots are areas that contain puddles in the earlier observation, but where in the later observation much of the water has drained through cracks and small holes too small to be detected at the ERTS resolution. The detection of surface characteristics in ERTS imagery is discussed more thoroughly in Section 4.

3.4 Techniques to Distinguish Glacial Ice from Sea Ice

Icebergs as small as the limiting ERTS resolution can be detected. In fact, because of the extreme contrast between a sunlit iceberg and the surrounding ocean, icebergs below the theoretical limiting resolution may at times be visible in ERTS imagery. Although glacial ice is readily detectable, distinction between icebergs and small floes can be ambiguous, since both appear as small bright "spots." In areas where most of the sea ice has become brash ice, however, small very bright spots can be identified fairly reliably as icebergs. In Figure 3-1b, for example, the bright spots are likely to be icebergs. Similarly, a very bright spot detected in the open ocean, where a floe would have broken up or melted, is almost certainly an iceberg.

Figure 3-3 ERTS-1 MSS-5 imagery (ID No. 1004-16324), 27 July 1972, showing northern Hudson Bay. Southampton Island (A), Coats Island (B).

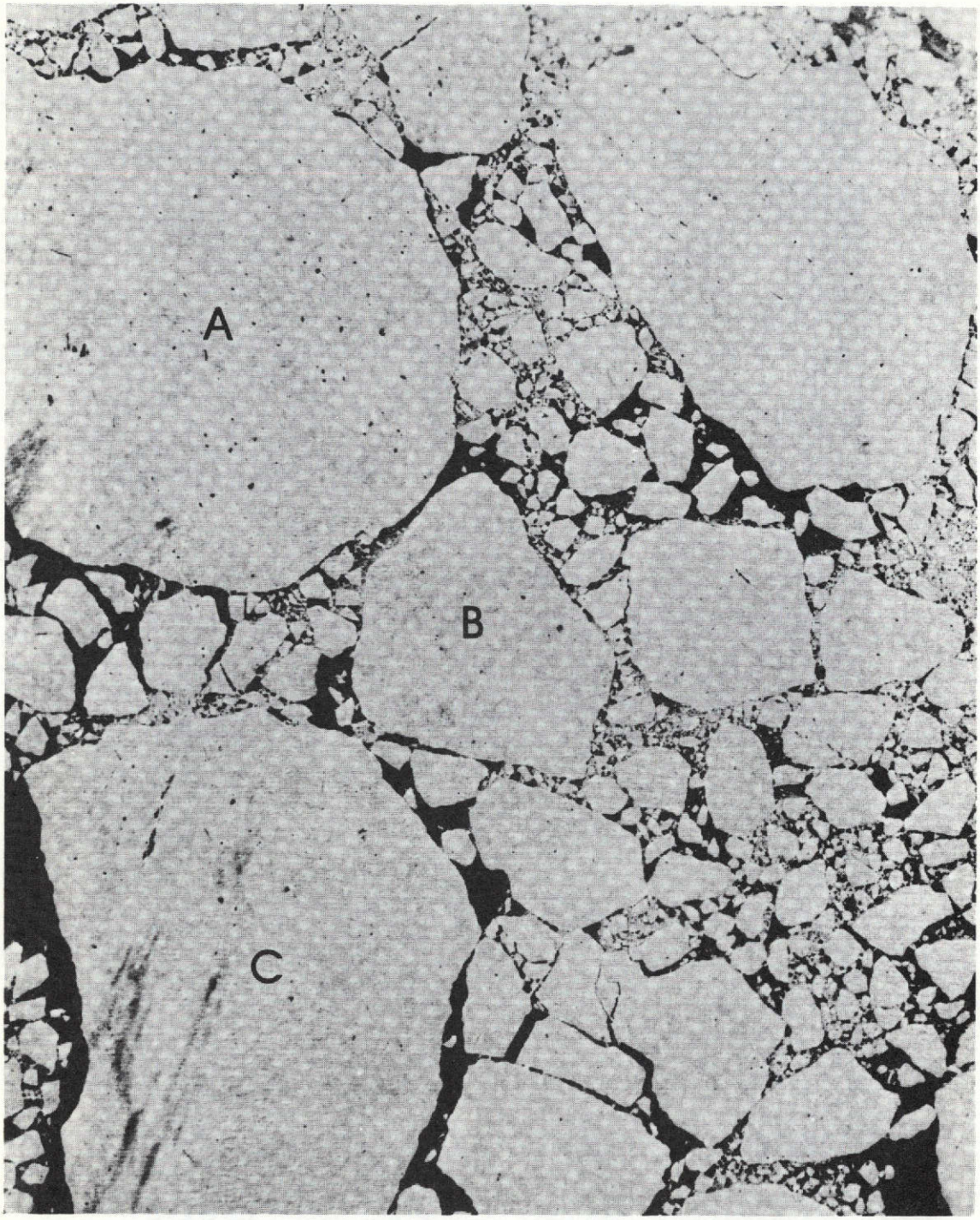

Figure 3-4a Portion of ERTS-1 MSS-7 image (ID No. 1010-20293), 2 August 1972, showing eastern Beaufort Sea, near 74°N, 130°W. Three ice floes that can also be identified in an ERTS image 20 days later are indicated. Floe A is about 50 km in width; some cloud shadows can be detected on floe C.

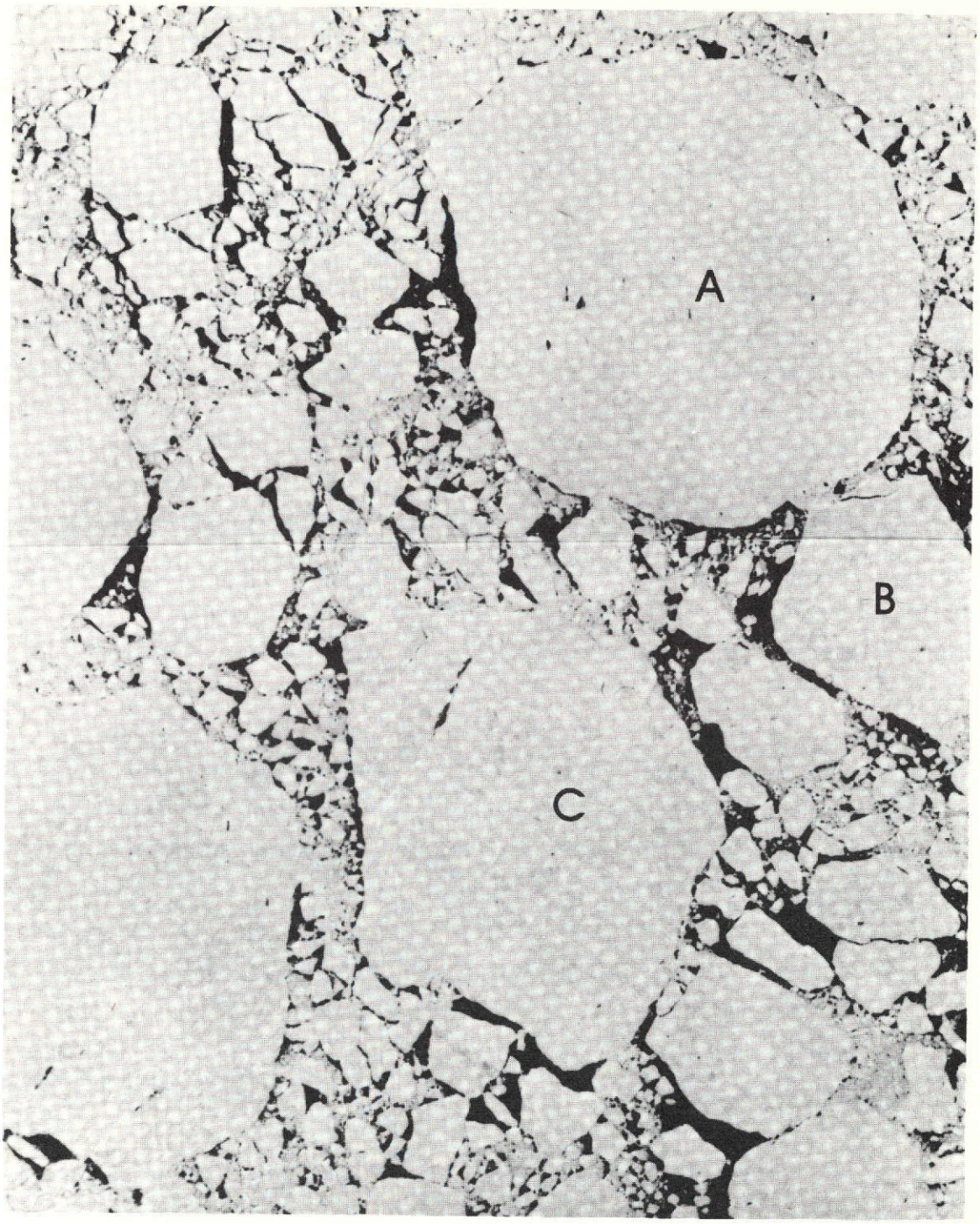

Figure 3-4b Portions of ERTS-1 MSS-7 images (ID Nos. 1030-20410 and 1030-20412), 22 August 1972, showing approximately the area as shown in Figure 3-4a. Floes A, B, and C and some other smaller floes can also be identified in Figure 3-4a.

Icebergs entrapped in fast ice or in close pack ice can be more positively identified, primarily because of their shadows on the surrounding ice and the higher reflectance off their vertical sides. In pack ice, an open water area may also form downwind of the iceberg, in the same way that wind flow often removes ice from the lee-side of an island. Examples of ERTS images in which glacial ice entrapped in fast ice and close pack ice can be distinguished are given in Figures 3-5 and 3-6.

A tongue of fast ice with a high concentration of embedded icebergs can be identified in Dove Bay on the east coast of Greenland (see map, Figure 2-3) in imagery from September 1972 and from March, June and August 1973. The image from 25 March is shown in Figure 3-5. The tongue extends into Dove Bay between Edvards Island and the adjacent island (one of the Godfred Hansens island group), a width of about 5.6 km. Storstrommen, a large glacier, has its mouth in Borge Fiord, just west of Edvards Island. The numerous iceberg shadows stand out particularly well in the March image, as the fast ice has a uniform brightness due to snow cover; also, the sun elevation angle of 16° is considerably lower than in the June and August imagery. In August and September, the iceberg tongue extends into ice-free water in Dove Bay.

Using prints that had been enlarged to a scale of approximately 1:250,000, the horizontal dimensions of the icebergs were measured and the heights were computed from measurements of the shadow lengths. In this instance, the measurements revealed that the size of the larger bergs in Borge Fiord ranged from 240 m to 450 m in length, with heights ranging from 40 m to 60 m. Two large, possibly tabular icebergs are evident close to the mouth of Storstrommen Glacier. The berg closest to the glacier measures approximately 1.1 km long, 360 m wide, and 33 m high; the smaller of the two, located some 5 km to the east, measures about 0.9 km long, 450 m wide, with a height of 33 m.

Numerous icebergs are also detectable in the Melville Bay area of northern Baffin Bay. For example, three icebergs that are trapped in coastal fast ice can be identified in data from September and March. In the March image, shown in Figure 3-6, icebergs can be seen in fast ice east of Kap York and embedded in the pack ice to the south. The wind effects producing open-water areas on the lee-sides of the icebergs drifting in the pack ice are evident. Measurements of the larger icebergs observed in the March imagery were, for the most part, similar to those of September, with the sizes ranging from 180 m to 480 m in length and heights of 45 m to 68 m.

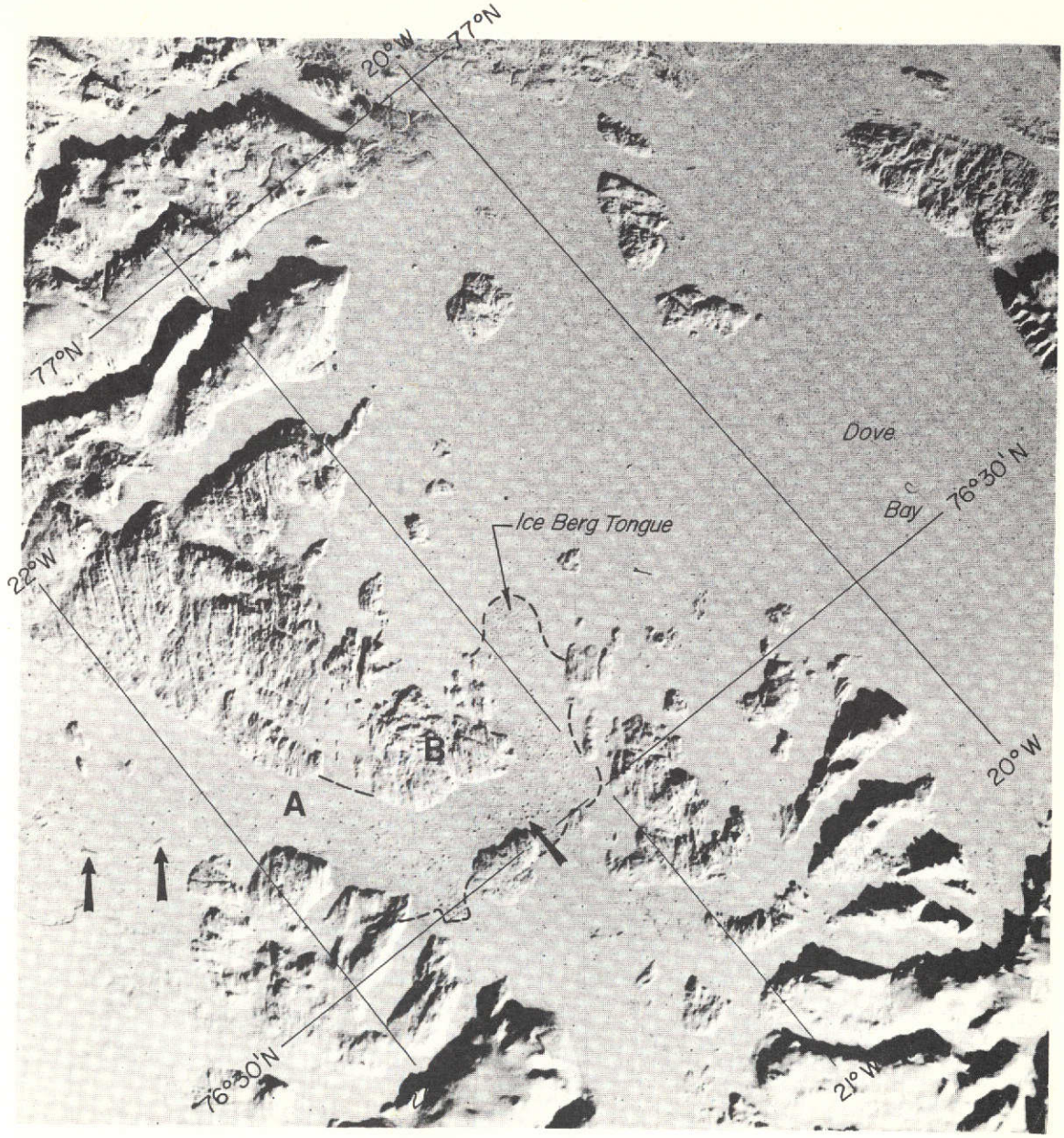

Figure 3-5 Portion of ERTS-1 MSS-7 image (ID No. 1245-13423), 25 March 1973, showing icebergs entrapped in fast ice along east coast of Greenland. The area of maximum iceberg concentration in Borge Fjorden (A) and near Edvards Island (B) is outlined. The positions of two tabular bergs in Borge Fjorden and four large bergs near Edvards Island are indicated by arrows. The area covered in this image is approximately 85 km across.

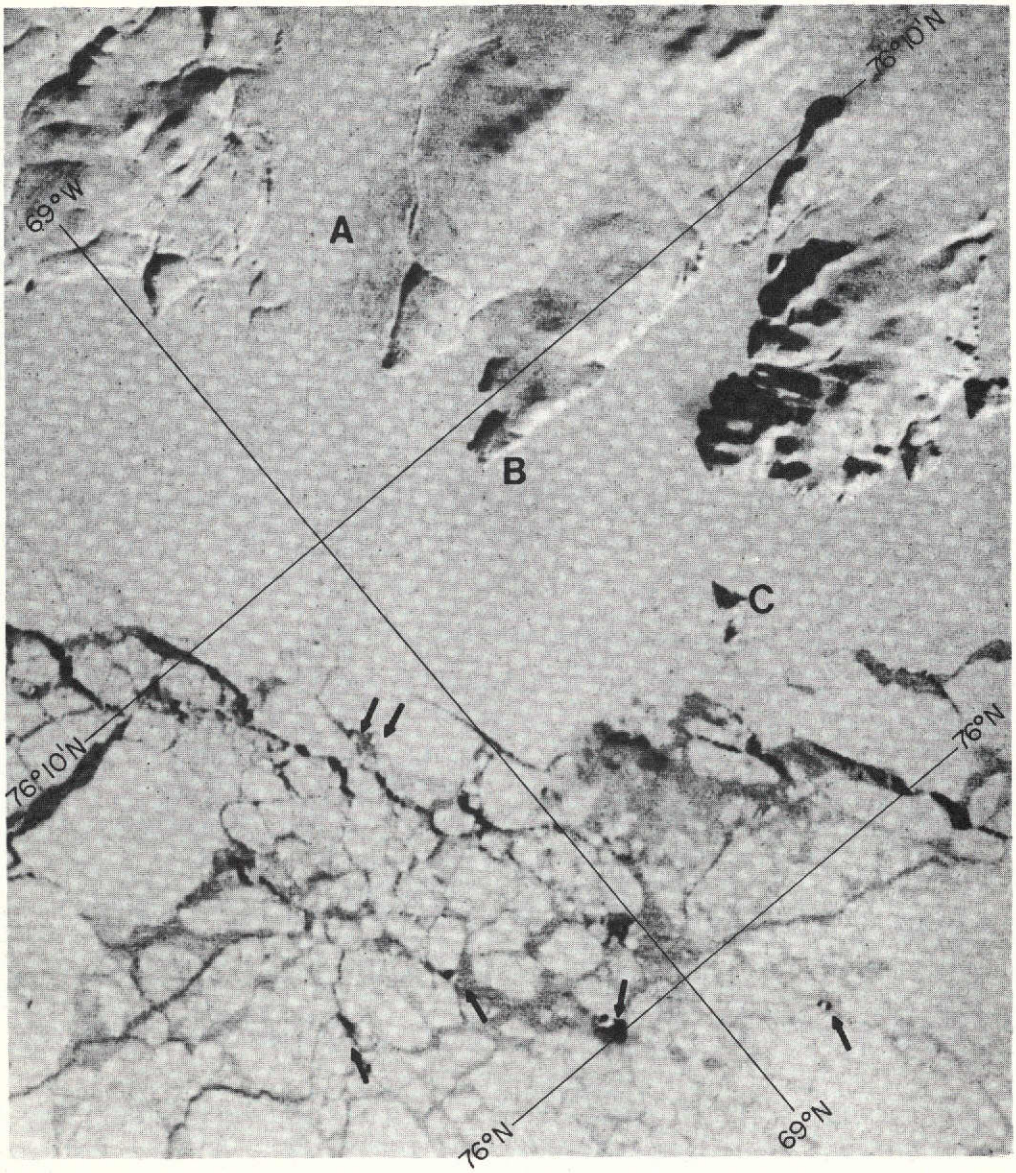

Figure 3-6 Portion of ERTS-1 MSS-7 image (ID No. 1244-17032), 24 March 1973, showing icebergs floating in the pack ice in Melville Bay, west coast of Greenland. The positions of icebergs are indicated by arrows. Land features include Petowik Gletscher (A), Cape Dudley Digges (B), and Conical Klippe (C). The area covered in this image is approximately 32 km across.

4. IDENTIFICATION OF ICE SURFACE CHARACTERISTICS AND ICE TYPES THROUGH MULTISPECTRAL ANALYSIS

4.1 Ice Surface Characteristics

The discussion in Section 3.2 indicates that sea ice can be detected in all of the MSS spectral bands because of its high reflectance as compared to that of open water. The distinct contrast between ice and water even in the near-IR (MSS-7) spectral band is seen in Figure 3-4. In certain instances, however, areas that have a high reflectance in the visible band, and, thus, are deduced to be ice covered, have a very low reflectance in the near-IR band. A striking example is given in Figure 4-1 (a and b), in which Crozier Channel and Kellett Strait between Prince Patrick and Melville Islands are viewed in mid-June 1973 (see map, Figure 2-2). In the near-IR image some ice covered areas appear nearly black, having a much lower reflectance than that of the surrounding land areas.

Differences in the reflectance of ice in the visible and near-IR bands in some of the initial data returned by ERTS-1 in late July 1972 was reported by McClain (1972). Previously, differences in the reflectance of ice and snow surfaces had been observed in visible and near-IR data from the Nimbus-3 satellite (Strong, et al, 1971). These investigations attribute the differing reflectances to the existance of meltwater on the ice or snow surface. As pointed out by McClain, even a thin film of water on the ice can cause a sharp drop in reflectance in the near-IR portion of the spectrum, whereas in the visible the reflectance does not change significantly.

At the time of the observation shown in Figure 4-1, daytime temperatures at Mould Bay, located on Prince Patrick Island are reported to be well above freezing, so that the snow cover on the ice would be melting. As a result, the ice in M'Clure Strait appears in a "mottled" pattern in the MSS-7 image, indicative of puddles and drainage channels. Further to the north, the ice appears uniformly black, indicative of an extensive covering of meltwater; Canadian ice observers who have overflown this region report that during the summer the ice in many of the bays and inlets becomes completely covered with a layer of meltwater.

In the near-IR image shown in Figure 4-1b, the areas that appear in a nearly continuous dark tone are seen to be interlaced with bright linear

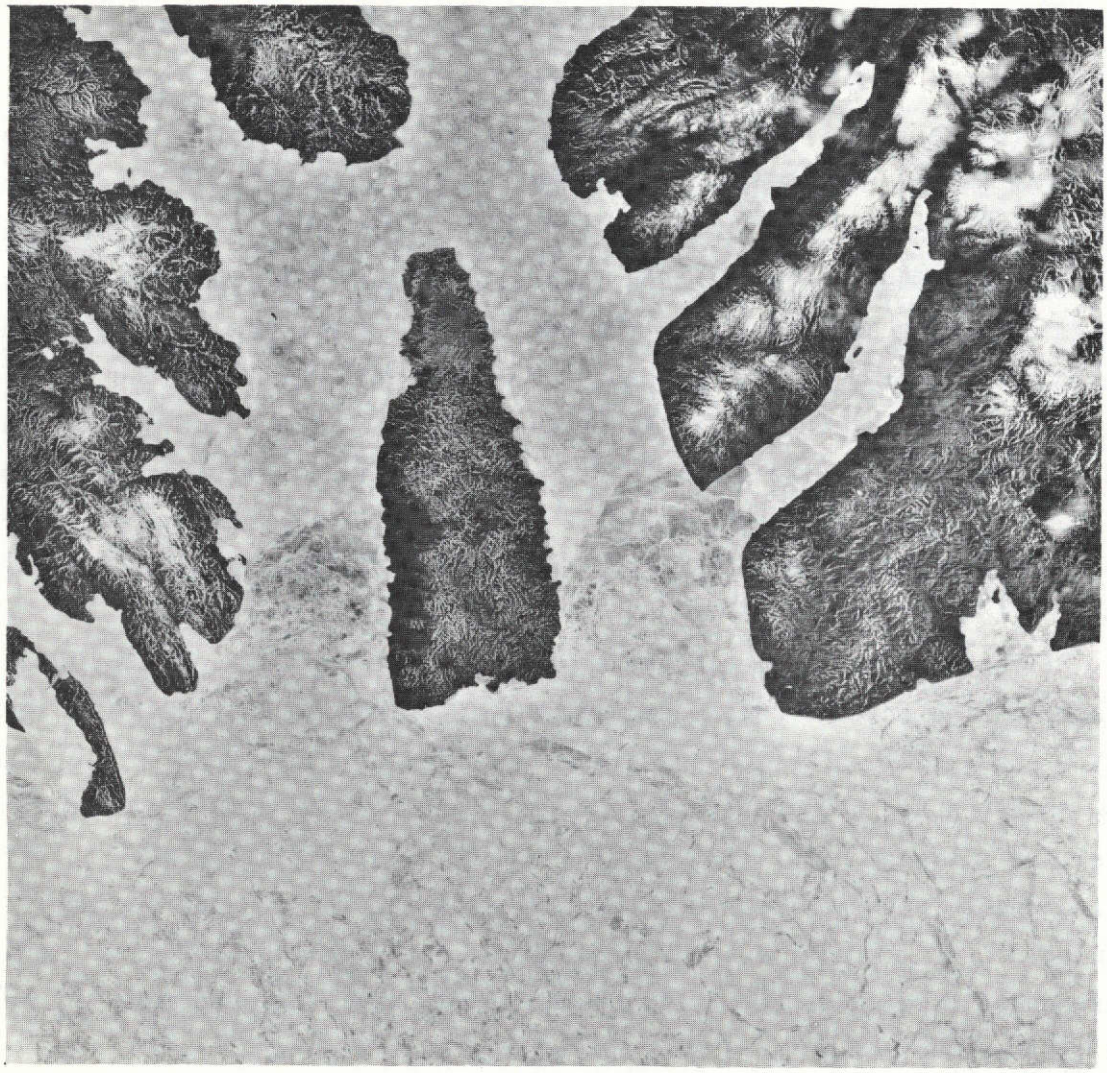

Figure 4-1a ERTS-1 MSS-4 visible band image (ID No. 1330-20064), 18 June 1973, showing ice in Crozier Channel and Kellett Strait just north of M'Clure Strait. Prince Patrick Island is at the left, Melville Island at the right, and Eglinton Island in the center.

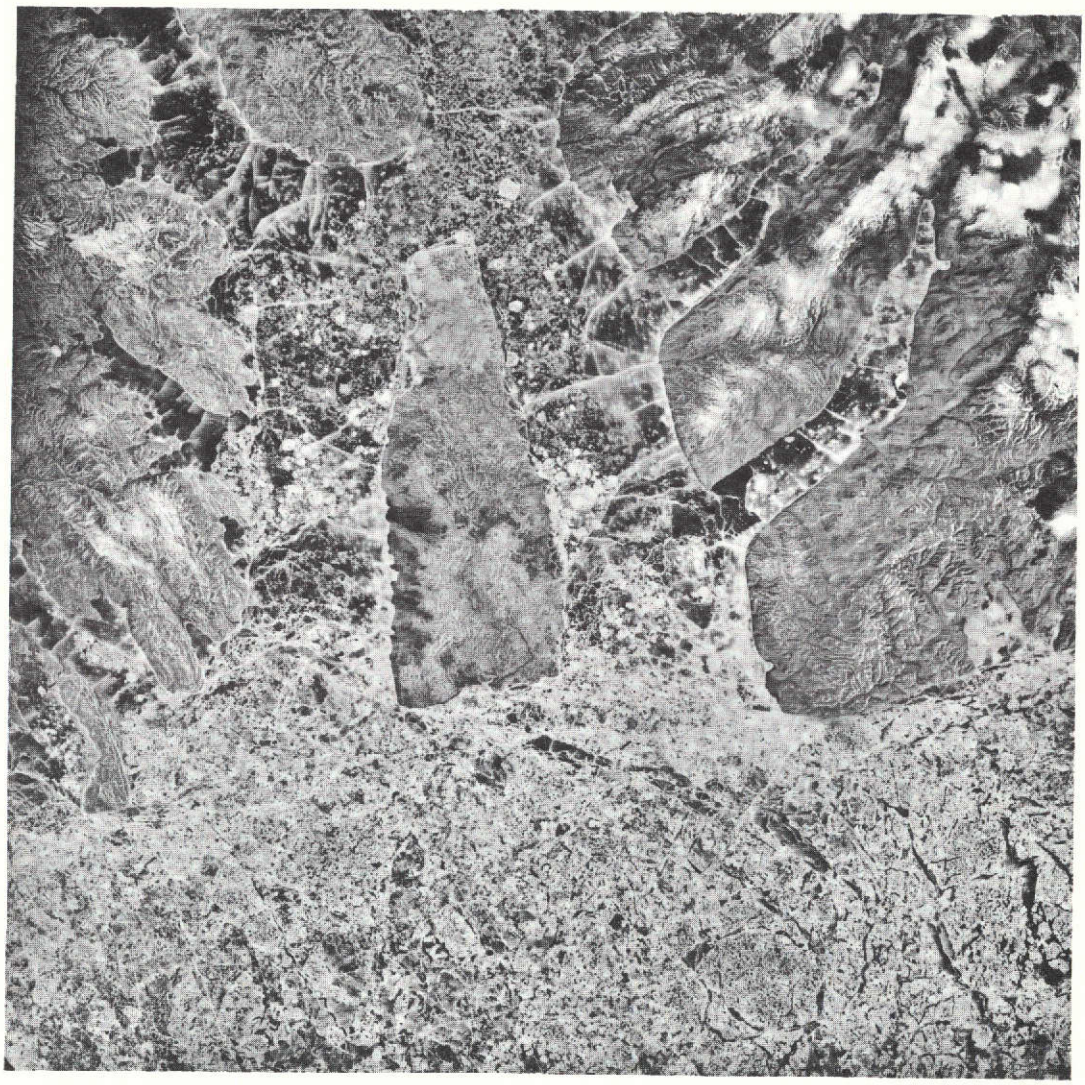

Figure 4-1b ERTS-1 MSS-7 near-IR band image, same scene as shown in Figure 4-1a. Note the decreased reflectance of much of the ice as compared to the visible band image. The dark patterns are related to melt water on the ice surface.

features and numerous bright spots. Similar linear features, many of which are in the same exact locations, can be detected in imagery from the previous summer, as well. The interpretation of these patterns is that leads or cracks too small to be resolved by the satellite have permitted the water on the sea surface to drain away; in the vicinity of the cracks, which develop in preferred locations from year to year, the ice becomes drier once again, and the reflectance in the near-IR increases. In fact, in M'Clure Strait as well as in other areas, imagery from later in the summer has an overall higher reflectance than the earlier imagery. Presumably, this is associated with the drainage of the meltwater, similar action to that which has apparently caused the changes in the surface characteristics of the ice floes shown in Figures 3-4 (a and b).

Cracks, leads, and thaw holes (definitions of ice features are given in the Appendix) can be distinguished from surface meltwater through multispectral analysis, as illustrated in Figure 4-2 (a and b). The visible and near-IR imagery covers the area just to the north of that covered in the previous figure, two days later. The areas in which the ice is covered by meltwater have a low reflectance in the near-IR image, but a relatively high reflectance in the visible image; however, the areas of open water within the pack ice to the west of Prince Patrick Island and the shore polynyas along the immediate west coast of the island have an equally low reflectance in both images.

The complexity of the meltwater patterns on the ice surface is illustrated even better, perhaps, in the near-IR image shown in Figure 4-2b. In the lower part of this image, the bright linear features can be compared with the features seen in the previous image. A particularly interesting ice feature is located in Moore Bay north of Fitzwilliam Strait; the feature is a circular area, about 18 km across, that is distinct in that it appears considerably smoother than the "mottled" ice around it. This same circular feature could also be detected in an image from the previous summer. Aerial reconnaissance reports no ice islands or other unusual ice formations in Moore Bay; it may be, therefore, that this feature is simply a large multi-year floe entrapped in a field of predominantly first-year ice. Extensive ground-truth surveys would be required to verify precisely the ice conditions deduced from ERTS imagery in areas such as this.

4.2 Ice Types

ERTS imagery of the eastern coastal area of Greenland on several dates during September and early October 1972 display wide variations in ice concentrations and apparent ice types, including compacted belts and eddies that apparently result from the combined effects of current flow and surface wind. An example is given in Figure 4-3 (a and b), where the visible and near-IR images covering the area near 77°N on 25 September are shown. In these scenes, the coast of Germania Land and the northern end of Store Koldeway are at the left (see map, Figure 2-3). A shore lead of about 2 km in width exists along the coast, and open water exists south of Germania Land into Dove Bay. An open water area also exists southeast of a giant ice floe (about 25 km across) located near the top of the respective images. This clearing out of the ice is presumed to be primarily the result of a wind flow from the northwest.

A comparison between Figures 4-3a and 4-3b reveals distinct differences in the sea ice characteristics in the two spectral bands. The ice in the eastern part of this scene appears much brighter in the MSS-4 band than in the MSS-7. Closer to the coast, the area of very close and consolidated pack ice has a nearly uniform reflectance in the MSS-4 band, whereas in the MSS-7 band the individual ice floes are distinctly brighter than the surrounding ice. This is particularly evident in the ice adjacent to the shore lead, which appears fairly bright in the MSS-4 band, but is nearly black in the MSS-7 band. Similarly, in the large ice floe near the top of the scene and in several of the smaller floes near the bottom, dark spots in the MSS-7 band are either much lighter or cannot be detected at all in the MSS-4 band.

As discussed above, the differences in reflectance in the visible and near-IR spectral bands are attributed to the existence of meltwater on the ice surface. The imagery shown in Figure 4-3 indicates that certain ice types can also be identified because of a significantly lower reflectance in the near-IR. The areas of low reflectance are identified as brash or rotten ice, where the ice field has become broken into small elements that have some amount of water on and around them. The ice floes which appear distinctly brighter in the MSS-7 band are deduced to be second-year or multi-year ice floes embedded in the first-year and brash ice. These older ice floes have a smoother, more uniform surface topography than first-year ice; also, be-

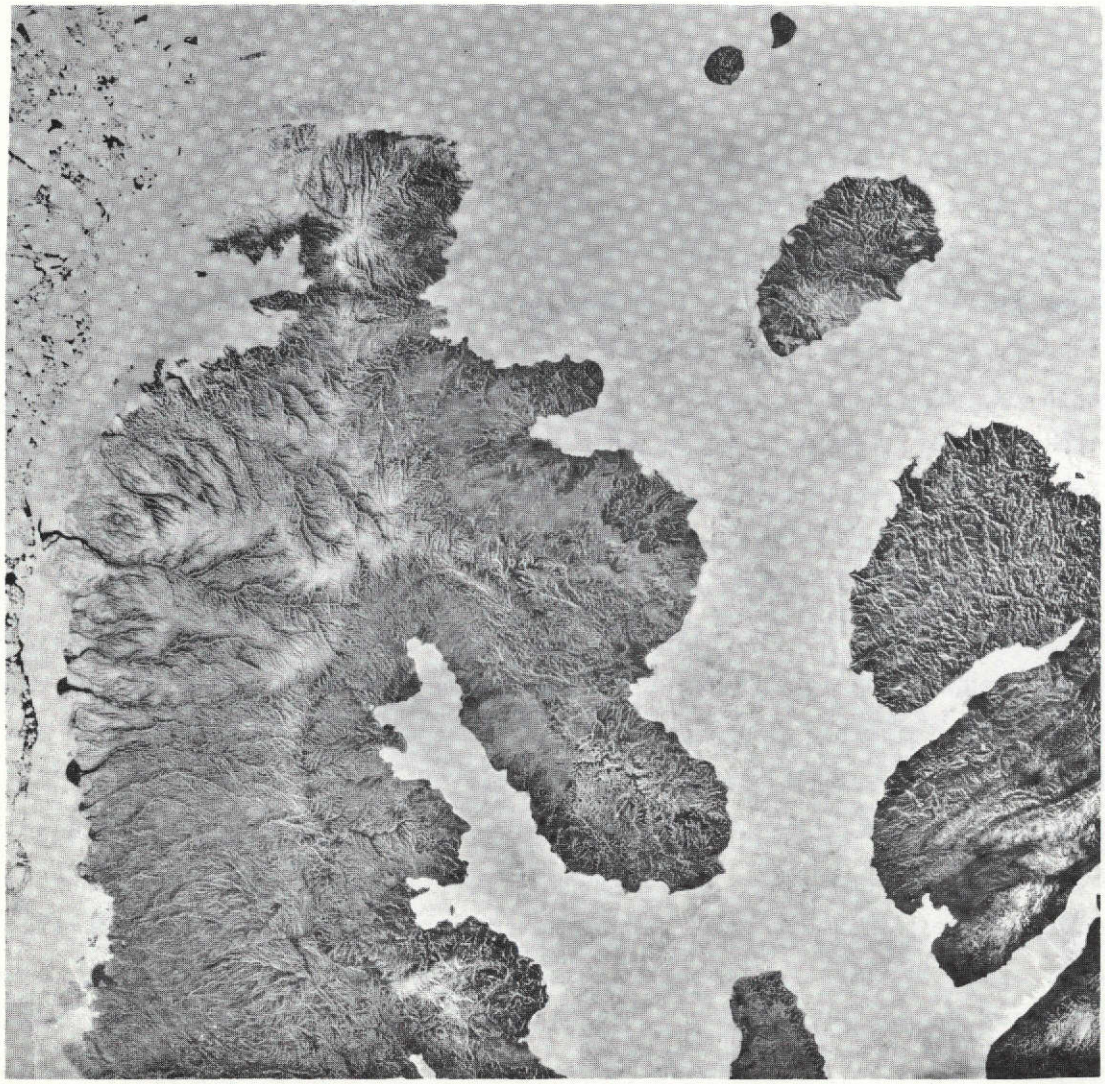

Figure 4-2a ERTS-1 MSS-4 visible band image (ID No. 1332-20174), 20 June 1973, showing ice in area just north of that shown in Figure 4-1. Shore Polynyas and other open water areas can be seen along the west coast of Prince Patrick Island.

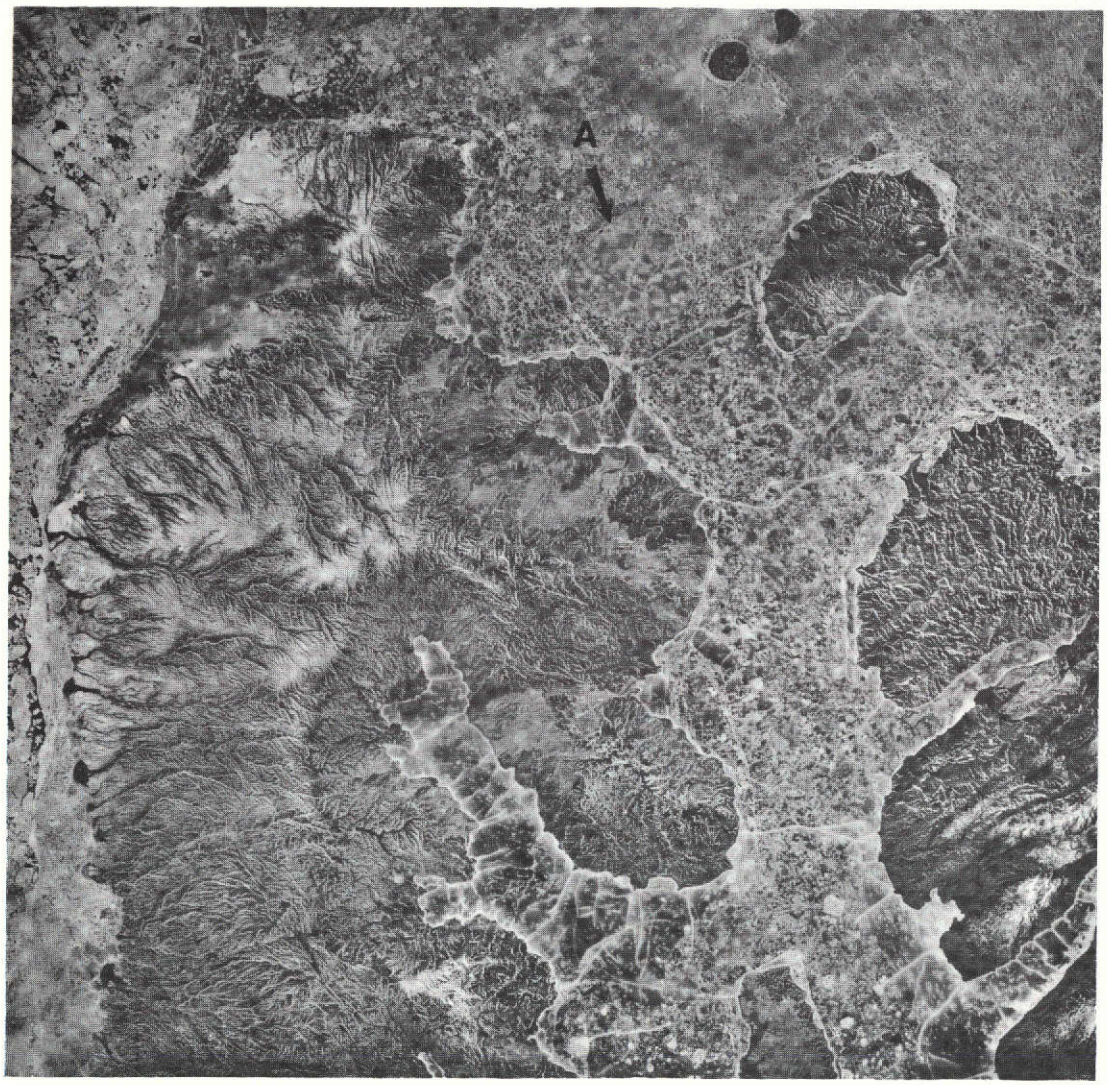

Figure 4-2b ERTS-1 MSS-7 near-IR band image, same scene as shown in Figure 4-2a. Patterns that are black in both the visible and near-IR images are open water, whereas patterns that are dark in the near-IR image but relatively bright in the visible image are related to melt water on the ice surface. The circular ice feature in Moore Bay (A) that cannot be detected in the visible image may be a multi-year floe surrounded by younger ice.

8540

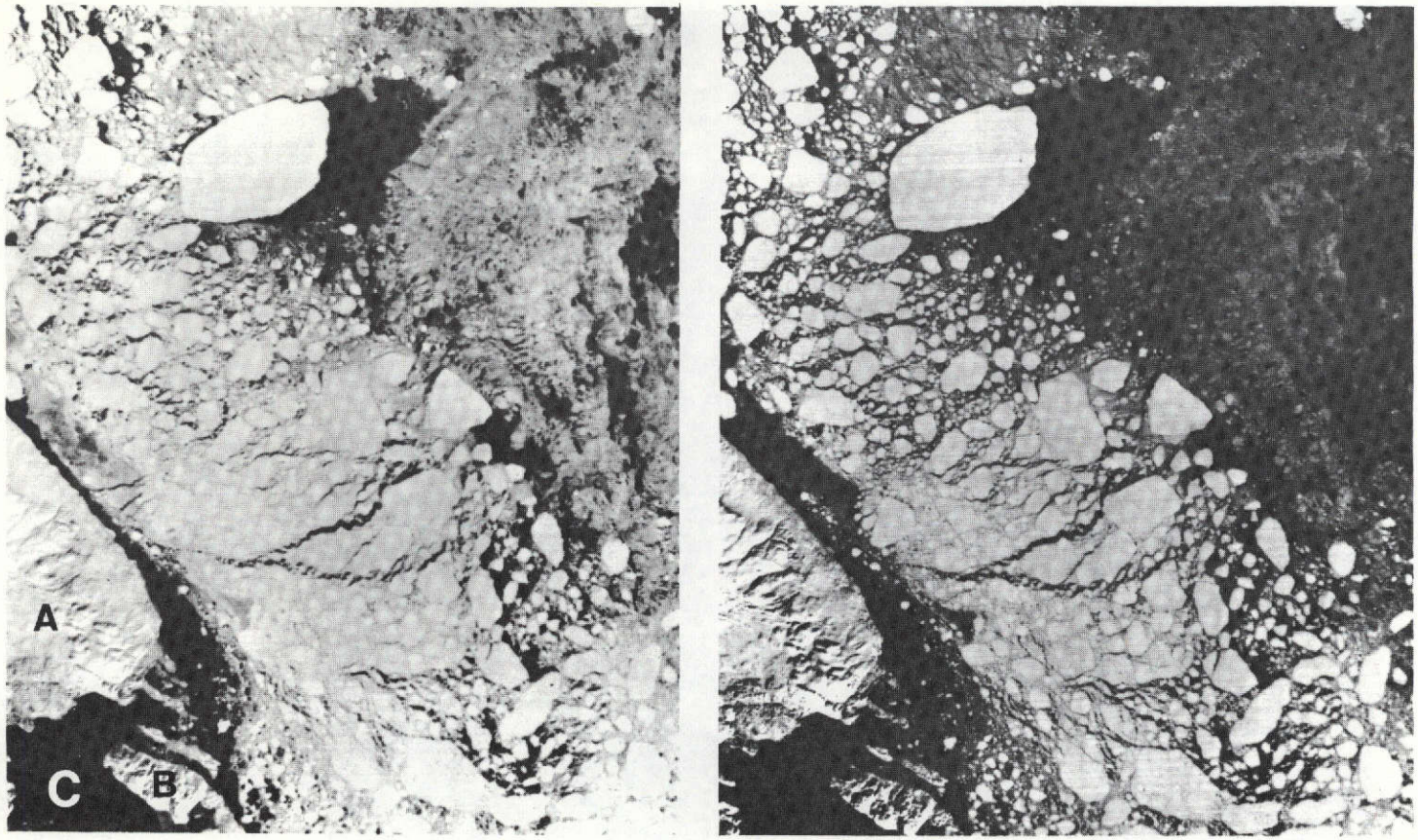

Figure 4-3 ERTS-1 imagery (ID No. 1064-13354), 25 September 1972, showing the east coast of Greenland in the area of Germania Land (A), Store Koldeway (B), and Dove Bay (C). The MSS-4 image is at the left, and the MSS-7 image at the right. Varying reflectances in the visible and near-IR images are related to ice type and ice surface features.

cause they have a much greater thickness (2.5 m to 3.2 m or greater) and are less dense than first-year ice, they stand higher out of the water and have a higher reflectance.

Variations in reflectance, particularly in the near-IR imagery, are also a key to distinguishing forms of new ice (such as grey and grey-white ice) from the older, first-year or multi-year ice. Different ice types can readily be distinguished in Baffin Bay in late March (Figure 4-4). During the early spring most arctic land areas that are visible in ERTS imagery appear to be surrounded by snow covered fast ice, making it difficult to distinguish the land itself from the ice. Moreover, in areas where much open water was observed in the late summer and fall of 1972, compact pack ice (10/10 concentration with no water visible) now exists. Although snow cover also obscures most surface features in the pack ice, the pack ice in most instances can be distinguished from the coastal fast ice because of variations in reflectance within the ice field in contrast to the extremely uniform reflectance of the fast ice. In some areas, flaw leads exist (a flaw lead is defined as a lead separating the pack ice from the fast ice).

In Figure 4-4, a band of fast ice as much as 45 km wide extends along the eastern coast of Baffin Island. The fast ice boundary is marked by a flaw lead, which is narrow in most areas (600-900 m wide) but opens to a width of 18 to 28 km near Henry Kater Peninsula. In the wide portion of the lead, distinct variations in reflectance can be seen. Along the immediate edge of the fast ice, a narrow band of open water exists. Next to the open water is an area of somewhat higher reflectance that is probably representative of newly formed grey ice. Finally, an area of higher reflectance, but still not as bright as either the fast ice or the pack ice, can be seen; this area is believed to consist of somewhat older, grey-white ice. Brighter floes, probably consisting of first-year ice, are embedded in the grey-white ice.

4.3 Land Features

In the ERTS imagery, considerable detail is evident in glaciers located along the east and west coasts of Greenland. Detectable features include moraines and crevassed areas. Of particular interest, is that through the combined analysis of the visible and near-IR data, it is possible to locate the glacial snow line. Several glaciers exhibit a uniform reflectance in

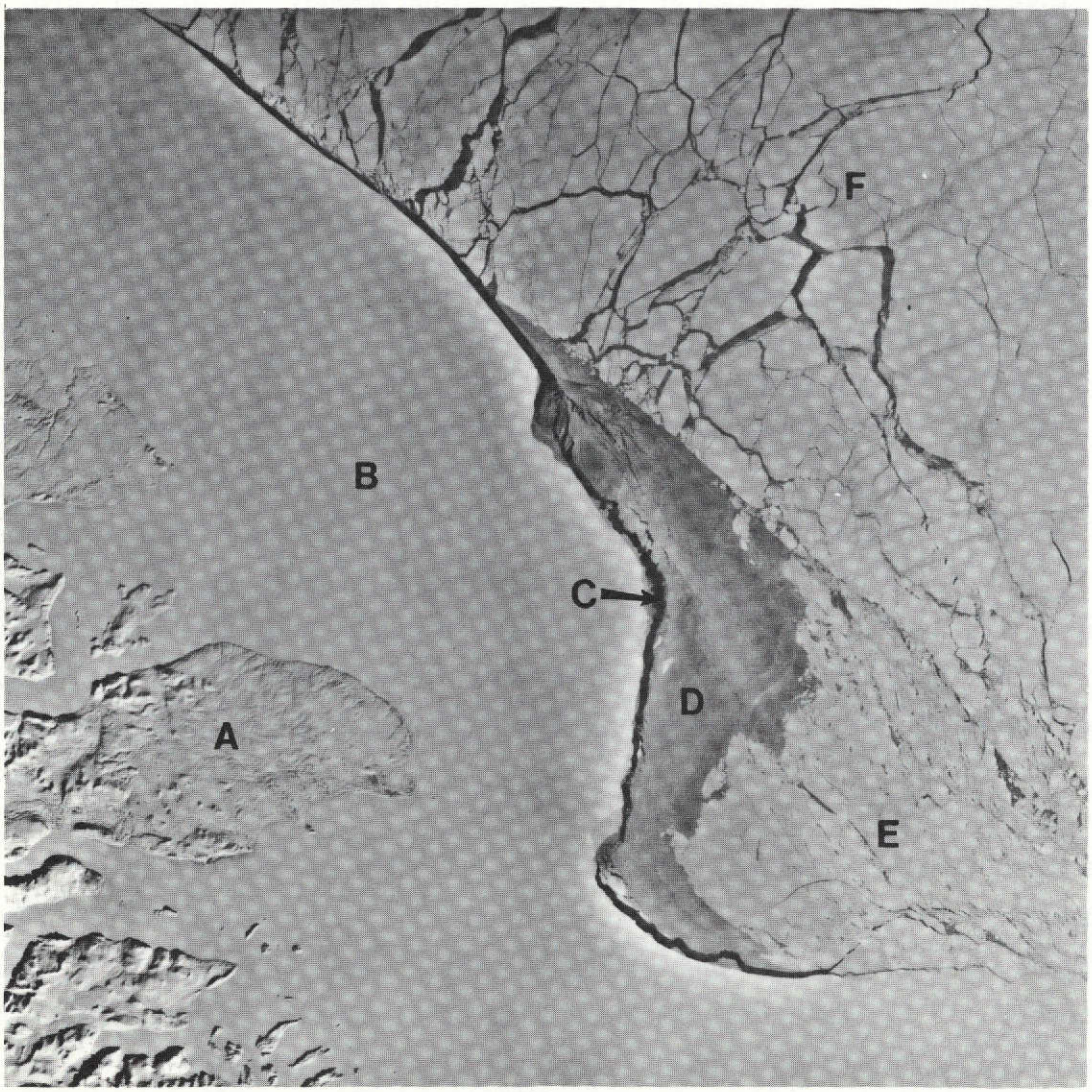

Figure 4-4 ERTS-1 MSS-7 image (ID No. 1248-15453), 28 March 1973, showing western Baffin Bay near Henry Kater Peninsula (A) on Baffin Island. Ice features are as follows: Fast ice (B), flaw lead (C), grey ice (D), grey-white ice (E), and pack ice (F).

the visible band, whereas in the near-IR band the lower elevation portions appear much darker than the higher elevation portions. This difference is attributed to the existence of meltwater on the surface of the glacier at the lower elevations and dry snow cover on the upper glacier.

Examination of land areas also indicates that during times of low sun angle and with a light snow cover on the ground, relatively small-scale terrain features, such as isolated hills, stream valleys, gullies, and ridges are greatly enhanced. The enhancement is particularly evident in the MSS-7 imagery, where large differences in brightness exist between sunlit features and shadows in the low-sun angle imagery. In Figure 4-3, for example, the land features are more distinct in the near-IR than in the visible image.

4.4 Use of Color Composite Imagery

A limited sample of color composite imagery in the positive print format was examined. The quality of most of the prints received from the NDPF, however, was not suitable for displaying ice features. As was the case with some of the black and white products (see Section 3.1), these prints have been exposed to retain the highly reflective snow covered and glacier areas along the east coast of Greenland; at this exposure the less reflective ice features are completely lost.

In the color composite prints, land definition is improved somewhat due to the increased contrast between the "brown" land, the "white" snow and ice, and the "blue" water. In some scenes, clouds appear "whiter" than does the ice, which tends toward the "blue." Thus, color composites may be useful for distinguishing quickly between ice and cloud. In certain scenes, there is also indication that ice floes and areas of fast ice are "whiter" than the surrounding broken ice fields and brash ice.

Overall, the examination of the limited data sample does not indicate any obvious advantages to the use of the color composites for ice detection. It may, of course, be possible to produce more useful color products through experimentation with different tonal combinations. Even with a better product, however, it appears that the use of the more readily available black and white products is sufficient for ice monitoring.

5. COMPARATIVE ANALYSIS BETWEEN ERTS AND AERIAL ICE OBSERVATIONS

5.1 Comparative Analysis with Aerial Ice Observation Charts

For the areas in which aerial ice observations were made nearly concurrent with the ERTS observation, the ice conditions mapped from the ERTS imagery were compared with the conditions indicated on the aerial ice observation charts. In all, some eight useful charts were available for the summer-fall period 1972 and one for the spring 1973. Six of the 1972 ice charts were from the Canadian Ice Forecasting Central and two from the Navy Ice Forecast Office; the spring 1973 chart was from the Canadian Ice Forecasting Central. The ERTS coverage and aerial survey were either one or two days apart in all instances except one, when they were on the same day. It is possible, therefore, that changes in the ice conditions could have taken place during the intervening periods. The results of the comparative analyses are discussed in the following sections.

5.1.1 Hudson Bay: ERTS Imagery for 27 July; Ice Chart for 29 July 1972

The principal ice features observed in northern Hudson Bay during the last week in July are indicated on the chart shown in Figure 5-1. The ERTS imagery for 27 July is shown in Figure 3-3. The aerial observation indicates: (a) A sharp, irregular (bights) ice edge extending southwest of Coats Island with ice-free water to the west; (b) an ice belt south of Southampton Island composed of 3/10's of first-year ice of which 1/10 is medium or larger size floes; (c) an area of open water with less than 1/10 ice concentration south of the ice belt and extending to the ice edge southwest of Coats Island; and (d) an area northwest of Coats Island in Fisher Strait comprised of 5/10's of first-year ice of which 2/10's is medium or larger size floes with ridges and hummocks.

The location of the ice edge extending southwest of Coats Island mapped from the ERTS imagery is also indicated in Figure 5-1; the location is in very close agreement with that mapped by radar two days earlier. Similarly,

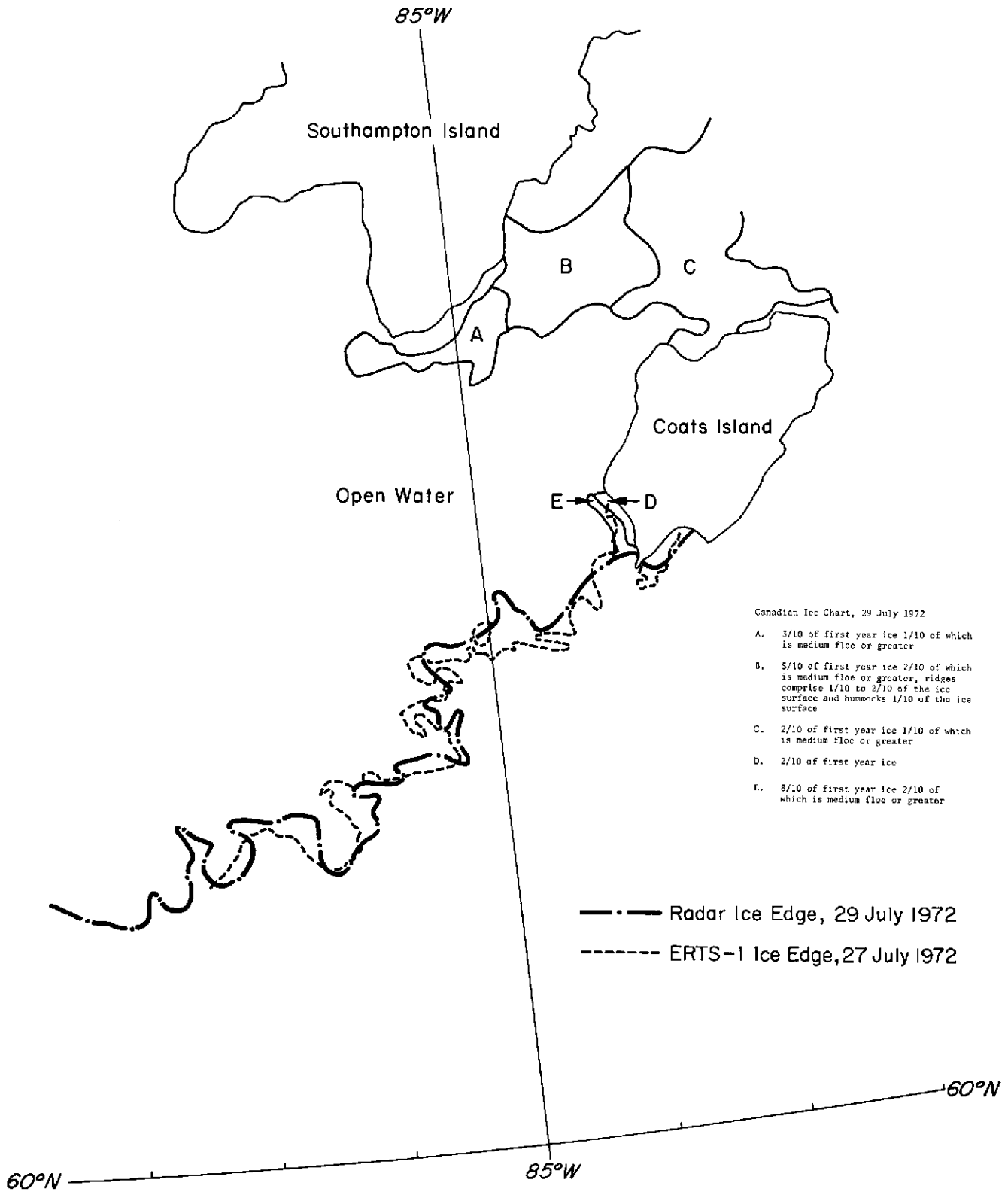

Figure 5-1 Aerial Ice Observation Chart, Northern Hudson Bay, 29 July 1972. ERTS imagery covering this area on 27 July is shown in Figure 3-3.

8072

a comparison between the imagery and the chart reveals that the ice belt south of Southampton Island is located almost exactly where the aerial observer reports it to be. The ice chart indicates that the majority of the floes are smaller than the "medium floe" category (100-500 m across), which also is in good agreement with the ERTS imagery. Surface features (ridges, hummocks, and puddles) that are reported to exist on the "small floes" (20-100 m across) cannot be detected in the ERTS data.

5.1.2 Beaufort Sea Near Alaskan Coast: ERTS Imagery for 7 October; Ice Chart for 7 October 1972

ERTS visible band imagery from a pass crossing the northwest coast of Alaska at Harrison Bay, just west of the Prudhoe Bay area, is shown in Figure 5-2. Ice conditions reported on an aerial observation chart for the same day are shown in Figure 5-3. In the imagery, although some clouds cover the area, much ice can be detected. The pack ice edge is located 80-100 km north of the coast, and is rather broken up consisting of ice strips along the southern limit of the pack. Along the immediate coast, ice can also be detected. Some ice is very bright and is difficult to distinguish from the snow covered land. In Harrison Bay, a well-defined area of ice with a much lower reflectance exists (this ice cannot be detected at all in the near-IR imagery); the low reflectance is indicative of newly formed grey ice.

A comparison between the imagery and the ice conditions reported in Figure 5-3 shows close agreement between the observed pack ice edge and the edge mapped from ERTS. Moreover, in the area where the grey and grey-white ice is detectable, the chart indicates new ice to be forming. Some nilas (new, dark) ice that is charted cannot, however, be positively identified in the imagery.

5.1.3 Eastern Beaufort Sea - Banks Island: ERTS Imagery for 18 June; Ice Chart for 17 June 1973

Of three aerial survey charts for the 1973 spring season received from the Canadian Ice Forecasting Central, only one chart was for an area covered by ERTS imagery on a nearby date. The chart depicts ice conditions in M'Clure Strait and southward along the west coast of Banks Island on 17 June; the corresponding ERTS imagery for the same area is one day later. The ERTS

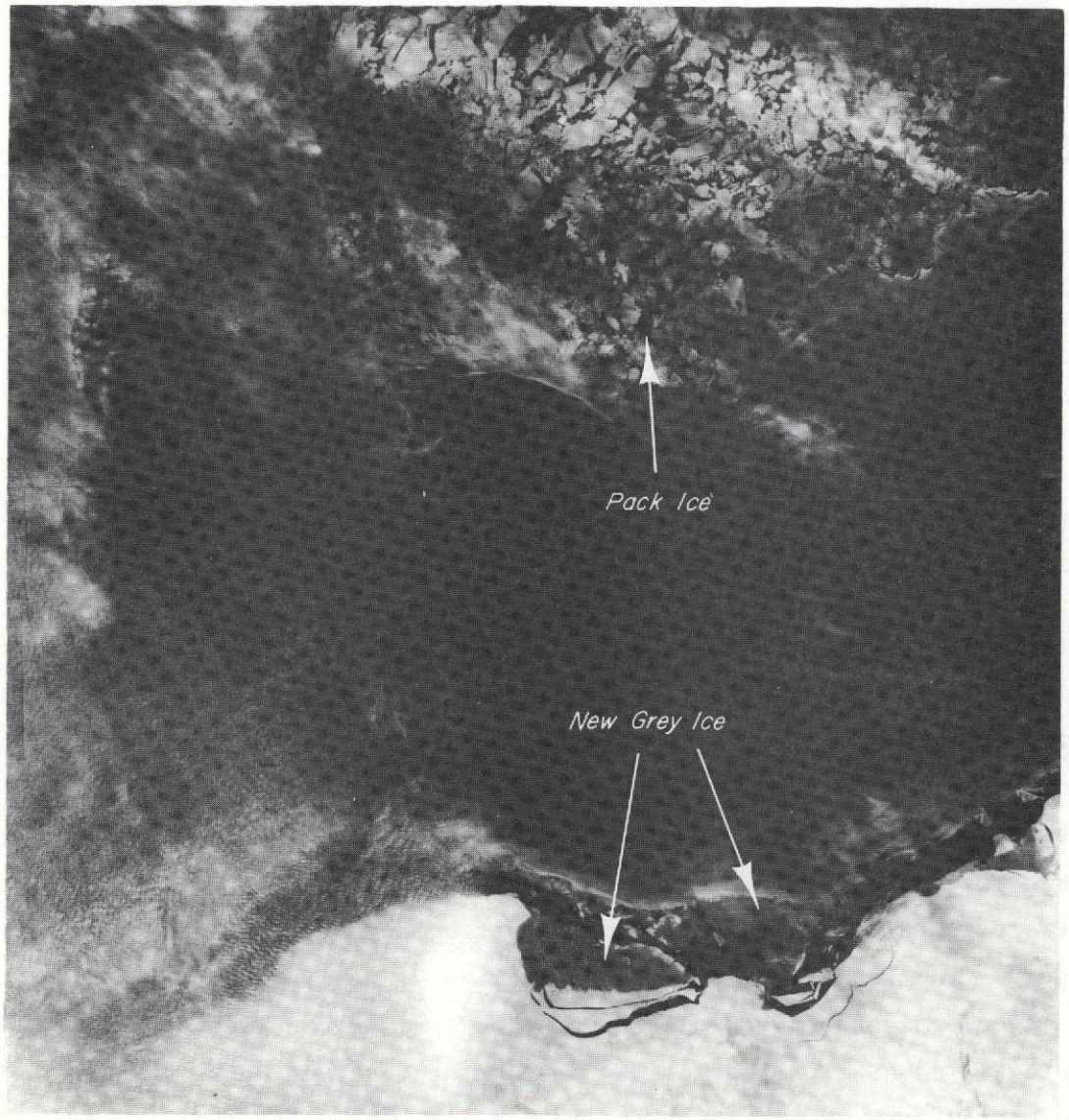

Figure 5-2 ERTS-1 MSS-5 imagery (ID Nos. 1076-21392 and 1076-21394), 7 October 1972, showing northern coast of Alaska at Harrison Bay. Newly formed ice is seen along the immediate coast; the edge of the pack ice is located 80-100 km off the coast.

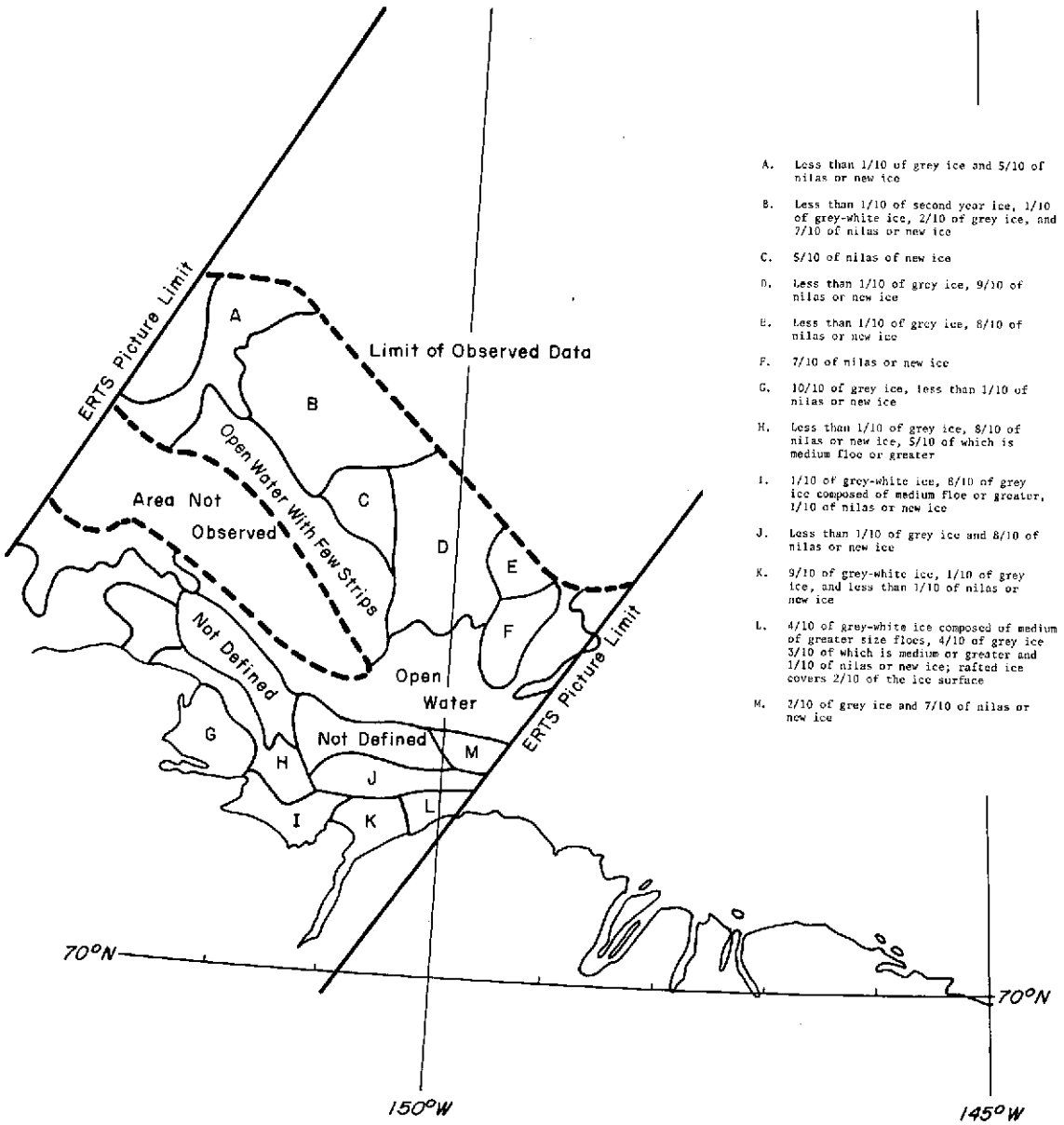

Figure 5-3 Aerial Ice Observation Chart, 7 October 1972, depicting reported ice conditions in the area covered by the image shown in Figure 5-2.

8071

imagery for a part of this area is shown in Figures 5-4a and 5-4b, and the aerial observation chart in Figure 5-5.

The comparative analysis indicates that the edge of the fast ice that extends southward from M'Clure Strait along the west coast of Banks Island is charted from 10 to 30 km farther west than is mapped from the ERTS imagery. The ice edge is very distinct in the ERTS image, and it is doubtful that the fast ice would have moved very much in the one-day interval; in this instance, therefore, the aerial observation seems questionable.

The ice chart reports the age and concentration of the fast ice in M'Clure Strait and along the west coast of Banks Island as 7/10 multi-year ice, and 1/10 first-year ice. The smoother topography of the ice surface and the melt pattern consisting of large interconnecting puddles and a well developed drainage system observed in the ERTS imagery appear to agree with this report in the region of M'Clure Strait; however, the numerous thaw holes and distribution of topographic features observed in the fast ice along the west coast of Banks Island appear more indicative of first year ice (much of the surface meltwater in this area has probably drained through small cracks and thaw holes, the process discussed in Section 4.1). ERTS imagery for late September 1972 had shown ice free conditions extending well to the west of Banks Island, whereas very close pack ice comprised of multi-year or second-year ice floes was observed in M'Clure Strait.

5.1.4 Additional Comparative Analyses

Comparative analyses were conducted for other aerial observation charts, as well. The results of these analyses are discussed briefly in the following paragraphs.

- Beaufort Sea: ERTS Imagery for 2 August; Ice Chart for 29 July 1972

The location of the pack ice boundary and the ice concentrations in various areas mapped from the imagery agrees well with the ice chart. Although various ice surface features are detectable on the larger floes (such as those shown in Figure 3-4a, which are located within the pack just north of the area covered by the aerial observation), hummocks and ridges cannot be identified precisely in the areas where they are reported to exist.

- Beaufort Sea: ERTS Imagery for 8 August; Ice Chart for 7 August 1972

This region was mostly cloud covered on 7 August, so only a small area was charted. Within the charted section, two areas that are reported as 9/10 and 6/10 first-year ice, respectively, appear to be consolidated pack ice in the ERTS data.

- Byam Martin Island and Viscount Melville Sound: ERTS Imagery for 22 August; Ice Chart for 21 August 1972

A radar ice edge reported north of Byam Martin Island is charted about 20-30 miles northwest of the ice edge mapped from the ERTS imagery. However, an open water area along the east coast of Melville Island reported on the chart is in very good agreement with open water mapped from ERTS. In this area, differences in ice age and some reported surface features cannot be detected in the imagery.

- Crozier Channel and M'Clure Strait: ERTS Imagery for 4 September; Ice Chart for 3 September 1972

Ice concentrations are in good agreement, but reported surface features are difficult to distinguish in the ERTS data.

- East Coast of Greenland: ERTS Imagery for 7 October; Ice Chart (Radar Ice Edge Only) for 6 October 1972

The location of the radar ice edge averages about 35 km east of the location of the ice edge mapped from ERTS. However, the ERTS imagery on this date is very dark, and a rather diffuse ice edge appears near the eastern limit of the ERTS coverage; therefore, additional ice patches or ice strips may very well exist farther to the east.

- East Coast of Greenland: ERTS Imagery for 10 October; Ice Chart (Radar Ice Edge Only) for 11 October 1972

As in above case, the radar ice edge is located well to the east of the apparent ice edge in the ERTS imagery.

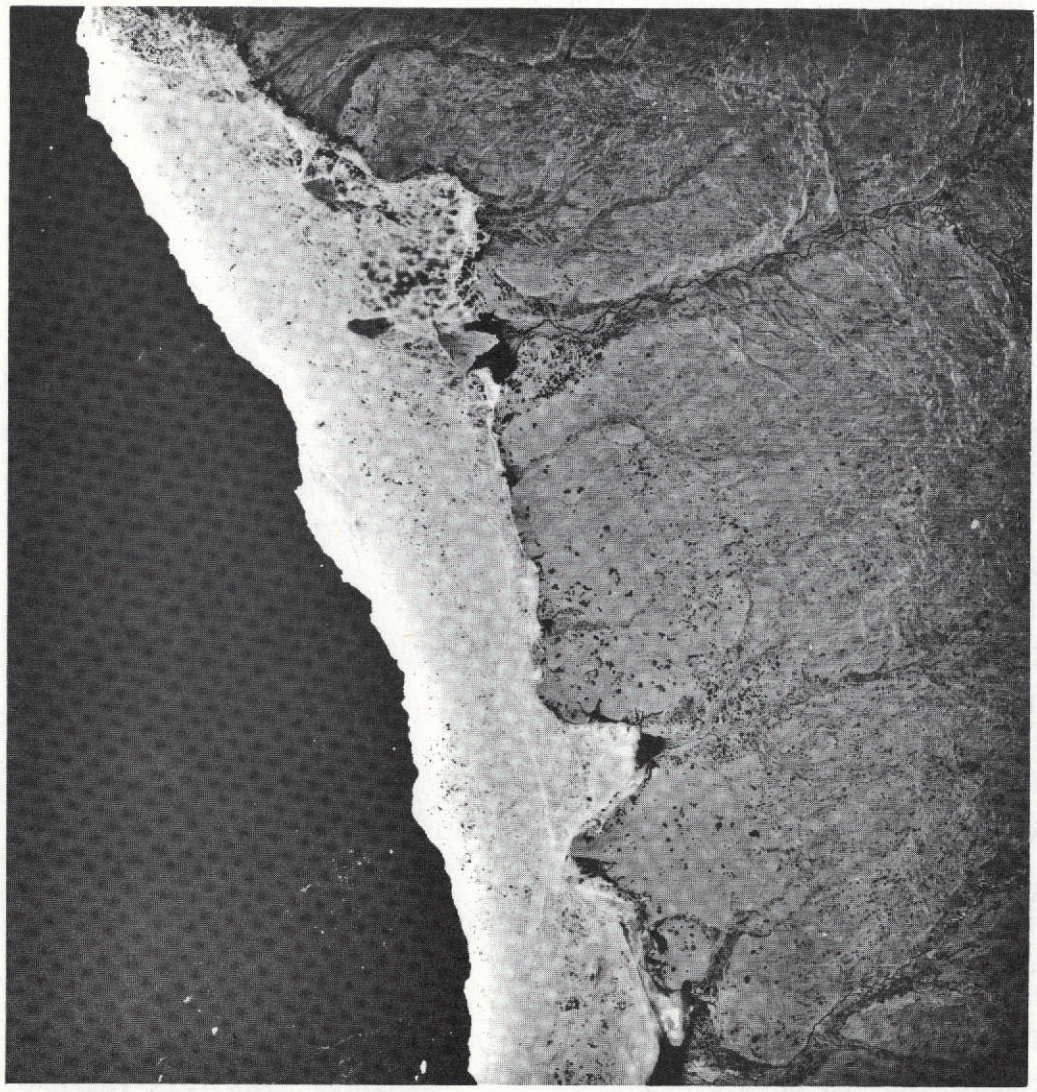

Figure 5-4a ERTS-1 MSS-7 image (ID No. 1330-20073, 18 June 1973, showing fast ice along the west coast of Banks Island.

Figure 5-4b ERTS-1 MSS-7 image (ID No. 1330-20080), 18 June 1973, showing area immediately to the south of the area shown in Figure 5-4a. Fast ice along the coast of Banks Island and ice pack can be seen.

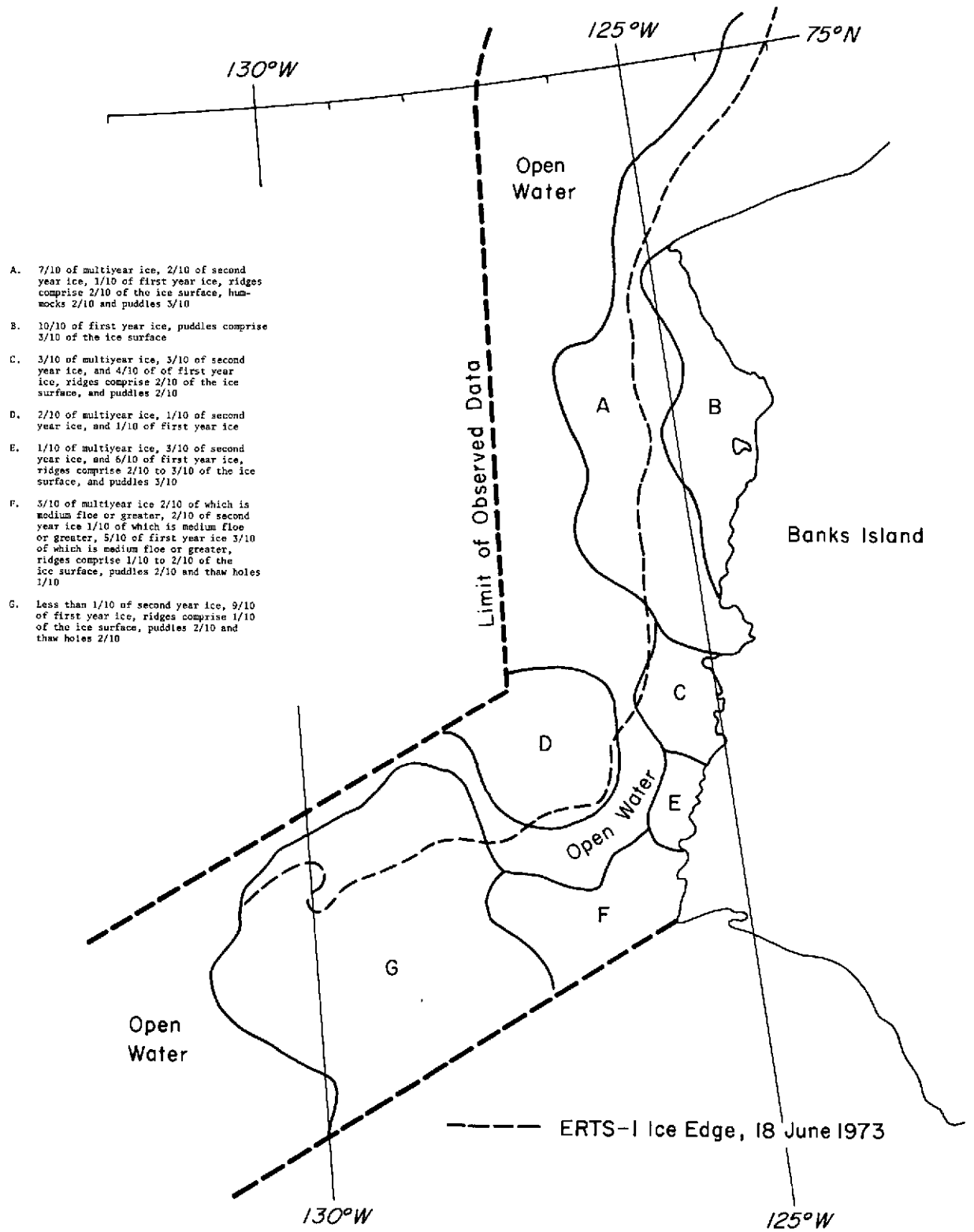

Figure 5-5 Aerial Ice Observation Chart, 17 June 1973, depicting reported ice conditions in the area covered by the images shown in Figures 5-4 (A and B).

5.1.5 Summary of Comparative Analyses with Aerial Observation Charts

In summary, the comparative analysis made to date have shown generally good agreement between the locations of ice edges and ice concentrations as indicated on aerial ice observation charts and as mapped from ERTS imagery. The agreement with two radar ice edges in the Greenland Sea, however, is not as close as is the agreement with most of the ice edges indicated to have been mapped visually. In the spring 1973 case near Banks Island, the apparent discrepancy in the location of the ice edge is difficult to explain because of the particularly well-defined ice features in the ERTS imagery.

Certain ice surface characteristics can be identified through multispectral analysis, as discussed in Section 4.1. It is difficult, however, to identify precisely some of the surface features reported on the charts, since many of the individual features are below the ERTS resolutions. For example, ridges, hummocks, individual puddles and frozen puddles, and rafted ice are not as readily detected in the imagery, although brightness variations can be distinguished on some ice surfaces, thereby suggesting their presence. In the ERTS imagery, younger forms of ice (grey and grey-white ice) are readily distinguished from older forms of ice because of their lower reflectance; also the first-year ice contains brightness variations suggesting the presence of ridges, thaw holes, puddles and hummocks, whereas the young ice appears much more uniform in reflectance. Areas indicated on ice charts to consist of the darker, new or nilas ice are more difficult to detect and may appear to be essentially ice free in the imagery. Also, in areas indicated to consist of mixtures of multi-year, second-year, or first-year ice, differences in reflectance in the ERTS imagery that could be associated with each ice type are not readily apparent.

5.2 Comparative Analysis between ERTS and BESEX Data

5.2.1 Comparative Analysis with Aerial Ice Observations

The Bering Sea Expedition (BESEX), which is described in Section 2, provided a unique opportunity to compare ERTS data with nearly concurrent aerial observations and aircraft photography. ERTS imagery for each of the four passes for which data were available during the BESEX period were acquired (the satellite was not programmed to collect data on any of the other

passes that crossed the Bering Sea during the mid-February to mid-March period). On two dates, 27 and 28 February, the ERTS passes crossed the easternmost part of the Bering Sea in the Nunivak Island area. On 6 and 7 March, the passes crossed St. Lawrence Island and the prime BESEX area of interest (see map, Figure 2-4). For each pass mosaics were prepared from the MSS-5 and MSS-7 data, and the geographic gridding was carefully checked using land features as a guide. For selected scenes enlarged prints (scale of 1:500,000) were processed. Imagery for 6 March and 28 February is shown in Figures 5-6 and 5-7, respectively.

Through reference to the CV-990 Navigational Flight Data it was possible to plot the segments of the flight paths that crossed the areas of the ERTS images. On 5 March an ice mosaic flight was conducted, and on 7 March an ocean roughness flight took place. Although the first flight was a day earlier than the ERTS data, two segments of the flight path did cross the area of ERTS coverage in the vicinity of St. Lawrence Island. On 7 March, much of the flight path was near the ice edge well south of St. Lawrence, where considerable cloud cover is evident in the ERTS imagery. The final leg of the flight, however, did pass just south of the island in an area that seems to be essentially cloud free. On 28 February a very small segment of the inbound leg of the flight crossed the area of ERTS coverage near Nunivak Island. On the 27th, the flight path was entirely north and west of the area shown in the ERTS imagery.

In the ERTS imagery of 6 March (Figure 5-6), an area of low reflectance, indicative of grey ice, extends southward from St. Lawrence Island. Along the immediate south coast of the island, a band of apparent open water exists. Over the open water, small streaks of stratus cloud can be seen; the ice to the south, however, appears to be cloud free. To the north and to the southeast of St. Lawrence, brighter ice floes exist surrounded by the grey ice. Numerous fractures and leads cut through the bright (first-year and multi-year) ice and the surrounding grey ice. Differences between the grey ice and the older ice are especially noticeable in the MSS-7 imagery.

The commentary by the ice observer onboard the CV-990, given in the Navigational Flight Data report, is in remarkably good agreement with the ice conditions deduced from the ERTS data, even though the flight is a day earlier. To the north of St. Lawrence the observer reports generally 80% first-year and multi-year ice and 20% grey ice. Where the observer reports

simple shearing leads, leads are detectable in the imagery. Also, the north coast of the island is reported as having heavily compacted ice; in the imagery, the ice in that area does appear solid, quite different from the ice south of the island.

As the flight approaches the western end of St. Lawrence Island the commentary indicates that the amount of first-year and multi-year ice is decreasing and that the ice ahead is mostly grey ice; the location of the ice boundary separating these different ice types in the ERTS imagery corresponds almost exactly with the location when the above comment was made. After crossing the island, the observer reports all grey ice a few days old, some of which has undergone deformation in the form of stretching to the southwest. This observation confirms the ice type deduced from the ERTS data; furthermore, leads indicative of stretching of the ice can be seen in the imagery.

The ice conditions displayed in the ERTS imagery on 7 March (not shown) are very similar to those of the previous day. On the 7th, however, the stratus streaks have increased, obscuring some of the grey ice south of St. Lawrence Island. Farther south some ice features can be detected, but much cloudiness exists. One segment of the CV-990 flight on this day follows the southern boundary of the grey ice, an area that is cloud free. The observer reports a vast expanse of grey ice, and then reports running into a stratus deck; the comment is made that the "stratus streaks are due to open water along the south shore of St. Lawrence." Thus, this commentary verifies exactly the ice and cloud conditions apparent in the ERTS imagery.

On 28 February (Figure 5-7), the ice conditions near Nunivak Island and along the Alaskan coast are similar to those near St. Lawrence Island on 6 March. Again, it appears that wind action is driving the ice away from the shore, and new grey ice is forming in the coastal areas. In this area, however, the distinct floes, such as are seen southeast of St. Lawrence Island, are not as numerous. On 28 February, although only a small segment of the flight crosses the area of ERTS coverage, open water can be detected near the coast where the observer reports a shore polynya. The observer also reports grey ice in the polynya, which is evident also in the ERTS data. The grey ice has a higher reflectance in the MSS-4 than the MSS-7 imagery; however, near Nunivak Island the distinction between grey and grey-white ice is much better defined in MSS-7 than in the visible band.

Figure 5-6 ERTS-1 MSS-5 imagery (ID Nos. 1226-22171 and 1226-22174), 6 March 1973, showing St. Lawrence Island area in the Bering Sea. Grey ice with numerous shearing leads extends southward from the island; an area of open water with developing stratus cloud streaks lies along the southern coast; first-year and multiyear floes cover the area east and north of the island.

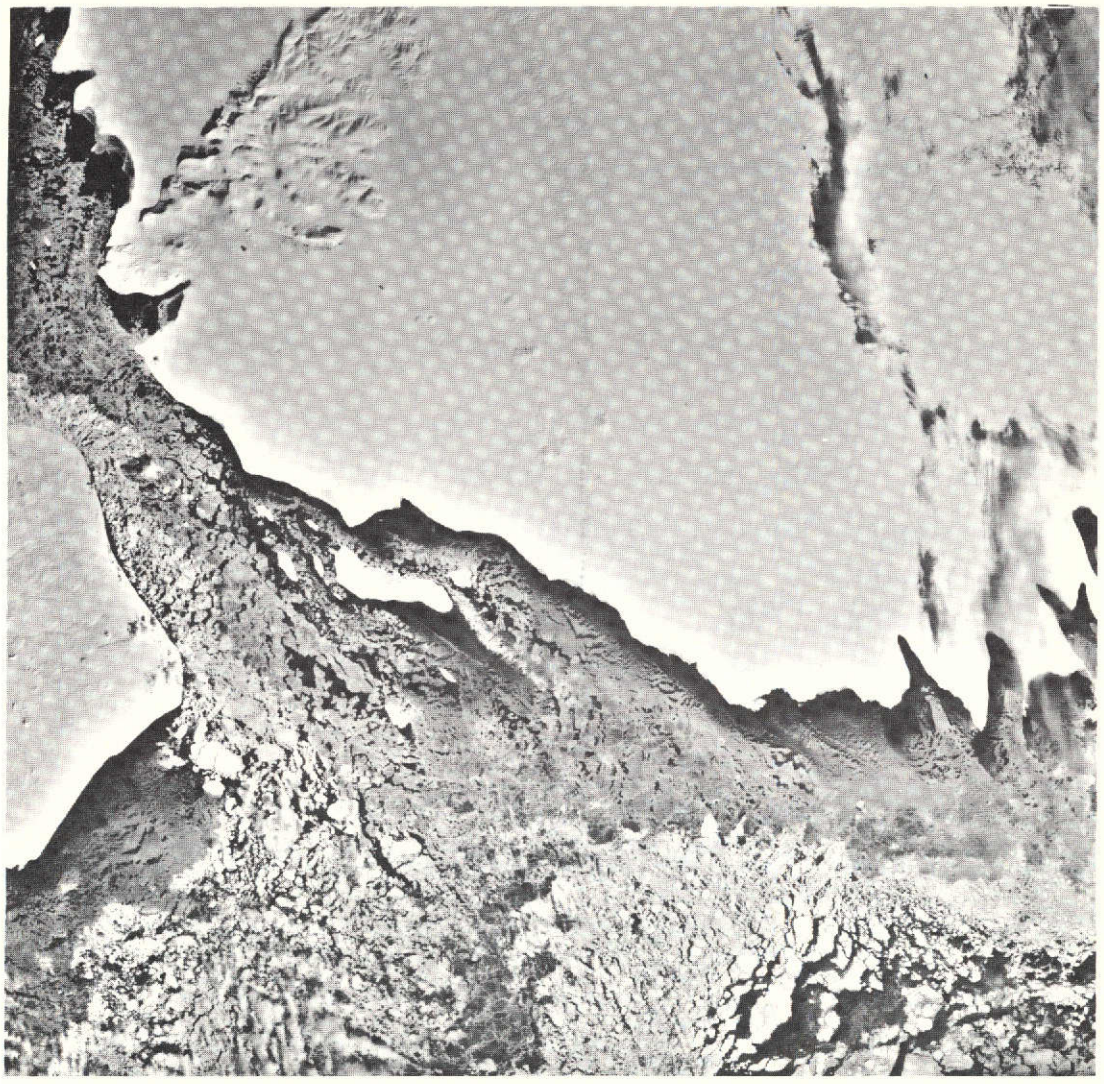

Figure 5-7 ERTS-1 MSS-5 image (ID No. 1220-21440), 28 February 1973, showing Nunivak Island and coast of Alaska. Much of the area is covered with grey and grey-white ice.

Some ice movement can be mapped by comparing the 28 February imagery with that of the previous day (not shown). It appears that the grey-white ice (and some of the first-year ice floes) has moved farther off-shore during the one-day interval. The ice edge does not change its position, however. The ice edge consists of numerous ice belts that appear very bright in both the MSS-5 and MSS-7 imagery. The ice belts likely result from wind and wave action.

5.2.2 Comparative Analysis with Aircraft Photography

Vertical viewing photography from the appropriate cloud-free segments of the CV-990 flights of 28 February - 1 March, 5 March, and 7 March was obtained from NASA/GSFC. The photographs consist of 70 mm positive prints for the earlier flight and 4.5 inch positive prints for the later two flights. The photography from the rather limited cloud-free segment of the 7 March flight was found to be not usable, however, because of difficulties encountered in locating the frames geographically.

Panchromatic Plus-X Aerographic film was used for the aircraft photography; the spectral response of the film is 0.40-0.71 μm. The field of view of the 4.5 inch camera system was ± 35°, providing an areal coverage for an individual frame of about 12.5 by 12.5 km at the altitude flown on the 5 March flight. Although information on the field of view of the 70 mm camera system was not available, the area covered by an individual frame was measured to be 15 x 15 km. Through a measurement of the scales of features detectable in the photographs as compared with those detectable in the corresponding ERTS images, the spatial resolution of the aircraft photographs was determined to be of the order of 5-10 m for the 4.5 inch camera and about 10 m for the 70 mm camera.

Four aerial photographs of inbound Flight No. 9 (1 March, 0308-0311 GMT) cover the area northeast of Nunivak Island in Baird Inlet, which ERTS viewed at 2144GMT, 28 February 1973. An enlarged portion of the ERTS image is shown in Figure 5-8a, and the earliest photograph of the sequence is shown in Figure 5-8b. In the area covered in the photograph, a polynya exists that separates fast ice (first-year, snow covered) from young ice (grey). Also, a narrow band of young ice (grey) approximately 100 m to 1.8 km wide is visible along the edge of the snow covered fast ice. Each of these features can be

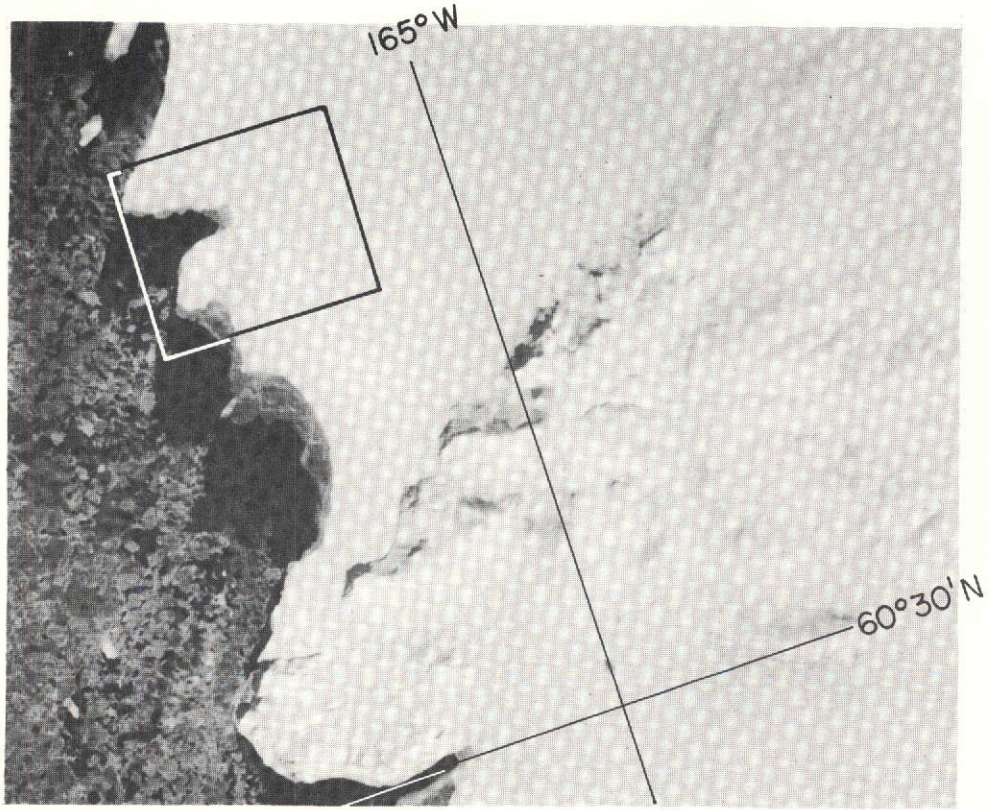

(a)

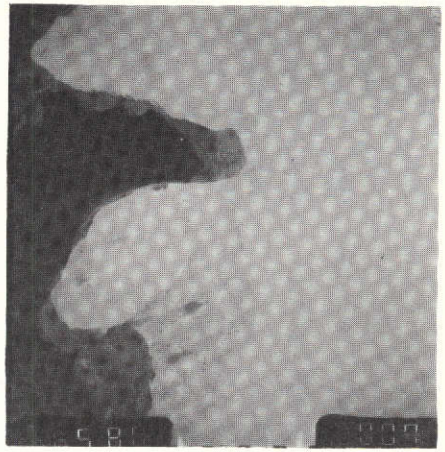

(b)

Figure 5-8 (a) Portion of MSS-5 image for same ERTS scene as shown in Figure 5-7; (b) Aircraft photograph taken a few hours later. The area covered in the photograph is outlined on the ERTS image. The shore polynya and grey ice seen in the photograph can also be detected in the ERTS image.

detected in the enlarged ERTS imagery. The three remaining aerial photographs show only solid fast ice (snow covered) and the coastline of Alaska.

Because of the higher resolution, certain ice features not detectable in the ERTS imagery can be seen in the photographs. For example, in Figure 5-8b, small dark features indicative of cracks or thaw holes can be seen in the band of young ice within the small bay. Although there is an indication of these features in Figure 5-8a, the individual dark spots cannot be distinguished. Also, in the ice to the north of the bay, individual ridges and other small topographic features can be detected because of their shadows. In other photographs (not shown), ridges and hummocks are even more pronounced.

Ice conditions photographed on two segments of Flight No. 12 (5 March, 2117-2130GMT) are in excellent agreement with the ice conditions mapped from the ERTS imagery a day later (6 March, 2217GMT). An enlarged portion of the ERTS image north of St. Lawrence Island is given in Figure 5-9, and the corresponding aircraft photography for this flight segment is given in Figure 5-10. The photography shows numerous first-year and multi-year floes (vast, big, medium and small) embedded in grey and grey-white ice, as well as several fractures. Twenty-four hours later these same vast, big and medium multi-year floes embedded in grey and grey-white ice can be identified in the ERTS enlargement. The small floes, however, are not as readily detected due to the overall brightness variations existing within the grey and grey-white ice. The fractures (approximately 70 to 90 m wide) seen in the photography are not visible in the ERTS imagery, indicating that they may have either closed or refroze during the 24-hour interval. A fracture which did not appear in a vast floe in the aerial photography is visible, however, in the ERTS image; the fact that this fracture is of the scale of those seen in the aircraft photography and is in a floe that can be positively identified indicates that changes have actually taken place in the ice (some fractures closing and others opening) during the 24-hour interval.

Another portion of the ERTS image is given in Figure 5-11 and the corresponding swath of aircraft photographs in Figure 5-12. This segment of aerial photographs shows young fast ice (grey and grey-white) 200 m to 1.4 km in width along the west coast of St. Lawrence Island. Pack ice off the southwest coast comprised of young (grey) ice is also visible. These same features are readily detectable in the ERTS image.

The availability of the BESEX data provides an opportunity to discuss the relative merits of the ERTS-1 and aircraft spatial resolutions. As stated above, the resolution of the aircraft photography is of the order of 10 m as compared to 70 m for ERTS. At the 10 m resolution, certain small scale ice features that are not visible in the ERTS imagery can be detected; these features include individual ridges, hummocks, and thaw holes. The comparative analysis does indicate, however, that essentially all of the significant ice features and different ice types can be detected by ERTS, as well.

The field of view of the aircraft camera is much smaller than that of ERTS, such that more than 100 photographs are needed to cover the area of a single ERTS scene. Furthermore, the multispectral ERTS data provide considerable information on ice type and on ice surface characteristics associated with meltwater. It is doubtful that at the ERTS resolution this information could be derived from the broad-spectral band film. When the respective fields of view are taken into account, the number of aircraft photographs needed to provide multispectral data for the area covered by a single ERTS scene becomes prohibitive. Thus, because of the expanse of sea ice that must be surveyed and the amount of information that can be derived from multispectral data, it does not appear worth the expense to furnish resolution comparable to the aircraft photography from a satellite system.

Figure 5-9 Portion of MSS-7 image for same ERTS scene as shown in Figure 5-6. The area viewed is just north of St. Lawrence Island; the area covered by the aircraft photography shown in Figure 5-10 is outlined, and certain ice floes are identified by letter.

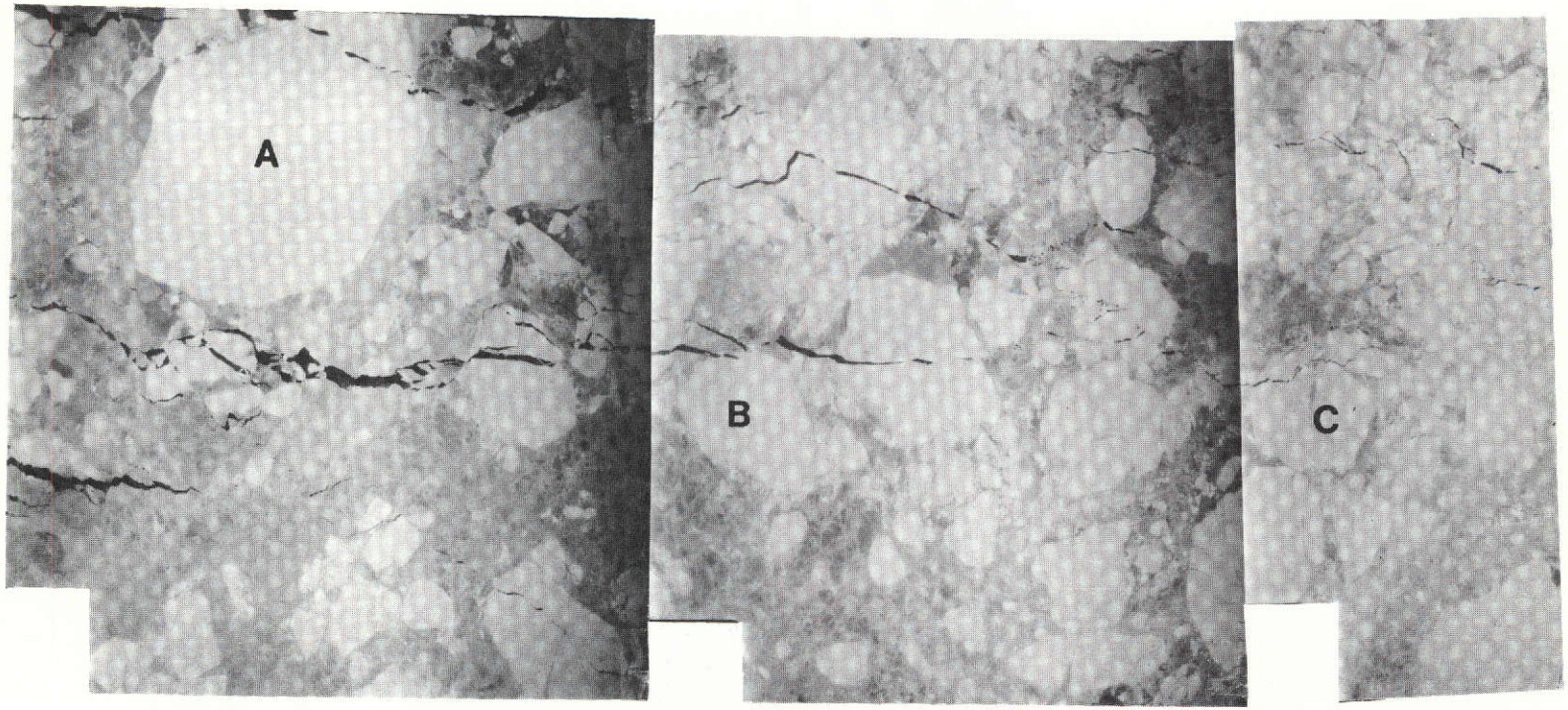

Figure 5-10 Aircraft photography covering the area outlined in Figure 5-9, taken one day earlier. The ice floes indicated by letter can be identified in Figure 5-9, as well. Many other ice features seen in the photography can also be detected in the ERTS imagery.

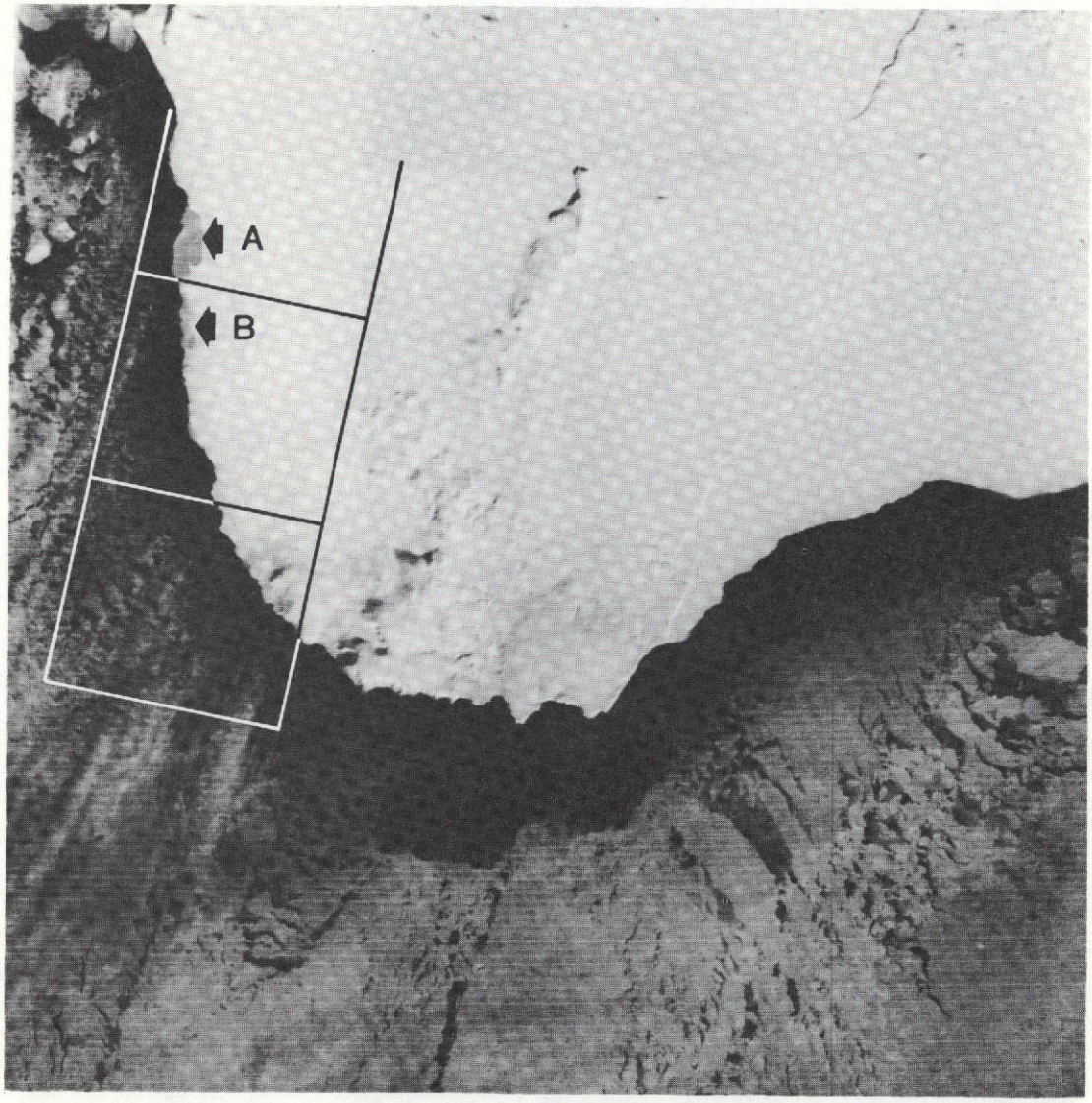

Figure 5-11 Portion of MSS-7 image for same scene as shown in Figure 5-6. The area viewed is the southwest coast of St. Lawrence Island. The area covered by the aircraft photography shown in Figure 5-12 is outlined, and areas of newly formed grey ice are indicated by letter.

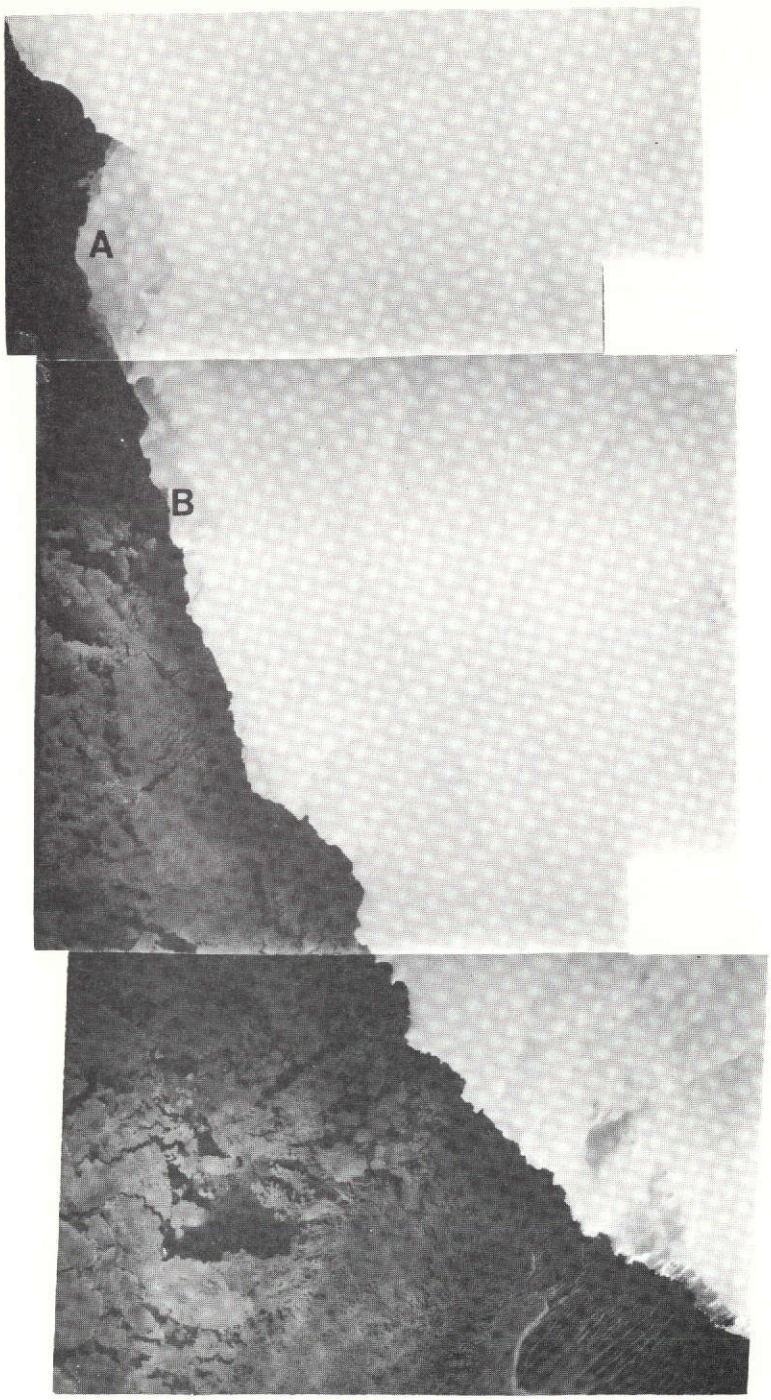

Figure 5-12 Aircraft photography covering the area outlined in Figure 5-11, taken one day earlier. The areas of newly formed grey ice indicated by letter can also be identified in the ERTS image.

8537

6. SEQUENTIAL ICE OBSERVATIONS

6.1 Synoptic-Scale Ice Deformation

Because of the repetitive coverage possible at high latitudes, ERTS is a powerful tool for collecting sequential, synoptic scale ice observations; such data are an important requirement for input to numerical ice models. In addition, other investigators have shown that ERTS imagery can be used to obtain quantitative measurements of mesoscale ice deformation (Crowder, et al, 1973). Selected examples of synoptic-scale ice deformations mapped from sequential ERTS observations are presented in the following sections; these sequential observations are but a few of the total data sample examined in only the initial few months of the operation of ERTS-1.

6.1.1 M'Clure Strait

Images from the near-IR spectral band (MSS-7) for two ERTS passes crossing the M'Clure Strait area, including parts of Prince Patrick, Eglinton, and Melville Islands to the north and Banks Island to the south, are shown in Figures 6-1 and 6-2. These data indicate that significant changes in the ice conditions in M'Clure Strait have occurred during the five-week interval between the time of the first pass, 29 July, and the second, 4 September. On the earlier date, fast ice exists along the northern coast of Banks Island; shore leads are observed, however, near the mouths of the rivers. Much of M'Clure Strait is covered by fast ice, although at the western end of the strait numerous fractures and leads can be detected. The structure of the ice breakup process seems to be evident in this imagery; fractures extending through the ice between Eglinton Island and Banks Island open into leads farther west and eventually into larger open water areas. Areas of surface melt water are also evident, particularly in Crozier Channel and Kellett Strait. On this date the islands are essentially snow-free, and some cloudiness covers the eastern part of M'Clure Strait and Melville Island. The clouds can easily be distinguished because of their shadows.

Five weeks later (Figure 6-2), the entire ice sheet in M'Clure Strait has broken up. No fast ice is evident, except along Prince Patrick Island and in Crozier Channel and Kellett Strait. Open water exists along the

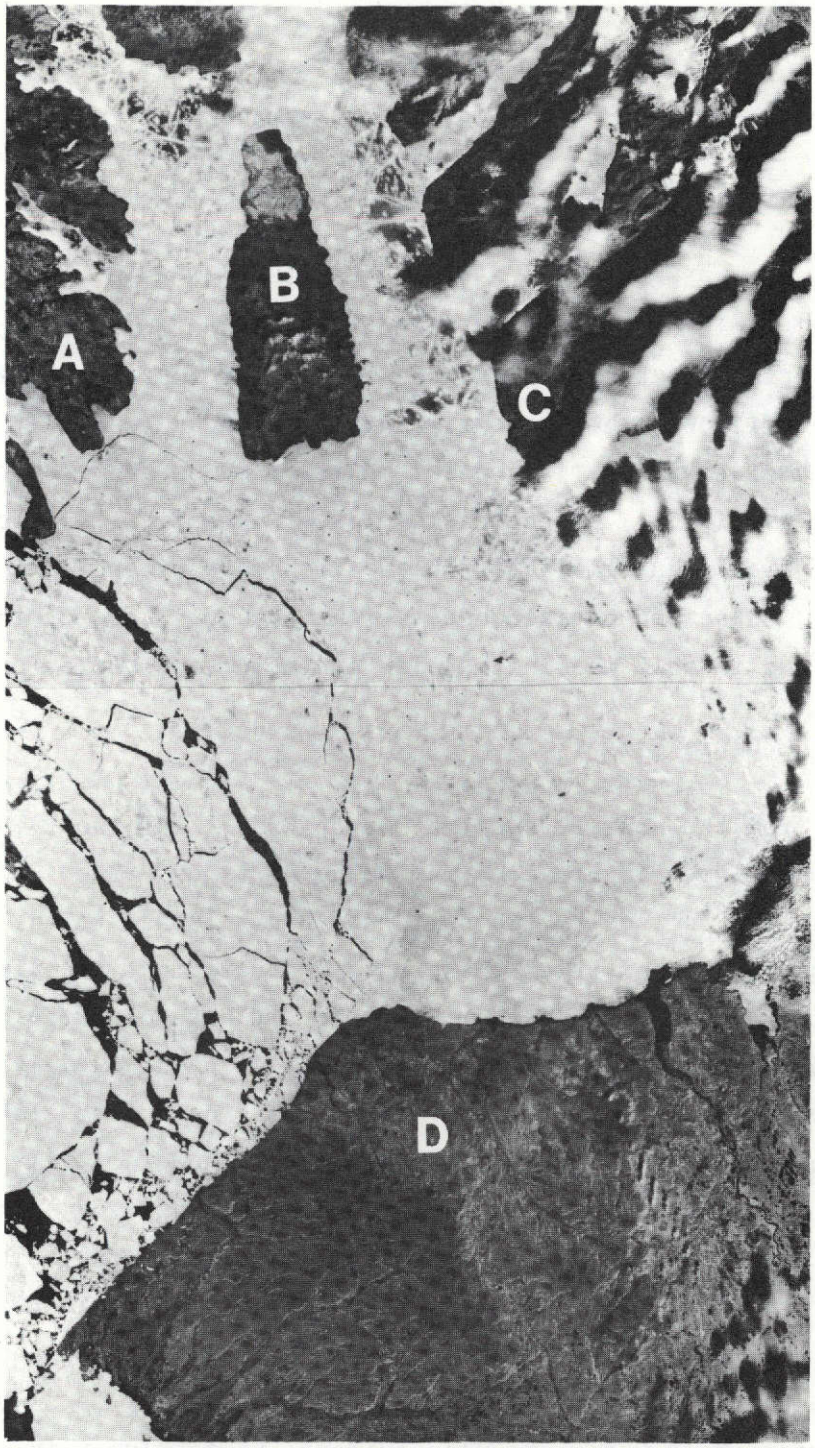

Figure 6-1 ERTS-1 MSS-7 imagery (ID Nos. 1006-20060 and 1006-20062), 29 July 1972, showing M'Clure Strait. Prince Patrick Island (A), Eglinton Island (B), Melville Island (C), Banks Island (D).

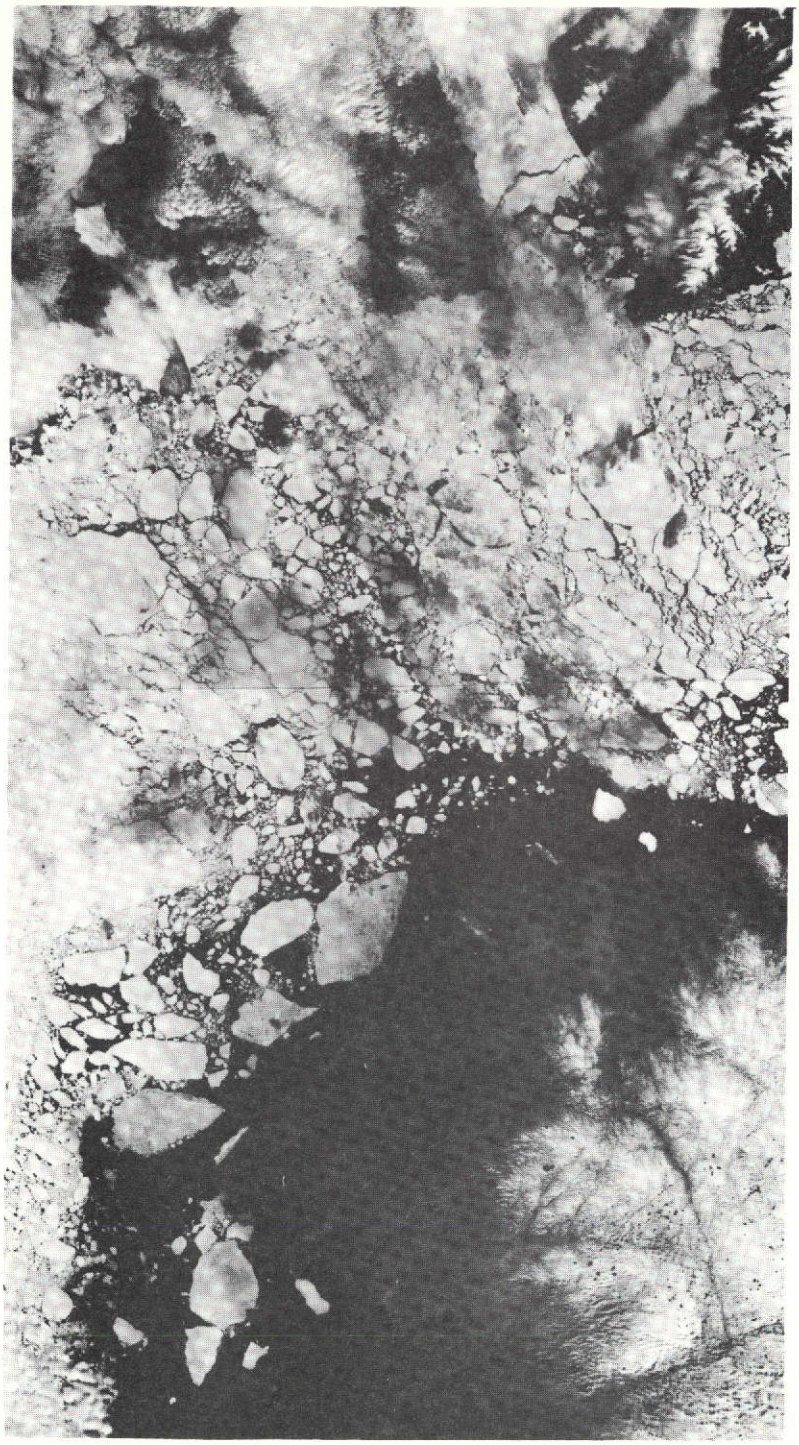

Figure 6-2 ERTS-1 MSS-7 imagery (ID Nos. 1043-20120 and 1043-20122), 4 September 1972, showing same area as in Figure 6-1. Note changes in ice conditions as compared with Figure 6-1, five weeks earlier.

coast of Banks Island, and breaks in the ice can be seen throughout M'Clure Strait. The ice concentration appears to be close (7/10 to 8/10) or very close pack ice (9/10 to less than 10/10), consisting of ice floes surrounded by brash ice; the apparent ice concentrations are verified by the aerial ice observation flight that crossed the area south of Eglinton Island on this date (see Section 5.1). The individual floes are distinctly brighter than the surrounding brash ice in the MSS-7 data. Considerable cloudiness covers the northern part of the area, and cloud shadows can be seen on the ice in M'Clure Strait, even though the clouds themselves are nearly transparent. By this date, a part of Banks Island and the higher terrain of Melville Island have again become snow covered.

6.1.2 Beaufort Sea

As stated in Section 2.2, the majority of the data received during Spring 1973 covers the Beaufort Sea. The individual scenes from several orbital passes were mosaiced, so that in some instances the ERTS coverage extends from coastal Alaska to about 80°N. In the mid-Beaufort Sea, because of the lack of landmarks for checking the geographic gridding of the images, ice movement cannot be measured as precisely as it can near coastal areas. However, it is possible to map relative changes in the ice from day to day and over longer time periods. In many of the mosaics, the entire swath is cloud-free; also, ice features can be detected at times through thin cloud cover.

ERTS imagery from several passes during the period from the first of April through mid-June covering the general area of 72-80°N and 126-150°W has been examined. This area contains compact (10/10) and very close (9/10 to less than 10/10) pack ice, but even in the early April data extensive leads can be seen, some being as much as 180 km or more in extent. In these early spring images, complex patterns are evident, with newer leads often intersecting older re-frozen leads. As the spring season progresses, the pack ice undergoes deformation from large ice fields into smaller ice floes. Images covering the same general area in the Beaufort Sea on 6 April and 18 June are shown in Figures 6-3 and 6-4, respectively.

In the imagery of early April, a large lead that is about 55 km wide at the widest point exists near 74°N, 140°W (a portion of this lead is

visible in Figure 6-3). Distinct tonal variations within the lead can be distinguished in both the visible and near-IR spectral bands, and are presumably representative of gradual re-freezing through formation of grey and grey-white ice. Twenty days later, on 21 April, the same lead can be seen, although it has narrowed considerably to a maximum width of only 18-22 km. On this date, the entire lead appears to contain grey-white ice. Within the grey-white ice small shearing leads are visible; the dark tone of these features indicates either open water or nilas ice. Finally, in an image on 7 May, the lead can barely be distinguished as only a very small difference in reflectance is detectable between the re-frozen lead and surrounding ice.

In the early April mosaics, a large lead containing some open water can also be mapped at about 77°N. North of the lead the pack ice is essentially solid, whereas south of the lead the ice is intersected with fractures and leads. In the imagery twenty days later, the area north of 77°N has also become fractured, and the lead visible earlier can no longer be detected.

Little change in the general ice structure of this area is evident between 21 April and 7 May, but a significant change appears to have taken place between 7 May and 18 June (Figure 6-4). By mid-June the entire area, although still consisting mostly of very close pack ice, has broken into ice floes. Moreover, on this date surface features can be detected on the individual floes in the southern part of the Beaufort Sea. In fact, a north to south progression in the visible surface features is noticeable. North of about 77°N, no surface features can be seen; from about 74° to 78°N, some features are visible; south of about 74°N, the ice appears to have deteriorated considerably, with the surface covered by features indicative of rotting ice. On this date, also, a large lead containing open water runs in a northwest-southeast direction near 80°N, 120°W; as was observed in the imagery more than two months earlier in the spring, the lead seems to be a boundary between more solid ice to the north and deformed ice to the south. The percentage of open water within the Beaufort Gyre (the general clockwise circulation of the Beaufort Sea) at different times of the year is an important consideration in ice dynamics and heat balance studies, but, as yet, is not precisely known (Campbell and Martin, 1973). ERTS imagery,

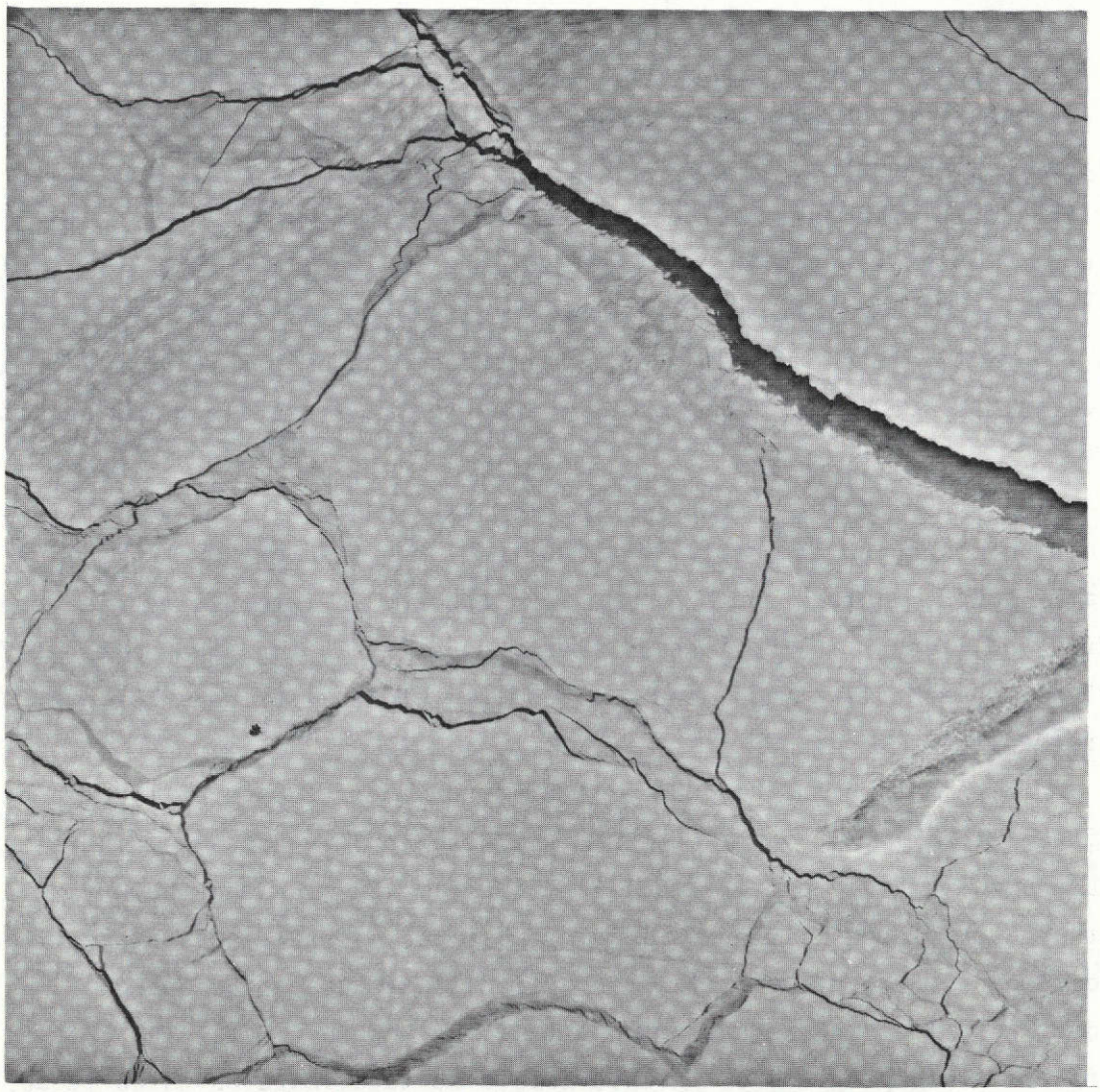

Figure 6-3 ERTS-1 MSS-7 image (ID No. 1257-21445), 6 April 1973, showing ice in Beaufort Sea near 75°N 142°W.

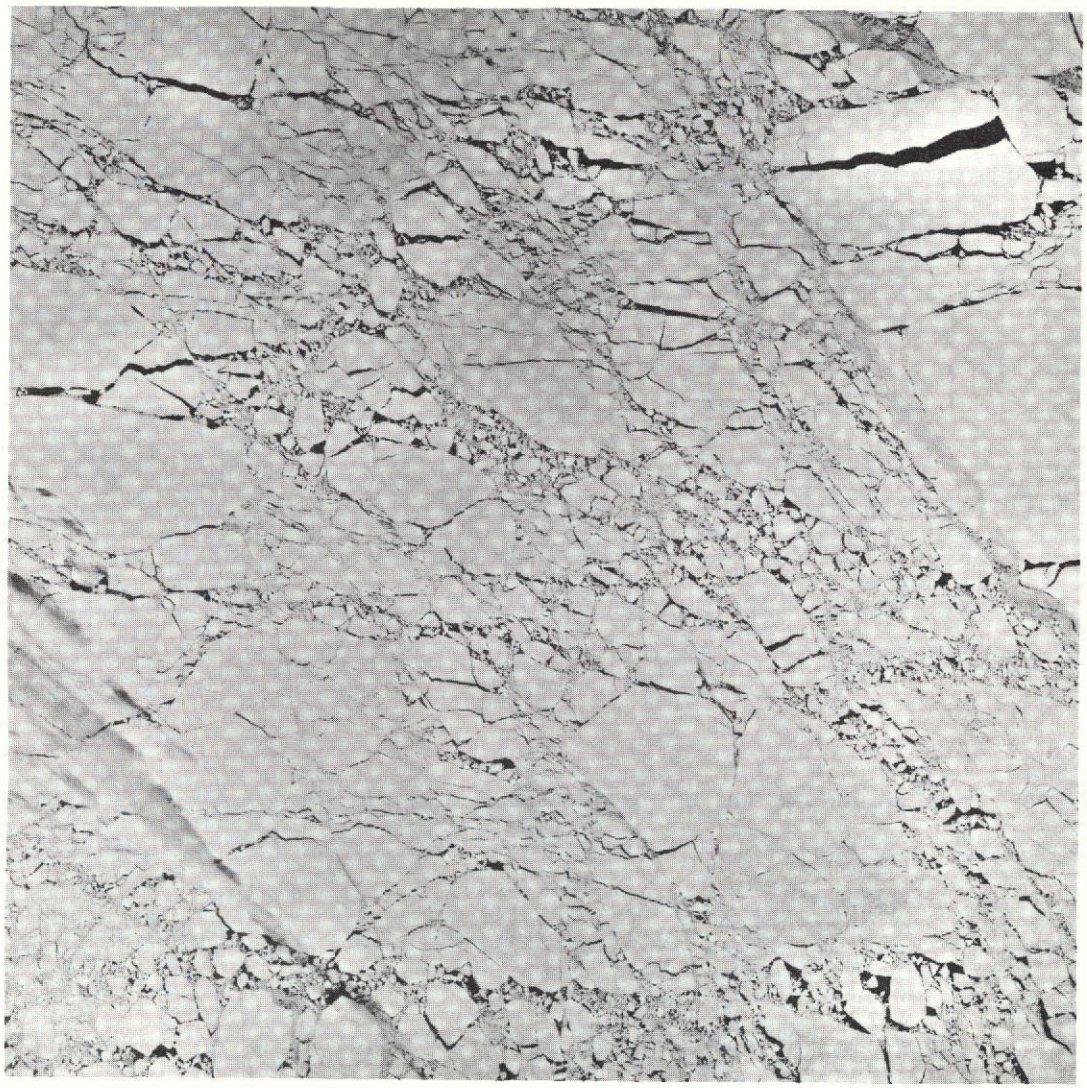

Figure 6-4 ERTS-1 MSS-7 image (ID No. 1330-21493), 18 June 1973, showing ice in Beaufort Sea at approximately the same area as in Figure 6-3.

such as is shown in Figures 6-3 and 6-4, has the potential for providing a measurement of the percentage of open water.

6.1.3 Eastern Beaufort Sea - Prince Patrick Island

Ice deformation in the eastern Beaufort Sea near Prince Patrick Island and the mouth of M'Clure Strait could be mapped throughout the spring season. Early in the spring, in imagery on 8, 10, 11, and 28 April (Figures 6-5, 6-6, 6-7, and 6-8), a quasi-permanent flaw lead can be observed just west of Prince Patrick Island. The lead separates fast ice along the coast and in M'Clure Strait from pack ice to the west. In the April imagery, all land and ice surfaces are snow covered and, therefore, appear smooth.

Significant changes in the configuration of the lead can be mapped from the imagery. On the 8th, the maximum width of the lead is about 4 km; two days later, it has widened to a width of 11 km near Prince Patrick Island and 28 km at M'Clure Strait; one day later, on the 11th, the maximum width is as much as 37 km. Later in the month the widening continues, so that on 28 April the lead is as much as 55 km wide. Detailed features along the edge can be mapped on the imagery and can be fit exactly with corresponding features on the eastern edge. As the lead opens, new ice formation is also evident. On the 10th and 11th, the low reflectance indicates the formation of grey ice, whereas on the 28th the higher reflectance in the western portion of the lead indicates that much of the ice has become grey-white. On each date the area of new ice formation is along the immediate eastern edge of the lead. Ice floes, judged to be either first-year or multi-year ice because of their high reflectance, are also embedded in the newer ice within the lead.

This same area is observed again in May and June. Images on 2 May, 17 May, 20 May, and 6 June are shown in Figures 6-9, 6-10, 6-11, and 6-12, respectively. During the short interval between 28 April (Figure 6-8) and 2 May (Figure 6-9), ice conditions have changed dramatically. The lead southwest of Prince Patrick Island has now closed in again and is full of ice floes, with very little grey or grey-white ice evident. Changes continue to take place, and by the next ERTS repeat cycle (17 May; Figure 6-10), the lead has once again reopened in the area south of Prince Patrick Island. In these observations, the formation of a giant floe (about 175 km across)

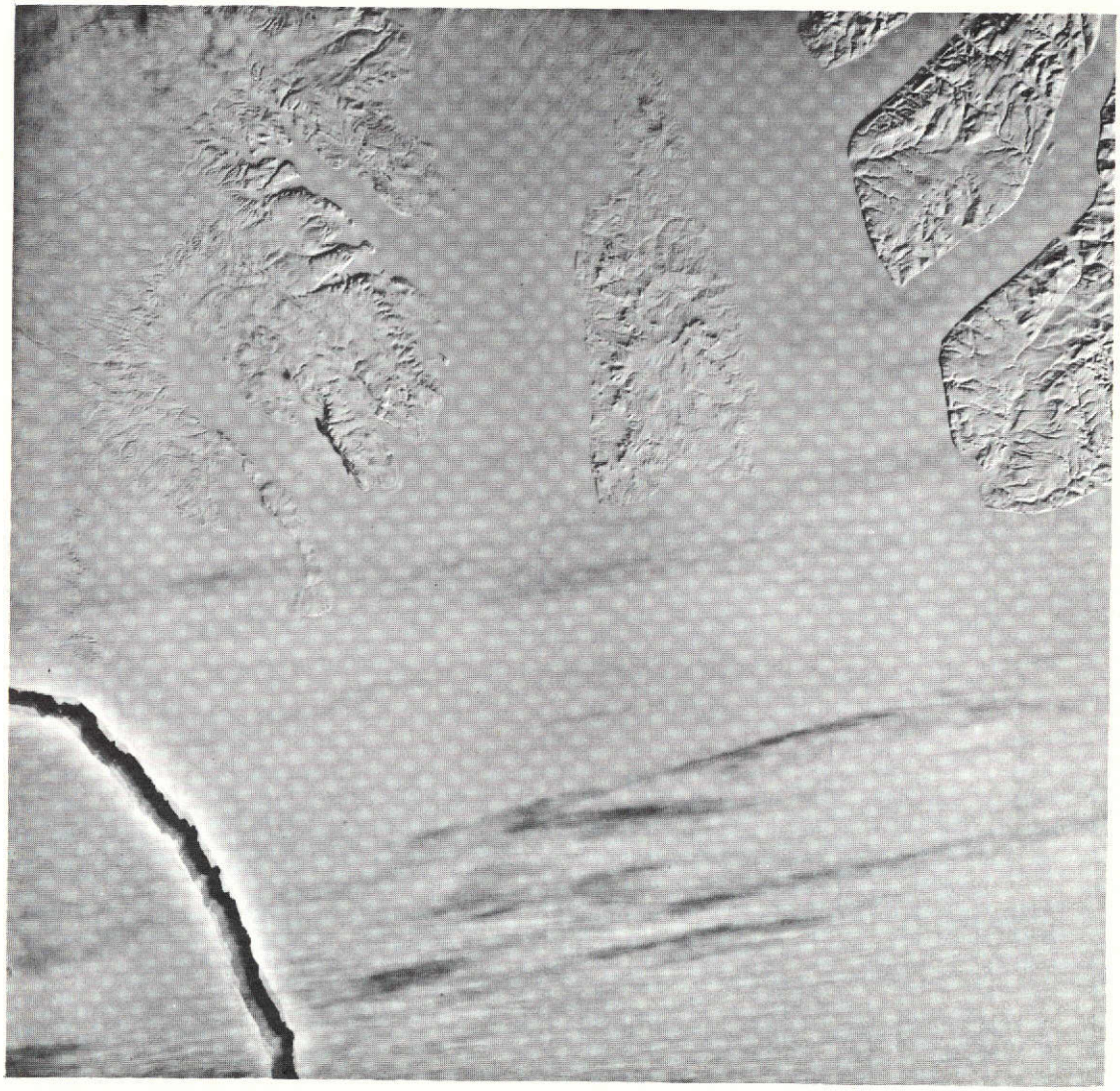

Figure 6-5 ERTS-1 MSS-7 image (ID No. 1259-20130), 8 April 1973, showing developing lead in eastern Beaufort Sea at M'Clure Strait, south of Prince Patrick Island.

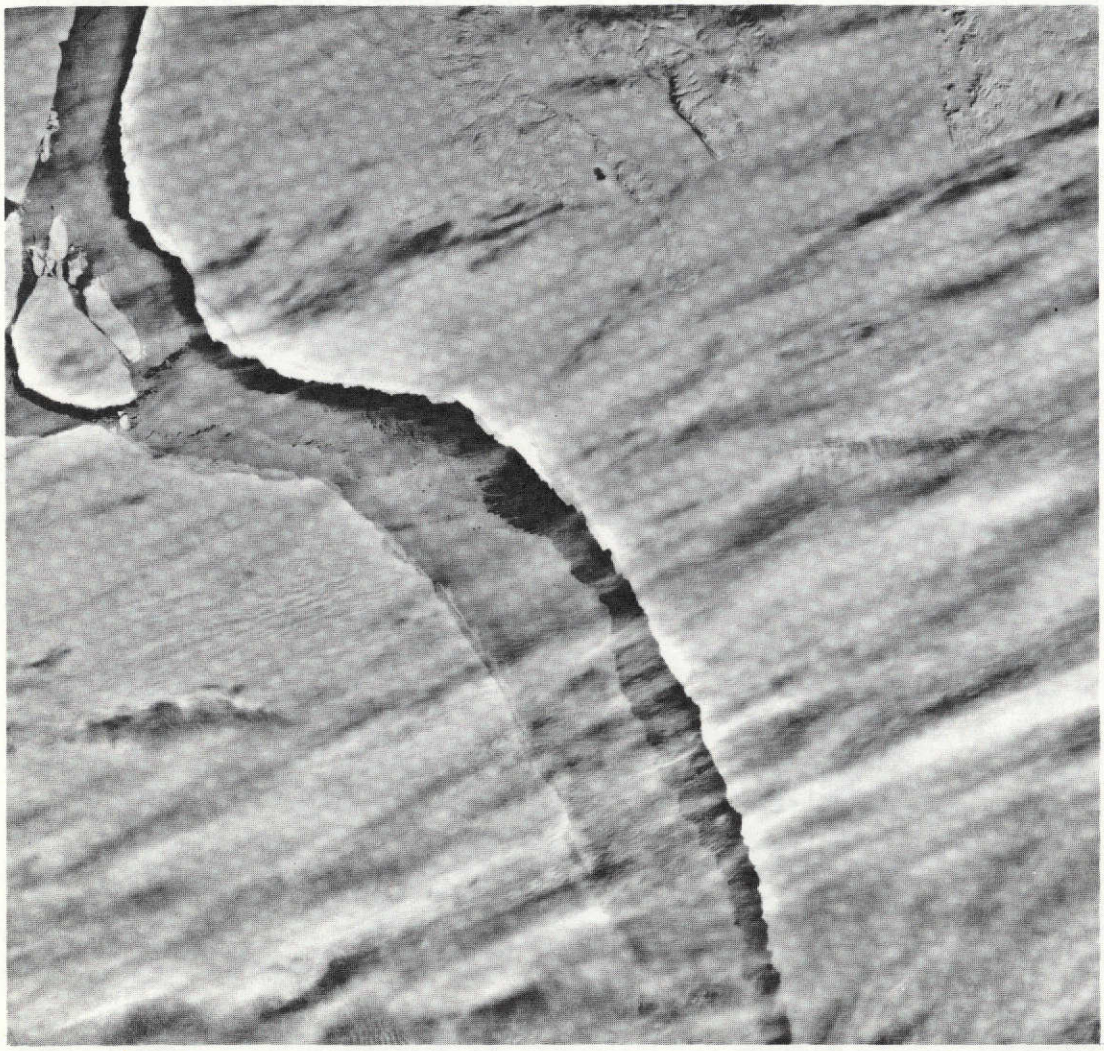

Figure 6-6 ERTS-1 MSS-7 image (ID No. 1261-20243), 10 April 1973, showing same area as in Figure 6-5.

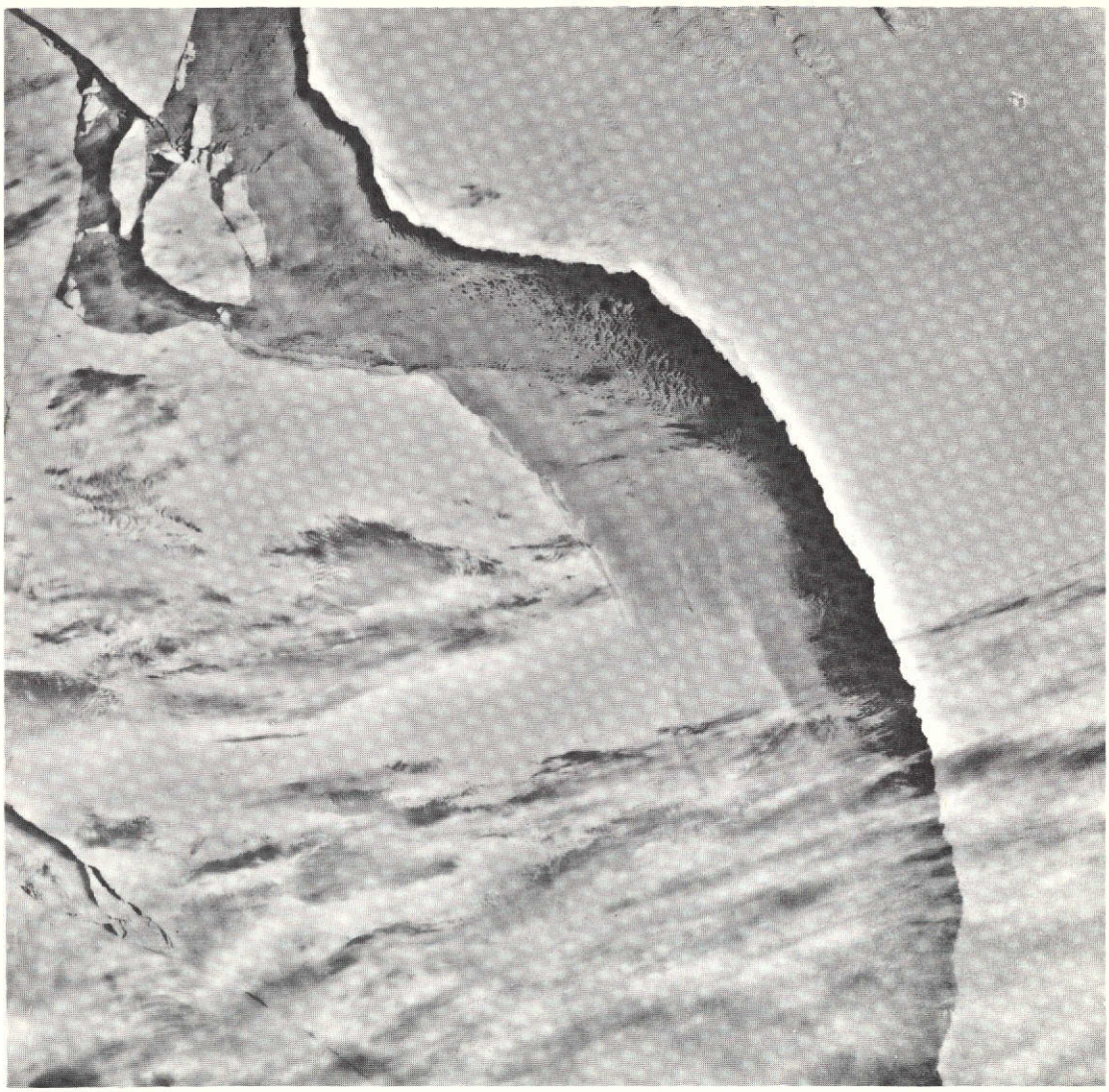

Figure 6-7 ERTS-1 MSS-7 image (ID No. 1262-20302), 11 April 1973, showing same area as in previous two figures.

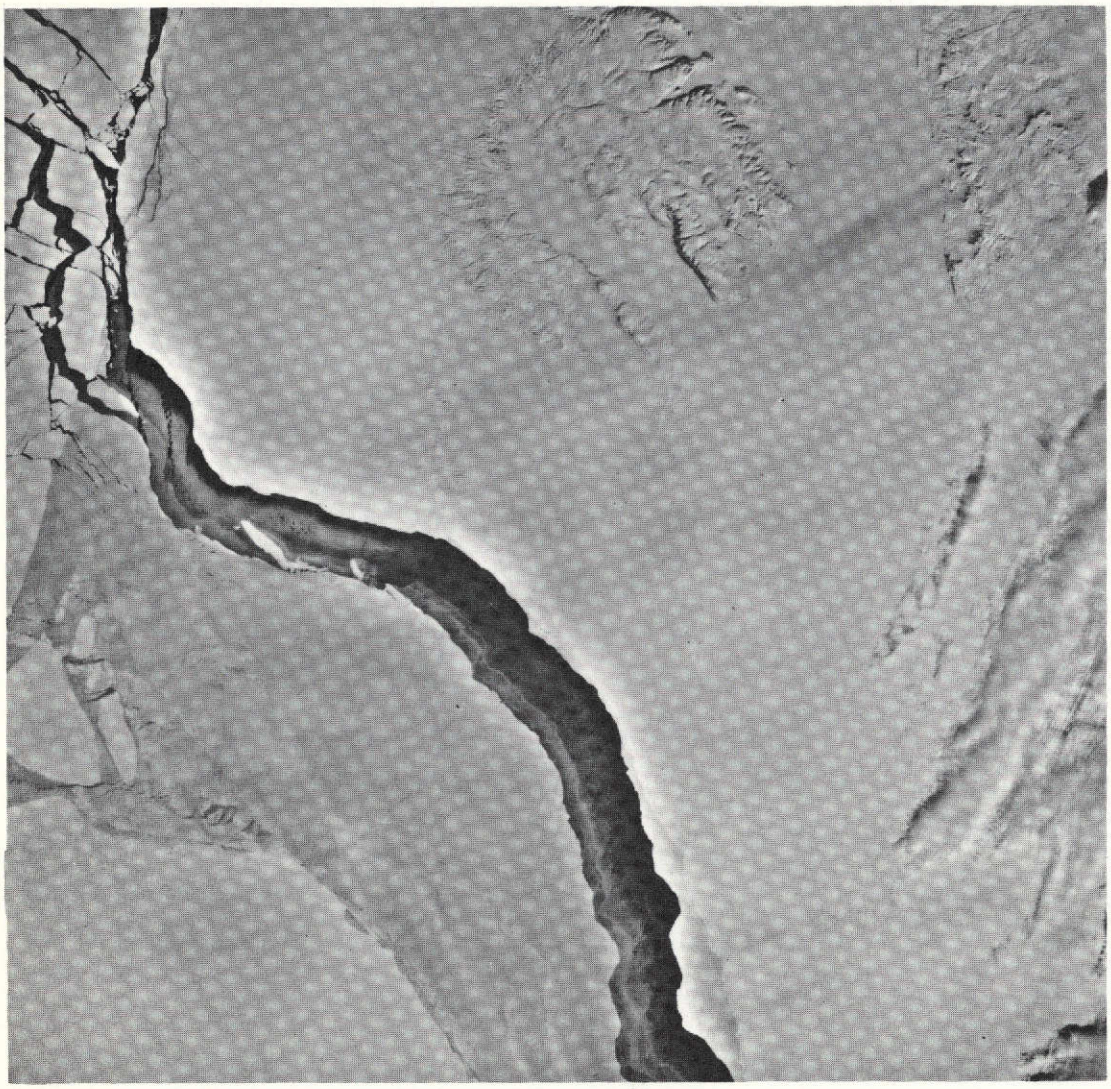

Figure 6-8 ERTS-1 MSS-7 image (ID No. 1279-20242), 28 April 1973, showing same area as in previous three figures.

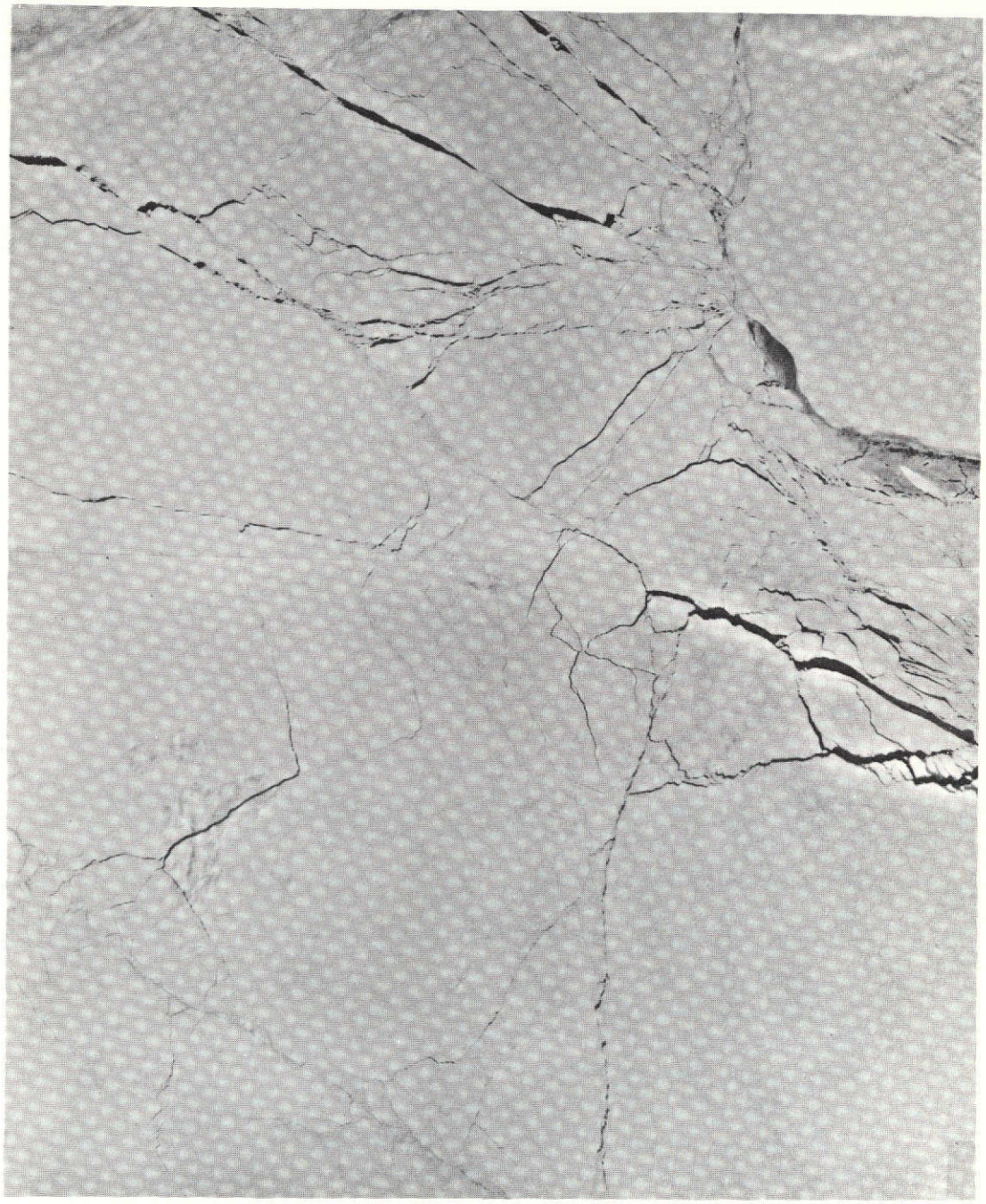

Figure 6-9 ERTS-1 MSS-7 imagery (ID Nos. 1283-20470 and 1283-20472), 2 May 1973, showing same area as in previous four figures.

Figure 6-10 ERTS-1 MSS-7 imagery (ID Nos. 1298-20300 and 1298-20302), 17 May 1973, showing same area as in previous five figures.

Figure 6-11 ERTS-1 MSS-7 imagery (ID Nos. 1301-20465 and 1301-20471), 20 May 1973, showing same area as in previous six figures.

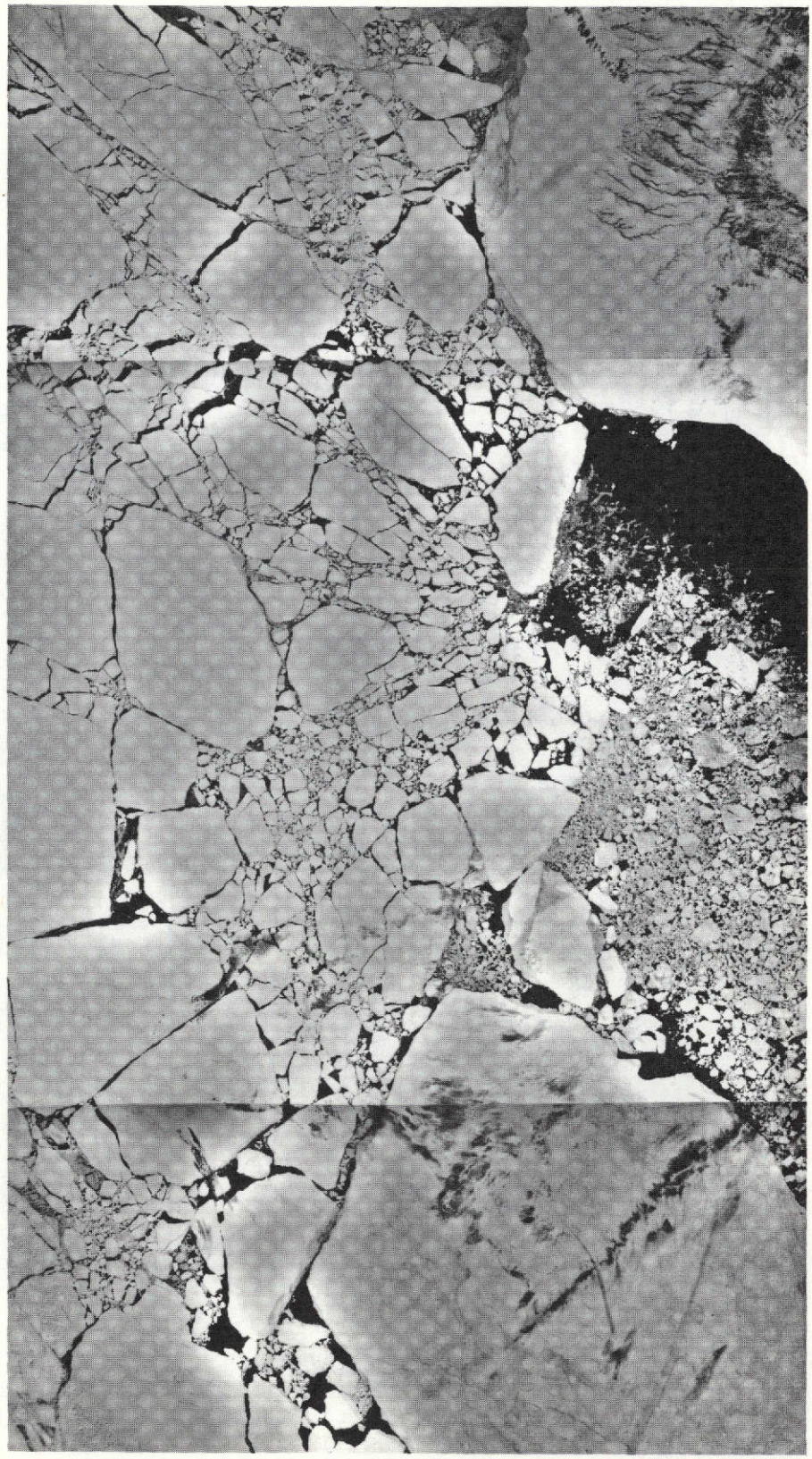

Figure 6-12 ERTS-1 MSS-7 imagery (ID Nos. 1318-20405, 1318-20411 and 1318-20414), 6 June 1973, showing same area as in previous seven figures.

can also be traced. The floe develops from fractures that can be detected on 2 May, and can be identified in later data on 20 May and 6 June (Figures 6-11 and 6-12). By the last date the floe has become surrounded by a broken ice field containing much smaller floes, and surface features can now be seen on the floe. Through careful study of these sequential observations, the deformation processes taking place in the ice field associated with the formation of this floe are evident.

6.1.4 Eastern Amundsen Gulf

Sequential observations covering the area of the eastern Amundsen Gulf and the Prince of Wales Strait were available throughout the period from 31 March to 29 June. The progression of the ice breakup, from smooth snow-covered fast ice early in the spring to a broken pack ice field at the end of June, can be mapped. Similarly, the deterioration of the ice surface as the reported temperatures in the area rise above freezing in late May and June can be observed; by the end of June the higher reflectivity of the ice surface suggests that considerable drainage of the meltwater has occurred.

Two images in mid-June are shown in Figures 6-13 and 6-14. On these dates (12 and 13 June) a boundary of fast ice with mostly open water to the west is observed extending southeast from Nelson Head, Banks Island to about 70°20°N - 122°W where it extends west-southwest to the tip of Parry Peninsula located between Franklin and Darnley Bays. Of particular interest is the appearance of several new fractures up to 1.8 km across on 13 June near the edge of the fast ice which extend from the mid-Gulf region westward to north of Darnley Bay. The imagery for the previous day showed only two fractures approximately 255 m to 360 m wide in the fast ice northwest of Darnley Bay. Also, during this one-day period, one giant floe (16 km across) and four vast floes (3.7 km to 11 km across) have moved some 18 to 25 km to the northwest, revealing a strong current flow in this region. A large shore polynya at the mouth of the Hornaday River in Darnley Bay is also evident in the 12 and 13 June imagery. On 13 June, however, a giant floe (18.5 km) not evident on the previous day, has broken away from the edge of the fast ice and has moved 3.7 km to the southeast.

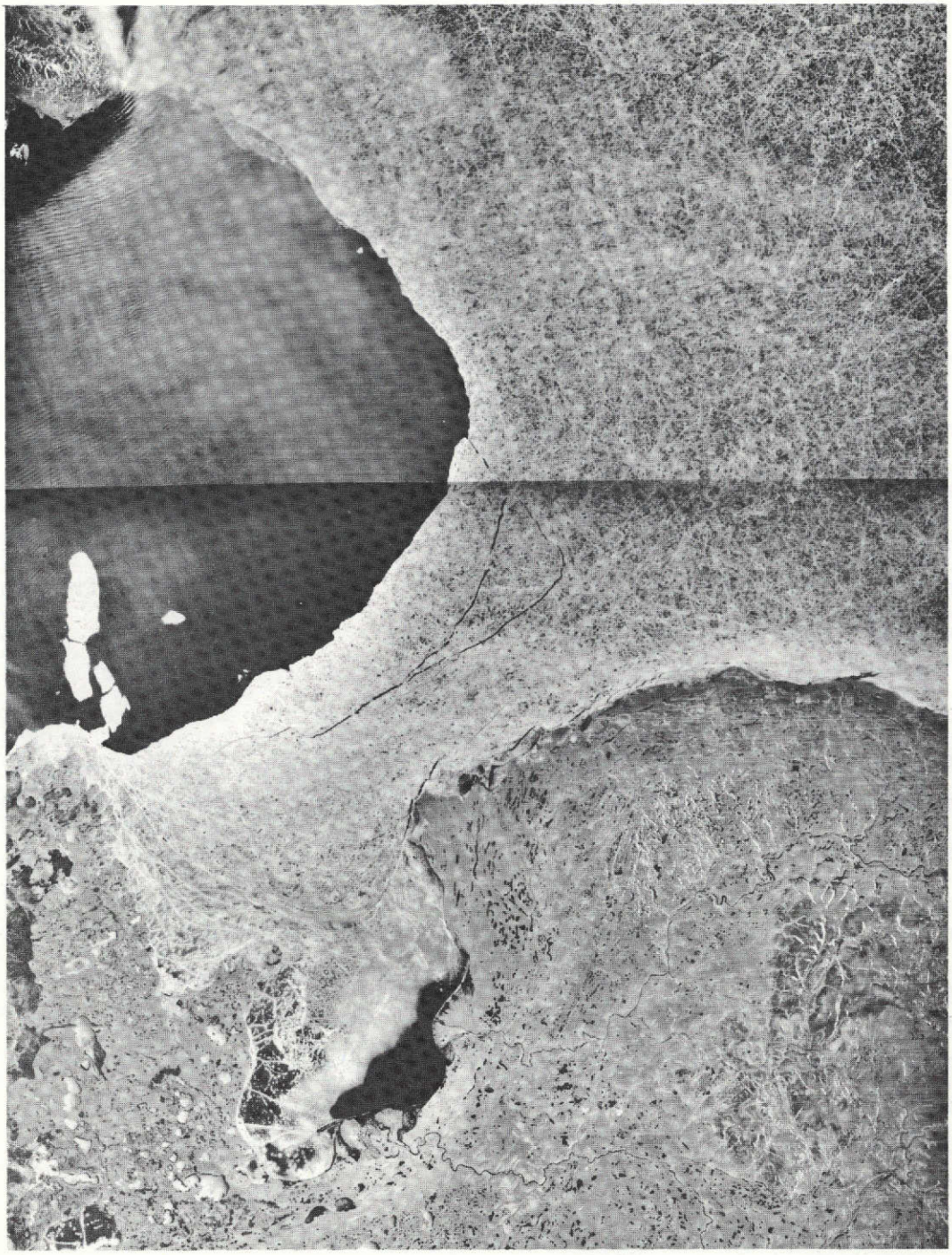

Figure 6-13 ERTS-1 MSS-7 imagery (ID Nos. 1324-19340 and 1324-19343), 12 June 1973, showing ice in eastern Amundsen Gulf. Banks Island is at upper left corner; Darnley Bay is at lower center of imagery.

Figure 6-14 ERTS-1 MSS-7 imagery (ID Nos. 1325-19394 and 1325-19401), 13 June 1973, showing same area as in previous figure.

6.2 Ice Movement

6.2.1 Amundsen Gulf

Through the use of the sequential ERTS observations it is possible to measure ice movements over 24-hour periods and over the longer periods associated with ERTS repeat cycles. In Amundsen Gulf, for example, the movements of floes were measured over 24-hour periods for a three day sequence of observations in late July 1972. The measurements of ice floes off the west coast of Banks Island indicated an overall direction of motion toward the west-southwest at about 15 km per day; the smaller floes nearer the coast appear to be moving more south-southwest at 15 to 20 km per day, whereas farther off-shore, the larger floes moved toward the west to southwest at 9 to 15 km per day. Little or no movement was observed in a giant floe to the north, although some deterioration (breaking off of smaller floes) did occur. Measurements of 24-hour motions of ice floes in western Franklin Bay off the coast of Cape Bathurst showed a mean direction toward the north-west at 13 to 28 km per day into Amundsen Gulf and the Beaufort Sea. Two floes closer to the coast moved southwest toward the coast of Cape Bathurst at about 11 km per day.

6.2.2 Beaufort Sea

In several instances it was possible to measure mean ice movements over longer time periods. Whereas the measurements discussed in the above section were determined from the motions of relatively small ice floes that could be easily recognized in the day-to-day images, the longer-period measurements require the existence of larger floes that retain their shapes over the intervals of 18 days or longer. In the Beaufort Sea, positive identification of 13 giant ice floes was possible over the 20-day period from 2 to 22 August (three of these floes are shown in Figures 3-4a and 3-4b). Mean motions of these floes were measured, using the geographic gridding of the images to locate the positions of the floes; because of the inherent gridding errors, the resulting measurements cannot be considered as precise as those where the grids can be adjusted using landmarks.

The measurements indicate a clockwise shift in the direction of motion from north to south, with the more northerly floes moving in a southward direction and the more southerly floes moving in a southwesterly direction. The latter floes are also indicated to be moving more slowly than those farther north. Measurements of four floes between 75°N and 74°N indicate a mean direction toward 176° at a speed of 4.3 to 3.5 km per day; measurements of six floes between 74°N and 73°N indicate a mean direction toward 206° at a speed of 3.7 to 3.0 km per day; and measurements of three floes between 73°N and 72°N indicated a mean direction toward 225° at 3.3 to 2.8 km per day.

6.2.3 Eastern Beaufort Sea - Prince Patrick Island Area

The sequential ERTS observations covering the eastern Beaufort Sea in the Prince Patrick Island area on several dates in May and June have enabled the formation and movement of 12 giant floes, ranging in size from 18 to 175 km across, to be determined (imagery for 2, 17, and 20 May and 6 June are shown in Figures 6-9 through 6-12).

The floes develop from fractures evident on the 2nd and 3rd of May and can be positively identified 34 days later on 6 June. As noted in the earlier measurements of the motions of 13 giant floes in the Beaufort Sea made on imagery of August 1972, a gradual clockwise shift in direction of movement is observed from north to south. Measurements of four floes between 76°N and 77°N off the west coast of Prince Patrick Island indicate a mean direction toward 198° at a speed of 1.3 to 1.7 km per day, whereas measurements of four floes between 75°N and 76°N indicate a mean direction toward 227° at a speed of 1.8 to 2.2 km per day. Measurements of two floes located farther to the west between 75°N and 76°N indicate a mean direction toward 248° at a somewhat slower speed of about 1.3 km per day. The measurements in this area also show that two larger-size giant floes located between 74°N and 75°N are moving at slightly different mean directions over the 34-day period. The giant floe closer to the coast measured 175 km across and is moving toward a mean direction of 214° at 2 km per day, whereas the giant floe (133 km across) immediately to the west is moving in a mean direction toward 256° at 2 km per day.

7. CONCLUSIONS

7.1 Practical Applications Resulting From the Use of ERTS Data for Monitoring Sea Ice

The results of the analysis of data for several arctic regions collected during the late summer and early fall of 1972 and the spring and early summer of 1973 indicate that the use of ERTS imagery has substantial practical application for monitoring sea ice. Most types of sea ice can be detected in all of the ERTS-1 spectral bands because of the high reflectance in comparison to that of the surrounding water. Moreover, glacial ice can usually be distinguished from sea ice, and ice can be distinguished from clouds through a number of interpretive keys. Experimentation has shown that the photographic processing of prints can be important for ice detection, since exposures selected to retain detail in bright, snow covered land areas may result in the loss of significant ice features. For ice mapping purposes, it appears that the color ERTS data products offer no significant advantages over the more readily available black and white products.

Ice features at least as small as 80-100 m in width can be detected in ERTS imagery. The visible spectral band imagery is the most useful for mapping overall ice extent, since some types of ice are difficult to detect in the near-IR spectral band imagery. A greater amount of detail in the ice features can be detected in the near-IR imagery, however, and the multispectral analysis of the visible and near-IR data is a powerful tool for identifying ice types and for determining certain ice surface characteristics. In regions such as the eastern Beaufort Sea, the combination of ERTS orbital overlap and a high incidence of cloud free conditions during the spring assures a high frequency of repetitive satellite coverage. The resulting sequential observations permit the deformation and movement of ice features to be mapped.

Ice features that can be identified in ERTS imagery include: the distinction between grey, grey-white, and older forms of ice, as well as the distinction between ice floes and surrounding brash ice; the growth and deterioration of leads; the formation of new grey ice within leads; the deterioration of the ice surface as evidenced by the formation of puddled areas and

flooded ice; linear dry areas within flooded ice fields caused by the drainage of meltwater; and icebergs embedded in fast ice or close pack, detectable by their shadows.

Comparative analyses have shown generally good agreement between the locations of ice edges and the ice concentrations as mapped from ERTS imagery and as depected on aerial ice observation charts. In addition to being compared with the standard aerial observation charts, data from ERTS passes crossing the Bering Sea in early March were compared with ice observations collected in the Bering Sea Expedition (BESEX). On two flights of the NASA-CV-990 aircraft, the ice conditions in the vicinity of St. Lawrence Island reported by the onboard observer are in remarkably close agreement with the ice conditions mapped from the corresponding ERTS imagery. The features identified in ERTS imagery and substantiated by the aerial observer include the locations of boundaries between areas consisting of mostly grey ice and of mostly first and multi-year ice, the existence of shearing leads, and the occurrence of open water with the associated development of stratus cloud streaks. Moreover, it appears that essentially all of the significant ice features near St. Lawrence Island visible in aircraft photographs taken from the CV-990 can also be detected in the ERTS imagery.

Personnel of the principal agencies responsible for ice reconnaisance in the Arctic, the Ice Forecast Office of the U.S. Navy Fleet Weather Central and the Canadian Ice Forecasting Central, have expressed considerable interest in the application of ERTS data to ice monitoring. In addition to the interest of these government agencies, at least one sector of private industry is also vitally interested in applications of ERTS data for ice monitoring. The oil and mineral exploration companies will be one of the principal users of ice data in the next few years. In fact, it is in this regard that one of the first operational uses of ERTS-1 data has been accomplished. As reported at a workshop on remote sensing of sea ice held recently in Ottawa and at the Third ERTS Symposium (Morley, 1973), useful operational ice formation from the Canadian "quick look" ERTS facility was supplied to a ship making seismic measurements in arctic waters; as a direct result of the ERTS data, the ship was able to penetrate 75 miles farther than had been anticipated.

Based on the results of the investigation, especially the comparative analysis between the ERTS and BESEX data, and the successful operational experience using the Canadian "quick-look" ERTS facility, it seems entirely feasible that ERTS imagery could be used to replace some currently flown aerial surveys. In fact, in a recent communication from the Canadian Ice Forecasting Central, Markham (1973) states that because of the high frequency of cloud free conditions in the Arctic during the spring season, he believes that the "quick-look" ERTS data - black and white product only - could replace at least the April ice survey flights, at a considerable saving in cost.

7.2 Recommendations

The ERTS-1 configuration is sufficient for collecting substantial amounts of sea ice data. Because of the overlapping of orbital passes at high latitudes, the potential for obtaining sequential observations of the Arctic is considerably greater than for lower latitudes. The sensor resolution and area viewed by ERTS are adequate for most ice monitoring purposes. Furthermore, ice monitoring is an application where the ERTS color data products appear to offer little advantage over the more readily available black and white imagery.

Despite the adequacy of ERTS-1 for most ice monitoring purposes, certain changes in the orbital configuration and sensor complement would enhance the potential for collecting arctic data. The orbital coverage should be extended farther north than the current 79 to 80° N limit, in order to permit data collection over additional arctic regions; for example, the northern coast of Ellesmere Island, which cannot be observed in the current ERTS configuration, is an important region to be monitored in future ice studies, because it is the origin of most of the arctic ice islands. Another limitation in the use of ERTS-1 data is that the existing sensors can provide ice observations only during the period of adequate solar illumination. For heat balance studies, in particular, wintertime ice monitoring is essential. The addition of a thermal-IR channel to the sensor complement would enable ice observations to be made during the wintertime dark period.

Further investigations using the ERTS-1 data sample should be conducted to document and verify the techniques for identifying and mapping ice developed under the initial study program. Besides the need to correlate ERTS data with

additional ground truth, it will now be possible to compare the data collected during the late summer and fall of 1973 with that from the same period of the previous year. In some arctic regions the ice distribution in 1973 may be quite different from that of 1972; the second year of data should be examined, therefore, to determine whether annual variations in ice distribution can be accurately mapped using ERTS data, and to compile statistics of ice distributions over two summer seasons.

Further studies should also emphasize the analysis of radiometric values from ERTS digitized data to determine more accurately the multispectral signatures of sea ice. Through the analysis of the digitized values it may be possible to develop techniques to differentiate ice types more reliably, and to obtain quantitative ice information.

The results of the initial investigation using ERTS-1 data have shown that the mapping of sea ice is one of the most immediately useful oceanographic applications of satellite observations. In fact, because of the expanse of sea ice that must be monitored, it does not appear worth the expense to furnish resolution comparable to that of aircraft photography from a satellite system. Clearly, the continued development of improved techniques to interpret ERTS and other satellite data will lead eventually to the use of operational satellite systems to collect ice data on a far more complete and economical basis than has heretofore been possible.

8. REFERENCES

Barnes, J.C. and C.J. Bowley, 1973a: Use of ERTS Data for Mapping Arctic Sea Ice, Symposium on Significant Results Obtained from the Earth Resources Technology Satellite-1, NASA SP-327, pp. 1377-1384.

Barnes, J.C. and C.J. Bowley, 1973b: Mapping Sea Ice from the Earth Resources Technology Satellite, Arctic Bulletin, 1 (1), pp. 6-13.

Barnes, J.C., C.J. Bowley, D.T. Chang and J.H. Willand, 1973: Application of Satellite and Visible Infrared Data to Mapping Sea Ice. Paper presented at the Interdisciplinary Symposium on Advanced Concepts and Techniques in the Study of Snow and Ice Resources, National Academy of Sciences, Monterey, California.

Barnes, J.C., D.T. Chang, and J.H. Willand, 1970: "Satellite Infrared Observation of Arctic Sea Ice," AIAA Paper No. 70-301, AIAA Earth Resources Observations and Information Systems Meeting, Annapolis, Maryland.

Barnes, J.C., D.T. Chang, and J.H. Willand, 1972: Image Enhancement Techniques for Improving Sea Ice Depiction in Satellite Infrared Data, Journal of Geophysical Research; Oceans and Atmospheres Edition, 77 (3), pp. 453-462.

Baliles, M.S. and H. Neiss, 1963: Conference on Satellite Ice Studies, Meteorological Satellite Laboratory Report No. 20, U.S. Department of Commerce, Weather Bureau.

Borisenkov, E.P. and A.F. Treshnikov: "Polar Experiment." Problemy Arktiki i Antarktiki, 38, Hydrometeoizdat, Leningrad, 1971.

Campbell, W.J., P. Gloersen, W. Nordberg, and T.T. Wilheit, 1973: Dynamics and Morphology of Beaufort Sea Ice Determined from Satellites, Aircraft, and Drifting Stations, NASA Publication X-650-73-194, NASA/GSFC.

Campbell, W.J. and S. Martin, 1973: Oil and Ice in the Arctic Ocean: Possible Large-Scale Interactions, Science, Vol. 181, pp. 56-58.

Committee on Polar Research, 1970: Polar Research, A Survey, National Research Council, National Academy of Sciences, Washington, D.C.

Crowder, W.K., H.L. McKim, S.F. Ackley, W.D. Hibler, III, and D.M. Anderson: Mesoscale Deformation of Sea Ice from Satellite Imagery. Paper presented at the Interdisciplinary Symposium on Advanced Concepts and Techniques in the Study of Snow and Ice Resources, Monterey, California, 1973.

Fletcher, J.O., 1966: "Forward," Proc. of the Symposium on the Arctic Heat Budget and Atmospheric Circulation, Memorandum RM-5233-NSF, The RAND Corporation.

Fletcher, J.O., 1968: "The Polar Oceans and World Climate," Proc. of the Long-Range Polar Objectives Conference, U.S. Department of Transportation, Washington, D.C.

Markham, W.E., 1973: Modern Demands on the Canadian Ice Advisory Service, Paper 3.12, Presented at Interdisciplinary Symposium on Advanced Concepts and Techniques in the Study of Snow and Ice Resources, Monterey, California.

Markham, W.E., 1973: Personal Communication.

Maykut, G.A., A.S. Thorndike and N. Untersteiner: "AIDJEX Scientific Plan." AIDJEX Bulletin No. 15, 1972.

Maykut, G.A. and N. Untersteiner, 1969: Numerical Prediction of the Thermodynamic Response of Arctic Sea Ice to Environmental Changes, Memorandum RM-6093-PR, The RAND Corporation.

McClain, E.P., 1972: Detection of Ice Conditions in the Queen Elizabeth Islands, Proc. of Symposium on Earth Resources Technology Satellite-1, September 29, 1972, National Aeronautics and Space Administration.

McClain, E.P., 1973: Some New Satellite Measurements and Their Application to Sea Ice Analysis in the Arctic and Antarctic, Paper 5.2, presented at Interdisciplinary Symposium on Advanced Concepts and Techniques in the Study of Snow and Ice Resources, Monterey, California.

McClain, E.P. and M.D. Baliles, 1971: Sea Ice Surveillance from Earth Satellites, Mariners Weather Log, 15 (1), pp. 1-4.

Morley, L.W., 1973: Report on the Canadian ERTS Program, paper presented at the Third ERTS Symposium, Washington, December 10-14, 1973, NASA/GSFC.

Morse, R.M., 1964: "Recommendations of Panel on Sea Ice," Oceanography from Space, Woods Hole Oceanographic Institution.

Strong, A.E., E.P. McClain and D.F. McGinnis, 1971: "Detection of thawing snow and ice packs through the combined use of visible and near-infrared measurements from earth satellites." Monthly Weather Review, 99 (11), pp. 828-830.

Wark, D. and R. Popham, 1962: Ice Photography from the Meteorological Satellites TIROS I and TIROS II, USWB, Meteorological Satellite Laboratory Report No. 8.

Wiesnet, D.R., 1973: "The Role of Satellites in Snow and Ice Measurements," Page 5.1, presented at Interdisciplinary Symposium on Advanced Concepts and Techniques in the Study of Snow and Ice Resources, Monterey, California.

Wittmann, W.I., 1966: "Report of Working Group on the Heat and Mass Budget of the Pack Ice," Proc. of the Symposium on the Arctic Heat Budget and Atmospheric Circulation, Memorandum RM-6233-NSF, The RAND Corporation.

APPENDIX

SEA ICE TERMINOLOGY

9. ACKNOWLEDGEMENTS

The authors wish to acknowledge the assistance provided throughout the study by Mr. James R. Greaves, Scientific Monitor, and Mr. Edmund F. Szajna, Technical Monitor, both of NASA Goddard Space Flight Center.

We also wish to thank Commander William Dehn, Director (recently retired) of the Ice Forecast Office of the U. S. Navy Fleet Weather Central, and Mr. William E. Markham, Director of the Canadian Ice Forecast Central, for providing aerial ice survey charts and for their helpful suggestions in the interpretation of various ice features detectable in ERTS imagery. Commander Dehn also kindly provided a considerable amount of useful material from the Navy aerial ice observer training course. The BESEX ice data were obtained through the courtesy of Dr. Per Gloersen of NASA Goddard Space Flight Center.

SEA ICE TERMINOLOGY

from WMO SEA ICE NOMENCLATURE

(WMO Publication No. 259.TP.145)

Belt	A large feature of pack ice arrangement; longer than it is wide: from 1 km to more than 100 km in width.
Bight	An extensive crescent-shaped indentation in the ice edge, formed by either wind or current.
Brash ice	Accumulations of floating ice made up of fragments not more than 2m across, the wreckage of other forms of ice.
Close pack ice	Pack ice in which the concentration is 7/10 to 8/10 (6/8 to less than 7/8), composed of floes mostly in contact.
Compacting	Pieces of floating ice are said to be compacting when they are subjected to a converging motion, which increases ice concentration and/or produces stresses which may result in ice deformation.
Compact pack ice	Pack ice in which the concentration is 10/10 (8/8) and no water is visible.
Concentration	The ratio in tenths of the sea surface actually covered by ice to the total area of sea surface, both ice-covered and ice-free, at a specific location or over a defined area.
Consolidated pack ice	Pack ice in which the concentration is 10/10 (8/8) and the floes are frozen together.
Crack	Any fracture which has not parted.
Diffuse ice edge	Poorly defined ice edge limiting an area of dispersed ice; usually on the leeward side of an area of pack ice.
Fast ice	Sea ice which forms and remains fast along the coast, where it is attached to the shore, to an ice wall, to an ice front, between shoals or grounded icebergs. It may extend a few metres or several hundred kilometres from the coast.

SEA ICE TERMINOLOGY

Fast-ice boundary	The ice boundary at any given time between fast ice and pack ice.
Fast-ice edge	The demarcation at any given time between fast ice and open water.
First-year ice	Sea ice of not more than one winter's growth, developing from young ice; thickness 30 cm - 2m. May be subdivided into thin first-year ice/white ice, medium first-year ice and thick first-year ice.
Flaw	A narrow separation zone between pack ice and fast ice, where the pieces of ice are in chaotic state; it forms when pack ice shears under the effect of a strong wind or current along the fast ice boundary.
Flaw lead	A passage-way between pack-ice and fast ice which is navigable by surface vessels.
Floe	Any relatively flat piece of sea ice 20 m or more across. Floes are subdivided according to horizontal extent as follows. Giant: Over 10 km across Vast: 2-10 km across Big: 500-2,000 m across Medium: 100-500 m across Small: 20-100 m across
Flooded ice	Sea ice which has been flooded by melt-water or river water and is heavily loaded by water and wet snow.
Fracture	Any break or rupture through very close pack ice, compact pack ice, consolidated pack-ice, fast ice, or a single floe resulting from deformation processes. Fractures may contain brash ice and/or be covered with nilas and/or young ice. Length may vary from a few metres to many kilometres.
Fracture zone	An area which has a great number of fractures.
Fracturing	Pressure process whereby ice is permanently deformed, and rupture occurs. Most commonly used to describe breaking across very close pack ice, compact pack ice and consolidated pack ice.

SEA ICE TERMINOLOGY

Glacier	A mass of snow and ice continuously moving from higher to lower ground or, if afloat, continuously spreading. The principal forms of glacier are: inland ice sheets, ice shelves, ice streams, ice caps, ice piedmonts, cirque glaciers and various types of mountain (valley) glaciers.
Grey ice	Young ice 10-15 cm thick. Less elastic nilas and breaks on swell. Usually rafts under pressure.
Grey-white ice	Young ice 15-30 cm thick. Under pressure more likely to ridge than to raft.
Hummock	A hillock of broken ice which has been forced upwards by pressure. May be fresh or weathered.
Iceberg	A massive piece of ice of greatly varying shape, more than 5 m above sea-level, which has broken away from a glacier, and which may be afloat or aground. Icebergs may be described as tabular, dome-shaped, sloping, pinnacled, weathered or glacier bergs.
Iceberg tongue	A major accumulation of icebergs projecting from the coast, held in place by grounding and joined together by fast ice.
Ice boundary	The demarcation at any given time between fast ice and pack ice or between areas of pack ice of different concentrations.
Ice cake	Any relatively flat piece of sea ice less than 20 m across.
Ice edge	The demarcation at any given time between the open sea and sea ice of any kind, whether fast or drifting. It may be termed compacted or diffuse.
Ice-free	No sea ice present. There may be some ice of land origin.
Ice island	A large piece of floating ice about 5 m above sea-level, which has broken away from an Arctic ice shelf, having a thickness of 30-50 m and an area of from a few thousand square metres to 500 sq km, or more, and usually characterized by a regularly undulating surface which gives it a ribbed appearance from the air.
Large fracture	More than 500 m wide.

SEA ICE TERMINOLOGY

Lead	Any fracture or passage-way through sea ice which is navigable by surface vessels.
Medium fracture	200 to 500 m wide.
Multi-year ice	Old ice up to 3 m or more thick which has survived at least two summers' melt. Hummocks even smoother than in second-year ice, and the ice is almost salt-free. Colour, where bare, is usually blue. Melt pattern consists of large interconnecting irregular puddles and a well-developed drainage system.
Nilas	A thin elastic crust of ice, easily bending on waves and swell and under pressure, thrusting in a pattern of interlocking "fingers" (finger rafting). Has a matt surface and is up to 10 cm in thickness. May be subdivided into dark nilas and light nilas.
Open pack ice	Pack ice in which the ice concentration is 4/10 to 6/10 (3/8 to less than 6/8), with many leads and polynyas, and the floes are generally not in contact with one another.
Open water	A large area of freely navigable water in which sea ice is present in concentrations less than 1/10 (1/8). When there is no sea ice present, the area should be termed ice-free, even though icebergs are present.
Pack ice	Term used in a wide sense to include any area of sea ice, other than fast ice, no matter what form it takes or how it is disposed.
Polynya	Any non-linear shaped opening enclosed in ice. Polynyas may contain brash ice and/or be covered with new ice, nilas or young ice; submariners refer to these as skylights.
Puddle	An accumulation on ice of melt-water, mainly due to melting snow, but in the more advanced stages also the melting of ice. Initial stage consists of patches of melted snow.
Ridge	A line or wall of broken ice forced up by pressure. May be fresh or weathered. The submerged volume of broken ice under a ridge, forced downwards by pressure, is termed an ice keel.
Rotten ice	Sea ice which has become honeycombed and which is in an advanced state of disintegration.

Second-year ice	Old ice which has survived only one summer's melt. Because it is thicker and less dense than first-year ice, it stands higher out of the water. In contrast to multi-year ice, summer melting produces a regular pattern of numerous small puddles. Bare patches and puddles are usually greenish-blue.
Shearing	An area of pack ice is subject to shear when the ice motion varies significantly in the direction normal to the motion, subjecting the ice to rotational forces.
Shore lead	A lead between pack ice and the shore or between pack ice and an ice front.
Shore polynya	A polynya between pack ice and the coast or between pack ice and an ice front.
Small fracture	50 to 200 m wide
Tabular berg	A flat-topped iceberg. Most tabular bergs form by calving from an ice shelf and show horizontal banding.
Thaw holes	Vertical holes in sea ice formed when surface puddles melt through to the underlying water.
Very close pack ice	Pack ice in which the concentration is 9/10 to less than 10/10 (7/8 to less than 8/8).
Very open pack ice	Pack ice in which the concentration is 1/10 to 3/10 (1/8 to less than 3/8) and water preponderates over ice.
Young coastal ice	The initial stage of fast ice formation consisting of nilas or young ice, its width varying from a few metres up to 100-200 m from the shoreline.
Young ice	Ice in the transition stage between nilas and first-year ice, 10-30 cm in thickness. May be subdivided into grey ice and grey-white ice.